

THE MULTIFRACTAL FORMALISM REVISITED WITH WAVELETS

J. F. MUZY*, E. BACRY*,† and A. ARNEODO*

*Centre de Recherche Paul Pascal, Avenue Schweitzer,
 33600 Pessac, France

†Université de Paris VII, UFR de Mathématiques,
 Tour 45-55, 2 Place Jussieu, 75251 Paris Cedex 05, France

Received December 13, 1993

The multifractal formalism originally introduced for singular measures is revisited using the wavelet transform. This new approach is based on the definition of partition functions from the wavelet transform modulus maxima. We demonstrate that the $f(\alpha)$ singularity spectrum can be readily determined from the scaling behavior of these partition functions. We show that this method provides a natural generalization of the classical box-counting techniques to fractal functions (the wavelets actually play the role of “generalized boxes”). We report on a systematic comparison between this alternative method and the structure function approach which is commonly used in the context of fully developed turbulence. We comment on the intrinsic limitations of the structure functions which possess fundamental drawbacks and do not provide a full characterization of the singularities of a signal in many cases. We show that our method based on the wavelet transform modulus maxima decomposition works in most situations and is likely to be the ground of a unified multifractal description of singular distributions. Our theoretical considerations are both illustrated on pedagogical examples, e.g., generalized devil staircases and fractional Brownian motions, and supported by numerical simulations. Recent applications of the wavelet transform modulus maxima method to experimental turbulent velocity signals at inertial range scales are compared to previous measurements based on the structure function approach. A similar analysis is carried out for the locally averaged dissipation and the validity of the Kolmogorov’s refined similarity hypothesis is discussed. To conclude, we elaborate on a wavelet based technique which goes further than a simple statistical characterization of the scaling properties of fractal objects and provides a very promising tool for solving the inverse fractal problem, i.e., for uncovering their construction rule in terms of a discrete dynamical system.

1. Introduction	246
2. The Multifractal Formalism	249
2.1. Fractal sets	249
2.1.1. Hausdorff dimension	249
2.1.2. Box dimension, capacity	249
2.2. Fractal measures	250
2.2.1. Spectrum of singularities	250
2.2.2. Generalized fractal dimensions	253
2.2.3. The multifractal formalism	254

2.3. Fractal functions	256
2.3.1. The concept of self-affinity.....	256
2.3.2. A first step towards a multifractal formalism for fractal functions: the structure function method	258
3. Singularity Detection and Processing with Wavelets	259
3.1. The continuous wavelet transform.....	259
3.1.1. Definitions	259
3.1.2. Inversion formula and reproducing kernel	260
3.1.3. Some examples of analyzing wavelets.....	261
3.2. Analysis of singularities with the continuous wavelet transform	262
3.2.1. Local regularity and Hölder exponents of a distribution.....	262
3.2.2. Wavelet analysis of local Hölder regularity	262
3.2.3. Detection and identification of singularities with the wavelet transform. Wavelet transform modulus maxima and maxima lines	263
4. A Multifractal Formalism for Distributions Based on Wavelets	265
4.1. Wavelet transform of multifractal measures.....	265
4.1.1. Wavelet analysis of the local scaling properties of singular measures.....	265
4.1.2. Wavelet transform and renormalization	267
4.2. The multifractal formalism for singular measures revisited with wavelets	274
4.3. Generalization of the multifractal formalism to fractal distributions: the wavelet transform modulus maxima method	276
5. Numerical and Experimental Applications of the Wavelet Transform Modulus Maxima Method	277
5.1. Generalized devil staircases	277
5.1.1. Deterministic and stochastic signals	277
5.1.2. The structure function approach versus the wavelet transform modulus maxima method	281
5.2. Non-everywhere-singular fractal functions	286
5.3. Brownian and turbulent signals	288
5.3.1. Fractional Brownian motions	288
5.3.2. Experimental velocity signals from fully developed turbulence data	290
6. Prospects: Solving the Inverse Fractal Problem from Wavelet Analysis	293
Acknowledgments	298
References	298

1. Introduction

Fractal and multifractal concepts [Mandelbrot, 1977, 1982; Halsey *et al.*, 1986; Paladin & Vulpiani, 1987] are now widely used to characterize multiscale phenomena that occur in a variety of physical situations [Stanley & Ostrowski, 1986, 1988; Pietronero & Tosatti, 1986; Guttinger & Dangelmayr, 1987;

Feder, 1988; Aharony & Feder, 1989; Vicsek, 1989; Family & Vicsek, 1991]. In its present form, the multifractal approach is essentially adapted to describe statistically the scaling properties of singular measures [Benzi *et al.*, 1984; Vul *et al.*, 1984; Halsey *et al.*, 1986; Badii, 1987; Collet *et al.*, 1987; Feingenbaum, 1987; Jensen *et al.*, 1987; Paladin & Vulpiani, 1987; Mandelbrot, 1989a; Rand, 1989].

Notable examples of such measures include the invariant probability distribution on a strange attractor [Halsey *et al.*, 1986; Collet *et al.*, 1987; Rand, 1989], the distribution of voltage drops across a random resistor network [Stanley & Ostrowski, 1986, 1988; Feder, 1988; Bunde & Havlin, 1991], the distribution of growth probabilities on the boundary of diffusion-limited aggregate [Feder, 1988; Meakin, 1988; Vicsek, 1989] and the spatial distribution of the dissipation field of fully developed turbulence [Mandelbrot, 1974; Paladin & Vulpiani, 1987; Frisch & Orszag, 1990; Meneveau & Sreenivasan, 1991]. The multifractal formalism involves decomposing fractal measures into interwoven sets which are characterized by their singularity strength α and their Hausdorff dimension $f(\alpha)$ [Halsey *et al.*, 1986]. The so-called $f(\alpha)$ singularity spectrum has been shown to be intimately related to the generalized fractal dimension D_q [Grassberger, 1983; Hentschel & Procaccia, 1983; Grassberger & Procaccia, 1984; Grassberger *et al.*, 1988]. Actually, there exists a deep analogy that links the multifractal formalism with statistical thermodynamics [Sinai, 1972; Bowen, 1975; Ruelle, 1978]. The variables q and $\tau(q) = (q-1)D_q$ play the same role as the inverse of temperature and the free energy in thermodynamics, while the Legendre transform $f(\alpha) = \min_q[q\alpha - \tau(q)]$ indicates that instead of the energy and the entropy, we have α and $f(\alpha)$ as the thermodynamic variables conjugated to q and $\tau(q)$ [Badii, 1987; Collet *et al.*, 1987; Feigenbaum, 1987; Bohr & Tél, 1988]. Most of the rigorous mathematical results concerning the multifractal formalism have been obtained in the context of dynamical system theory. It has recently been developed into a powerful technique accessible also to experimentalists. Successful applications have been reported in various fields and the pertinence of the multifractal approach seems, nowadays, to be well admitted in the scientific community at large.

However, in physics as well as in other applied sciences, fractals appear not only as singular measures, but also as singular functions. The examples range from plots of various kinds of random walks, e.g., Brownian signals [Mandelbrot & Van Ness, 1968; Peitgen & Saupe, 1987], to financial time series [Mandelbrot, 1967; Mandelbrot & Taylor, 1967; Li, 1991], to geologic shapes [Mandelbrot, 1977; Goodchild, 1980], to rough interfaces developing in far from equilibrium growth processes [Family & Vicsek, 1991], to turbulent velocity signals [Anselmet *et al.*, 1984; Gagne, 1987; Gagne *et al.*,

1988] and to DNA "walk" coding of nucleotide sequences [Peng *et al.*, 1992]. There have been several attempts to extend the concept of multifractality to singular functions [Frisch & Parisi, 1985; Barabási & Vicsek, 1991]. In the context of fully developed turbulence, the multiscaling properties of the recorded turbulent velocity signals have been investigated by calculating the moments $S_p(l) = \langle \delta v_l^p \rangle \sim l^{\zeta_p}$ of the probability density function of longitudinal velocity increments $\delta v_l(x) = v(x+l) - v(x)$ over inertial separation [Anselmet *et al.*, 1984; Gagne *et al.*, 1988]. By Legendre transforming the scaling exponents ζ_p of the structure functions S_p of order p , one expects to get the Hausdorff dimension $D(h) = \min_p(ph - \zeta_p + 1)$ of the subset of \mathbb{R} for which the velocity increments behave as $\delta v_l \sim l^h$ [Frisch & Parisi, 1985]. In a more general context, $D(h)$ will be defined as the spectrum of Hölder exponents for the singular signal under study and thus will have a similar status than the $f(\alpha)$ singularity spectrum for singular measures [Muzy, 1993]. But there are some fundamental limitations to the structure function approach which intrinsically fails to fully characterize the $D(h)$ singularity spectrum [Arneodo *et al.*, 1991; Muzy *et al.*, 1993a]. Actually, only the singularities of Hölder exponent $0 < h < 1$ are potentially amenable to this method (singularities in the derivatives of the signal are not identified). Moreover it has fundamental drawbacks which may introduce drastic bias in the estimate of the $D(h)$ singularity spectrum (e.g. divergencies in $S_p(l)$ for $p < 0$). Even though the structure function method was an interesting first step towards a multifractal theory of singular functions, this theory was still lacking and there was a need for an appropriate powerful technical tool to deal with fractal functions.

Our purpose here, is to elaborate on a novel strategy that we have recently proposed and which is likely to provide a practical way to determine the entire $D(h)$ singularity spectrum from any experimental signal [Arneodo *et al.*, 1991; Muzy *et al.*, 1991, 1993a, 1993b; Bacry *et al.*, 1993]. This approach is mainly based on the use of a mathematical tool introduced in signal analysis in the early eighties: the wavelet transform [Combes *et al.*, 1989; Lemarié, 1990; Meyer, 1990, 1992; Daubechies, 1992; Ruskai *et al.*, 1992; Meyer & Roques, 1993]. The wavelet transform (WT) has been recently emphasized as a very efficient technique to collect microscopic information about the scaling properties of multifractal measures [Arneodo *et al.*, 1988, 1989,

1990, 1992a; Holschneider, 1988a, 1988b; Argoul *et al.*, 1989a, 1990]. Extensive applications to various multifractal measures including the invariant measures of some well known discrete dynamical systems have clearly demonstrated the fascinating ability of this mathematical microscope to reveal the underlying hierarchy that governs the spatial distribution of the singularities. What makes the wavelet transform such an attractive tool in the present study is that its singularity scanning ability applies to any distribution including singular measures as well as singular functions [Holschneider, 1988a, 1988b; Jaffard, 1989, 1992; Holschneider & Tchamitchian, 1990; Arneodo *et al.*, 1991; Muzy *et al.*, 1991; Mallat & Hwang, 1992].

The simplest and classical way of performing a multifractal analysis of a singular measure is to partition its support using boxes of size ε [Halsey *et al.*, 1986; Grassberger *et al.*, 1988]. Then the measure in each ε -box can be characterized by a singularity strength α according to its scaling behavior $\mu_i(\varepsilon) \sim \varepsilon^{\alpha_i}$, where the index i denotes the box location. The number $N_\alpha(\varepsilon)$ of occurrences of a particular α defines the $f(\alpha)$ singularity spectrum: $N_\alpha(\varepsilon) \sim \varepsilon^{-f(\alpha)}$. Moreover, the generalized fractal dimensions $D_q = \tau(q)/(q-1)$ can be extracted from the power law behavior of the partition function $Z(q, \varepsilon) = \sum \mu_i^q(\varepsilon) \sim \varepsilon^{\tau(q)}$, in the limit $\varepsilon \rightarrow 0^+$. Since a wavelet can be seen as an oscillating variant of the characteristic function of a box (i.e., a “square” function), one can generalize in a rather natural way the multifractal formalism by defining some partition functions in terms of the wavelet coefficients [Arneodo *et al.*, 1991; Muzy *et al.*, 1991, 1993a, 1993b; Bacry *et al.*, 1993]. Let us note that by choosing a wavelet which is orthogonal to polynomial behavior up to order N , one can make the wavelet transform blind to regular behavior, remedying in this way one of the main failures of the classical approaches (box-counting method in the case of measures and structure function method in the case of functions). Then, from the Legendre transform of the scaling exponents $\tau(q)$ of these wavelet based partition functions, one can extract the whole $D(h)$ spectrum of Hölder exponents. At a given scale, instead of using a continuous integral over space (like in the structure function method), one sums discretely over the local maxima of the modulus of the wavelet transform so that, on the one hand the divergencies of the negative order moments are removed and on the other hand the multiplicative structure (if there is any) of the singularity

arrangement is directly incorporated into the calculation of the partition functions [Arneodo *et al.*, 1991; Muzy *et al.*, 1991]. According to Mallat & Hwang [1992], each connected line of local maxima is likely to emanate from a singularity of the considered signal. Along these maxima lines, the wavelet transform behaves, at small scales, as a power-law with an exponent $h(x)$ which is equal to the Hölder exponent of the signal at the point x . The number of such lines corresponding to the same h , defines the $D(h)$ singularity spectrum: $N(h) \sim a^{-D(h)}$ in the limit $a \rightarrow 0^+$. For a large class of fractal distributions, it can be rigorously established that the so-obtained $D(h)$ spectrum corresponds to the Hausdorff dimension of the set of singularities of Hölder exponent h .

The content of this tutorial paper is a detailed description of what is called the wavelet transform modulus maxima (WTMM) method and which is likely to be a good candidate to achieve a unified thermodynamical description of singular distributions including measures and functions. Moreover, beyond this statistical characterization of the scaling properties of fractal objects, one can hope to take further advantage of the wavelet transform microscope to address the fundamental issue of solving the inverse fractal problem. In many cases, the self-similarity properties of fractal objects can be expressed in terms of a dynamical system which leaves the object invariant. The inverse fractal problem consists in recovering this dynamical system (or its main characteristics) from the data. In this context, the wavelet transform modulus maxima can potentially be used to extract a one-dimensional map which accounts for its construction process [Arneodo *et al.*, 1993a, 1993b]. In a concluding section devoted to prospects, we will elaborate on a wavelet based tree matching algorithm which provides a very attractive alternative methodology to the approaches developed in the theory of iterated function systems (IFS) [Barnsley & Demko, 1985; Barnsley, 1988; Handy & Mantica, 1990].

The paper is organized as follows. Section 2 contains some background material on fractal sets, fractal measures and fractal functions. The foundations of the multifractal formalism, originally introduced for fractal measures, are described and some basic ingredients of the thermodynamics of fractals are discussed. In Sec. 3, we review some basic definitions concerning the one-dimensional continuous wavelet transform. We present the continuous wavelet transform as a mathematical

microscope which is well suited to scanning the singularities of fractal functions as well as singular measures. In Sec. 4, we revisit the multifractal formalism using the wavelet decomposition. We describe the WTMM method within the mathematical framework of the continuous wavelet transform and its modulus maxima representation. We emphasize the WTMM method as a natural generalization of the multifractal formalism to fractal distributions. Section 5 is devoted to numerical and experimental applications of the WTMM method. We illustrate our theoretical considerations on pedagogical examples including recursively generated fractal signals and fractional Brownian motions. We report on a systematic comparison between the structure function approach and the WTMM method which reveals the fundamental drawbacks and insufficiencies of the former approach. Further applications of the WTMM method to fully developed turbulence data are shown. They provide unambiguous quantitative evidence for the multifractal nature of a turbulent velocity signal at inertial range scales. We conclude in Sec. 6 with some perspectives for future research. A wavelet based tree matching algorithm is proposed as a very promising tool for solving the inverse fractal problem.

2. The Multifractal Formalism

2.1. Fractal sets

2.1.1. Hausdorff dimension

The usual notion of dimension of a set corresponds to the number of degrees of freedom, i.e., the number of parameters one has to use to indicate the position of a point in this set. The so-called *topological dimension* d_T takes only positive integer values. In the 19th century, the mathematician Peano [1973] builds a curve which uniformly “covers” the plane i.e., he gives a one-to-one map between a curve of topological dimension 1 and a set of topological dimension 2. Thus, the notion of topological dimension is not well adapted to this particular case. In 1919, Hausdorff [1919] suggests another definition of the dimension based on the generalization of the notion of length. The following definition has first been stated by Besicovitch [1935] (see also Falconer [1985] and Kahane [1985]).

Let S be a set in a metric space E (for the sake of simplicity, we will always consider $E = \mathbb{R}^n$). We

then define the Hausdorff measure of S , indexed by the parameter $\delta \in \mathbb{R}$, in the following way:

$$l_\delta(S) = \lim_{\varepsilon \rightarrow 0^+} l_{\delta, \varepsilon}(S), \quad (1)$$

where

$$l_{\delta, \varepsilon}(S) = \inf_{K(\varepsilon)} \sum_{B_i \in K(\varepsilon)} |B_i|^\delta, \quad (2)$$

and where the lower bound is taken over all the coverings $K(\varepsilon)$ of the set S made of balls $\{B_i\}_i$ of diameter smaller than ε . The *Hausdorff dimension* of S , $d_H(S)$, is then defined as the unique value of δ such that $l_\delta(S)$ is finite:

$$\begin{cases} \delta > d_H(S) \Rightarrow l_\delta(S) = 0, \\ \delta < d_H(S) \Rightarrow l_\delta(S) = +\infty. \end{cases} \quad (3)$$

Let us note that d_H can take noninteger values. The Hausdorff measure associated to the dimension d_H is l_{d_H} . It is a generalization of the Lebesgue measure (length, surface, volume, ...) in the sense that for any positive integer n , l_n is the Lebesgue measure in \mathbb{R}^n . Thus, in order to evaluate the relative “size” of two given sets, one just needs to compare their Hausdorff dimensions and, if they are equal, the values of their Hausdorff measures. Although the Hausdorff dimension is very well defined mathematically, it is generally hard to estimate numerically. To circumvent this difficulty, a more practical definition of the dimension of a set is generally used.

2.1.2. Box dimension, capacity

The *capacity* (also called the *box dimension*) has been introduced by Kolmogorov [1958]. Let S be a subset of \mathbb{R}^n and $K(\varepsilon)$ a covering of S with balls of size ε . Let $N(\varepsilon)$ be the number of balls in $K(\varepsilon)$. The capacity of S , $d_C(S)$, is then defined as the limit:

$$d_C(S) = \lim_{\varepsilon \rightarrow 0^+} \sup \frac{\ln N(\varepsilon)}{\ln(1/\varepsilon)}. \quad (4)$$

Thus the box dimension quantifies how the “size” of a set varies when one changes the unit measure. Like the Hausdorff dimension, it classifies sets according to their relative “dimensions.” However, let us note that it does not give any way of “measuring” (as we did with the Hausdorff measure) two sets with the same dimension.

In order to understand the differences between the three dimensions we have just defined (the topological dimension d_T , the Hausdorff dimension d_H

and the capacity d_C), we present below a list of sets for which we indicate their respective dimensions.

Examples

- The Hausdorff dimension and the capacity dimension of the empty set are equal: $d_H = d_C = -\infty$. In this particular case the topological dimension is not defined.
- For common sets such as a point, a segment, a surface, the Hausdorff dimension and the capacity are equal to the topological dimension which is respectively 0, 1 and 2. Actually, one can prove that these three dimensions are equal for any differentiable manifold.
- Let us consider the triadic Cantor set. This set is constructed in the following way: the segment $[0, 1]$ is divided into three parts of equal length and the middle part is taken out. Then, we repeat the same process on the two remaining sub-segments and so on recursively. The limit set so obtained is called the *triadic Cantor set* [Falconer, 1985]. An illustration of its construction process is shown in Fig. 1. Let us note that it is a closed set whose interior is empty and which is only made of nonisolated points. At the step n of the construction process, the set is made of 2^n intervals of equal length 3^{-n} : its total length is $(2/3)^n$. Thus, the Lebesgue measure of the triadic Cantor set obtained when $n \rightarrow +\infty$ is 0, and its topological dimension is $d_T = 0$. Let us consider the covering corresponding to the step n of the construction process. As we already pointed out, it is made of $N(\varepsilon) = 2^n$ intervals of size $\varepsilon = 3^{-n}$. When ε goes to 0 (i.e., $n \rightarrow +\infty$), one thus deduces that the capacity of the triadic Cantor set is $d_C = \ln 2 / \ln 3$. The Hausdorff dimension can be obtained in a similar way [Falconer, 1985] and is found to be the same as d_C . The triadic Cantor set is then characterized by the following dimensions:

$$d_T = 0; \quad d_H = d_C = \frac{\ln 2}{\ln 3}. \quad (5)$$

Let us note that in the former examples the different dimensions verified

$$d_T \leq d_H = d_C. \quad (6)$$

Actually, one can prove [Farmer et al., 1983] that:

$$d_T \leq d_H \leq d_C. \quad (7)$$

A classical example for which $d_H < d_C$ is the set of all the rational numbers in $[0, 1]$. As it is dense in

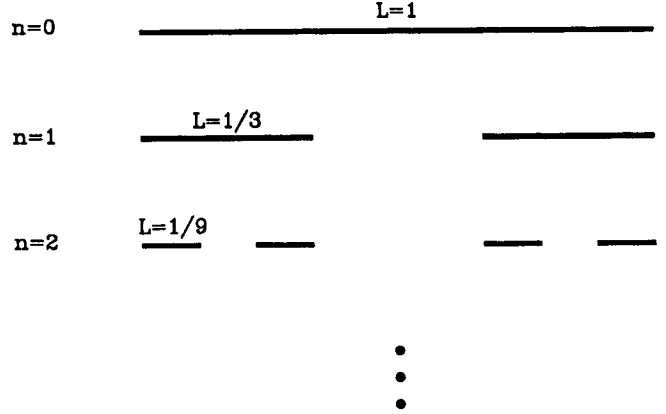


Fig. 1. The construction process of the triadic Cantor set.

$[0, 1]$, the capacity is $d_C = 1$. However the Hausdorff dimension is equal to the topological dimension which is 0.

A definition of a fractal set. Originally Mandelbrot [1977, 1982] suggested that a fractal set should be defined as a set whose Hausdorff dimension is strictly greater than its topological dimension. Even though this definition is adequate for a lot of sets, there exists a whole class of sets (of the same type as the triadic Cantor set) whose Lebesgue measure is finite and thus whose Hausdorff dimension is $d_H = 1$. These sets, which are generally referred to as *fat fractals* [Farmer, 1984], are not fractal sets according to the latter definition. Thus, along with Mandelbrot [Mandelbrot, 1988, 1989b; Evertsz & Mandelbrot, 1992], we will rather say that a *fractal set* is a set which has some self-similar properties in the sense that its singular structure is the same at any scale. In other words, the set is invariant (either in a deterministic or in a statistical sense) by the iterative action of some elementary similitudes. This definition is much wider than the one based on the Hausdorff dimension and, as we will see later on, can be applied to a larger class of objects such as measures and functions.

2.2. Fractal measures

2.2.1. Spectrum of singularities

The concept of fractal measure first appeared in the works by Mandelbrot [1974] on the spatial distribution of dissipative regions in turbulent flows. Since, this new concept has proved very fruitful for modelling singular objects arising in a variety of phys-

ical situations. It has notably been developed in the framework of dynamical systems by Grassberger [1983], Hentschel & Procaccia [1983] and Grassberger & Procaccia [1984]. The term “multifractal” and the concept of singularity spectrum have first been introduced by Frisch & Parisi [1985] in the context of fully developed turbulence, and formalized by Halsey *et al.* [1986] who made the link with the original works mentioned above.

A measure assigns weights to different parts of a set. It could represent, for instance, a distribution of charge or of mass, the distribution of energy in a turbulent flow or of course any probability distribution such as equilibrium measures in statistical physics or invariant measures of dynamical systems. In many cases, a measure μ on \mathbb{R} can be described by its density $\rho(x) = \lim_{\varepsilon \rightarrow 0^+} \mu([x, x+\varepsilon])/\varepsilon$. However, a point charge in electrostatic theory represented as a Dirac distribution $\delta(x)$ does not correspond to any density function. A measure which cannot be expressed in terms of either a density function or a sum of Dirac distributions is called a *singular measure*. An example of such a measure is the Hausdorff measure $l_{\ln 2/\ln 3}$ on the triadic Cantor set [Eq. (1)].

In the same way the Hausdorff (or capacity) dimension is used to describe sets whose Lebesgue measure (in \mathbb{R}) is 0 and which are made of nonisolated points, the *f(α) singularity spectrum* gives a characterization of singular measures which do not have any density component [Farmer *et al.*, 1983; Halsey *et al.*, 1986; Grassberger *et al.*, 1988; Mandelbrot, 1988, 1989b]. For the sake of simplicity, we will work exclusively in \mathbb{R} and we will use indifferently the words “interval,” “ball” or “box.”

Definition 1. Let μ be a measure on \mathbb{R} and $\text{Supp } \mu$ its support.

- We call *singularity exponent* at the point $x_0 \in \text{Supp } \mu$, the limit:

$$\alpha(x_0) = \lim_{\varepsilon \rightarrow 0^+} \frac{\ln \mu(B_{x_0}(\varepsilon))}{\ln \varepsilon}, \quad (8)$$

where $B_{x_0}(\varepsilon)$ is the ball centered at x_0 and of size ε . Let us note that when this limit does not exist, one can use either a limsup or a liminf in the above equation.

- The *f(α) singularity spectrum* of a measure μ associates with any given α , the Hausdorff dimension of the set of all the points x_0 such that $\alpha(x_0) = \alpha$:

$$f(\alpha) = d_H(\{x_0 \in \text{Supp } \mu, \alpha(x_0) = \alpha\}). \quad (9)$$

The *support of the f(α) singularity spectrum* is the set of all α values for which $f(\alpha) \neq -\infty$

The exponent $\alpha(x_0)$ represents the singularity “strength” of the measure μ at x_0 . Indeed, if μ is singular, $\mu(B_{x_0}(\varepsilon))$ does not correspond to any density function, therefore it cannot be written as $\rho(x_0)\varepsilon$; according to the definition (8) of $\alpha(x_0)$, it can be expressed as

$$\mu(B_{x_0}(\varepsilon)) \sim C\varepsilon^{\alpha(x_0)}. \quad (10)$$

The smaller the exponent $\alpha(x_0)$, the more singular the measure μ around x_0 and the “stronger” the singularity. The limit $\alpha = 0$ corresponds to a behavior similar to a Dirac distribution at x_0 . Let us note that C in Eq. (10) can be a function of ε which varies slower than any power of ε . The singularity spectrum describes the statistical distribution of the singularity exponents $\alpha(x)$. If we cover the support of the measure μ with balls of size ε , the number of such balls that scale like ε^α for a given α is [Halsey *et al.*, 1986; Mandelbrot, 1988, 1989b]:

$$N_\alpha(\varepsilon) \sim \varepsilon^{-f(\alpha)}. \quad (11)$$

Thus, $f(\alpha)$ describes how the “histogram” $N_\alpha(\varepsilon)$ varies when ε goes to 0. Let us illustrate this concept on two examples.

Examples

- Let μ be a uniformly distributed measure on the triadic Cantor set. One can cover this set by 2^n disjointed intervals of size $\varepsilon = 3^{-n}$ (the same ones as the ones obtained at the step n of the construction process in Fig. 1). Each of these intervals $B_{x_i}(\varepsilon)$ has a mass $\mu(B_{x_i}(\varepsilon)) = 2^{-n}$, thus we get $\ln \mu(B_{x_i}(\varepsilon))/\ln \varepsilon = \ln 2/\ln 3$. In the limit $\varepsilon \rightarrow 0^+$, each point of the Cantor set will correspond to the same singularity exponent $\alpha(x) = \ln 2/\ln 3$. Moreover, the Hausdorff dimension of the Cantor set is $\ln 2/\ln 3$. The support of the singularity spectrum of the measure μ thus reduces to a single point $f(\alpha = \ln 2/\ln 3) = \ln 2/\ln 3$.
- Let us consider a nonsingular measure $\mu(A) = \int_A \rho(x)dx$. Generically, for all x in the support of μ , we have $\alpha(x) = 1$. Since the Lebesgue measure of the support of μ is not zero, its Hausdorff dimension is 1. Thus, the singularity spectrum of this nonsingular measure is $f(\alpha) = -\infty$ for $\alpha \neq 1$ and $f(1) = 1$. The support of $f(\alpha)$ is a single point.

Remark. Let us point out that, as a direct consequence of the example just above, the $f(\alpha)$ singularity spectrum fails to account for singularities of exponent $\alpha > 1$ as soon as some density component is present in the measure.

The first example corresponds to a singularity spectrum whose support is a single point $(\alpha_0, f(\alpha_0))$: only one “sort” of singularity is found in the measure. Such measures are called *homogeneous measures* [Mandelbrot, 1977, 1982, 1988; Halsey *et al.*, 1986; Tél, 1988]. Let us note that for this type of measures, the relation $f(\alpha_0) = \alpha_0$ is always true. Indeed, if we cover the support of μ with $N(\varepsilon)$ disjointed balls of size ε : $\{B_i(\varepsilon)\}_{i=1 \dots N(\varepsilon)}$, we have

$$\mu(\text{Supp } \mu) = \sum_{i=1}^{N(\varepsilon)} \mu(B_i(\varepsilon)) = 1. \quad (12)$$

Moreover, as μ is homogenous of exponent α_0 , we get

$$\mu(\text{Supp } \mu) \sim N(\varepsilon) \varepsilon^{\alpha_0} \sim \varepsilon^{-f(\alpha_0)} \varepsilon^{\alpha_0}, \quad (13)$$

and thus $f(\alpha_0) = \alpha_0$.

However, there exist nonhomogeneous measures, i.e., measures whose singularity spectrum is supported by more than a single point. One can build such a measure on the triadic Cantor set in the following way: at the step $n = 0$ of the construction process, we associate the weight $\mu_0 = 1$ to the interval $[0, 1]$. At step $n = 1$, μ_0 is distributed on the two subintervals: $\mu_1 = p_1 \mu_0$ for the interval $[0, 1/3]$ and $\mu_2 = p_2 \mu_0 = (1 - p_1) \mu_0$ to the interval $[2/3, 1]$. We then repeat recursively this process: μ_1 (resp. μ_2) is distributed in two parts $p_1 \mu_1$ (resp. $p_1 \mu_2$) and $p_2 \mu_1$ (resp. $p_2 \mu_2$) and so on. The same weights p_1 and p_2 are used at each step. Clearly the so obtained measure is not homogeneous, i.e., it involves singularities of different strengths α . Indeed, let us consider at each step n the first interval on the left side $B_1(\varepsilon = 3^{-n}) = [0, 1/3^n]$. This interval always contains $x_0 = 0$ and is such that $\mu(B_1) = p_1^n \mu_0 = p_1^n$. Thus, the singularity exponent of the measure μ at the point $x_0 = 0$ is $\alpha(0) = \ln p_1 / \ln(1/3)$. In a similar way, by considering the last interval on the right side $B_{2^n}(\varepsilon = 3^{-n})$, one can prove that the singularity exponent at the point $x_0 = 1$ is $\alpha(1) = \ln p_2 / \ln(1/3)$. As we chose $p_1 \neq p_2$ then $\alpha(0) \neq \alpha(1)$. Moreover, one can prove that there exist a “lot” of points corresponding to the singularity exponent $\alpha(0)$ [respectively

$\alpha(1)$]. Thus the corresponding Hausdorff dimensions $f(\alpha(0))$ and $f(\alpha(1))$ are both different from $-\infty$ and therefore the support of the singularity spectrum is not reduced to a single point. Actually one can prove that the support of $f(\alpha)$ is a whole interval $[\alpha_{\min}, \alpha_{\max}]$ where $\alpha_{\min} = \min\{\alpha(0), \alpha(1)\}$ and $\alpha_{\max} = \max\{\alpha(0), \alpha(1)\}$. Moreover $f(\alpha_{\min}) = f(\alpha_{\max}) = 0$ and $f(\alpha)$ is a single humped curve whose maximum is $f(\alpha_M) = d_H = \ln 2 / \ln 3$. Figure 2(a) illustrates the construction process of this measure. The singularity spectrum for $p_1 = 0.6$ and $p_2 = 0.4$ is displayed in Fig. 2(b). This spectrum can be computed analytically [Halsey *et al.*, 1986]: each point of the triadic Cantor set can be addressed by an infinite sequence of symbols L and R according to the successive choice of the left (L) or the right (R) subinterval at each construction step. The $f(\alpha)$ singularity spectrum is then obtained by

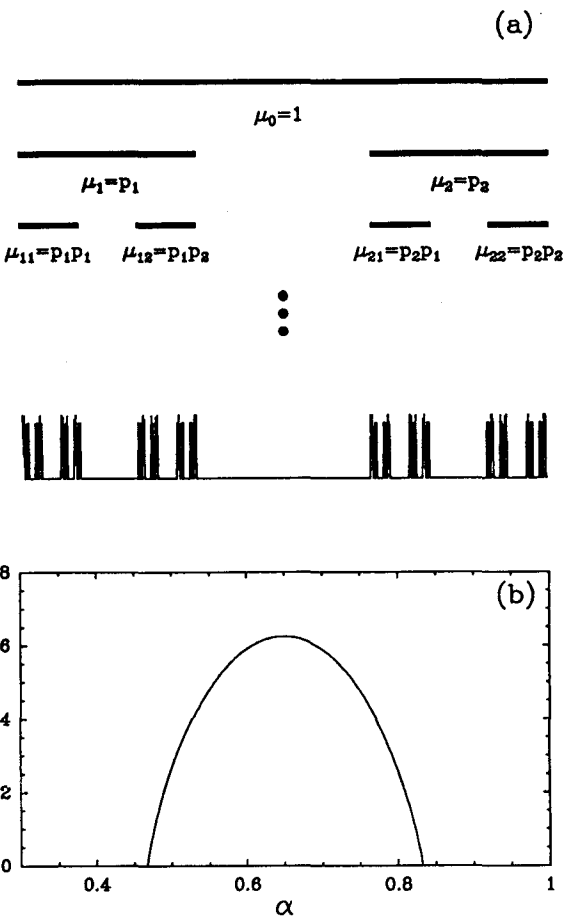


Fig. 2. Binomial measure distributed on the triadic Cantor set with the weights $p_1 = 0.6$ and $p_2 = 0.4$. (a) Construction rule. (b) $f(\alpha)$ singularity spectrum. The support of the singularity spectrum is a whole interval; therefore the measure μ is not homogeneous.

counting the number of symbolic sequences such that the ratio of the numbers of symbols L and R converges to a given value; these sequences correspond to a same singularity α .

But generally, one cannot compute analytically the singularity spectrum of any given measure. One must then define a numerical algorithm for computing singularity spectra. The most natural way would be to use directly Eqs. (8) and (9): one first scans the support of μ measuring $\alpha(x)$ at each point x by estimating the slope of the curve $\log \mu(B_x(\varepsilon))$ as a function of $\log \varepsilon$; then one computes the fractal dimension $f(\alpha)$ by using the *box counting method* corresponding to Eq. (4). However, such a method would lead to dramatic errors since, for any ε , $\mu(B_x(\varepsilon))$ takes into account a lot of points with very different singularity exponents; the estimate of $\alpha(x)$ on a finite range of scales is thus extremely unstable. One can use a slightly different method called the *histogram method* [Arneodo *et al.*, 1987; Badii & Broggi, 1988; Grassberger *et al.*, 1988]. It consists in covering the support of the measure μ with balls $\{B_i(\varepsilon)\}_i$ of size ε . For each ball $B_i(\varepsilon)$, we define the exponent $\alpha_i(\varepsilon) = \ln \mu(B_i(\varepsilon))/\ln \varepsilon$. This exponent is like a singularity exponent “seen” at the scale ε . Then if $N_\alpha(\varepsilon)$ is the histogram of the values $\{\alpha_i(\varepsilon)\}_i$, $f(\alpha)$ can be computed using the following relation:

$$N_\alpha(\varepsilon) \sim \varepsilon^{-f(\alpha)}. \quad (14)$$

Even though this method is stable under certain conditions, the convergence when ε goes to 0^+ is very slow [Grasseau, 1989]. In most cases, the range of scales available in the numerical data is too small and the histogram method leads to very approximate results because of scale dependent prefactors. Basically, this is due to the fact that this method is based on the computation of scaling exponents which represent “local” quantities that can vary a lot from one point to another. In the next paragraph, we present the multifractal formalism which uses the generalized fractal dimensions of a measure as intermediate “global” quantities from which one can compute the $f(\alpha)$ singularity spectrum.

2.2.2. Generalized fractal dimensions

Let μ be a measure on \mathbb{R} , $K(\varepsilon)$ a covering of the support of μ with intervals of size ε and $N(\varepsilon)$ the number of intervals in $K(\varepsilon)$, i.e., $K(\varepsilon) = \{B_i(\varepsilon)\}_{i=1 \dots N(\varepsilon)}$. Let $\mu_i(\varepsilon) = \int_{B_i(\varepsilon)} d\mu$. For all

$q \in \mathbb{R}$, we consider the *partition function*:

$$\mathcal{Z}(q, \varepsilon) = \sum_{i=1}^{N(\varepsilon)} \mu_i^q(\varepsilon). \quad (15)$$

We then define the $\tau(q)$ spectrum from the power law scaling behavior of $\mathcal{Z}(q, \varepsilon)$ when $\varepsilon \rightarrow 0^+$:

$$\mathcal{Z}(q, \varepsilon) \sim \varepsilon^{\tau(q)}. \quad (16)$$

The spectrum of *generalized fractal dimensions* D_q is obtained from the spectrum $\tau(q)$ [Grassberger, 1983; Hentschel & Procaccia, 1983; Grassberger & Procaccia, 1984]:

$$D_q = \frac{\tau(q)}{(q-1)}. \quad (17)$$

Let us note that the notion of generalized fractal dimensions has first been introduced in the dynamical system theory to characterize an ergodic measure associated to a given dynamical system. The capacity [Eq. (4)] of the support of μ corresponds to D_0 , whereas D_1 characterizes the scaling behavior of the information $I(\varepsilon) = \sum_i \mu_i(\varepsilon) \ln \mu_i(\varepsilon)$: it is called the *information dimension* [Renyi, 1970]. Moreover, for $q \geq 2$, the D_q 's can be related to the q -point correlation integrals [Grassberger, 1983; Grassberger & Procaccia, 1983, 1984; Hentschel & Procaccia, 1983].

The spectrum $\tau(q)$ is a “global” quantity which describes the behavior of the “mean” value $\mathcal{Z}(q, \varepsilon)$. Thus, it is likely that a “ $\tau(q)$ -based” method for computing $f(\alpha)$ will be much more stable than any “ α -based” method such as the histogram method. Let us see how one can relate the $f(\alpha)$ singularity spectrum to the $\tau(q)$ spectrum. At the scale ε , if we consider that the distribution of the α 's is of the form $\rho(\alpha) \varepsilon^{-f(\alpha)}$ and if we use this expression in Eq. (15), it follows [Frisch & Parisi, 1985; Halsey *et al.*, 1986] that

$$\mathcal{Z}(q, \varepsilon) \simeq \int \rho(\alpha) \varepsilon^{q\alpha - f(\alpha)} d\alpha. \quad (18)$$

In the limit $\varepsilon \rightarrow 0^+$, this sum is dominated by the term $\varepsilon^{\min_\alpha(q\alpha - f(\alpha))}$. Then, from the definition of $\tau(q)$, we obtain

$$\tau(q) = \min_\alpha(q\alpha - f(\alpha)). \quad (19)$$

Thus the $\tau(q)$ spectrum is obtained by Legendre transforming the $f(\alpha)$ singularity spectrum. By inverting this transformation one gets

$$f(\alpha) = \min_q(q\alpha - \tau(q)). \quad (20)$$

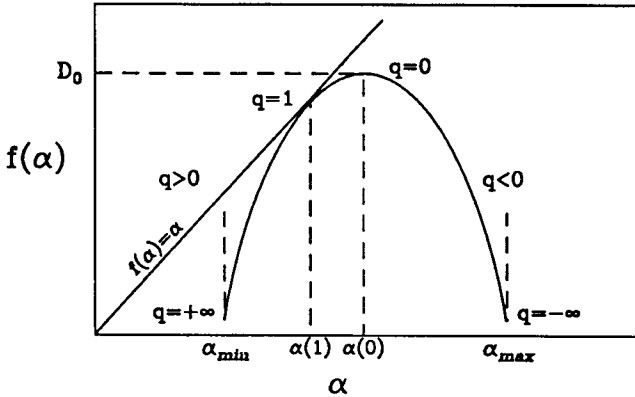


Fig. 3. Generic shape of the $f(\alpha)$ singularity spectrum considered as the Legendre transform of $\tau(q)$ [Eq. (20)].

One can thus compute the $f(\alpha)$ singularity spectrum from the scaling exponents $\tau(q)$ of the partition functions $Z(q, \varepsilon)$. In the case $\tau(q)$ is a continuously differentiable function, the relation (19) can be rewritten in the following way:

$$\begin{cases} q = df/d\alpha, \\ \tau(q) = q\alpha - f(\alpha). \end{cases} \quad (21)$$

In the same way, Eq. (20) becomes:

$$\begin{cases} \alpha = d\tau/dq, \\ f(\alpha) = q\alpha - \tau(q). \end{cases} \quad (22)$$

Let us study these last equations for some particular values of q (Fig. 3).

- For $q = 0$, by using both the definitions of $\tau(q)$ [Eq. (16)] and of D_q [Eq. (17)], one gets from Eq. (21):

$$-\tau(0) = D_0 = d_C(\text{Supp } \mu) = \max_{\alpha} f(\alpha). \quad (23)$$

Thus the fractal dimension of the support of the measure corresponds to the maximum of the $f(\alpha)$ curve. By definition of f , one can deduce that the value $\alpha(q = 0)$ corresponding to $f(\alpha(q = 0)) = \max_{\alpha} f(\alpha) = D_0$ is the most “frequent” singularity.

- For $q = 1$, Eq. (19) becomes $\tau(1) = \min_{\alpha} (\alpha - f(\alpha)) = \alpha(q = 1) - f(\alpha(q = 1))$. Moreover, we know from the definition of τ (Eq. (16)) that $\tau(1) = 0$ ($\sum \mu_i(\varepsilon) = 1$). We thus get $f(\alpha(q = 1)) = \alpha(q = 1)$. The singularity spectrum $f(\alpha)$ stands below the diagonal $f(\alpha) = \alpha$ and reaches it for $\alpha = \alpha(q = 1)$. Let us note that if f is

differentiable at $\alpha = \alpha(q = 1)$, then $df/d\alpha = 1$ [Eq. (21)] and thus $f(\alpha)$ is tangent to the diagonal at $\alpha(1)$.

- For $q = \pm\infty$, one can deduce from Eqs. (17) and (19) that:

$$D_{+\infty} = \alpha_{\min}; \quad D_{-\infty} = \alpha_{\max}. \quad (24)$$

Thus, in these limits, the D_q spectrum directly gives the strongest and the weakest singularity exponents that respectively characterize the densest and the most rarefied regions of the support of μ . Moreover, Eq. (21) shows that the tangent of $f(\alpha)$ at α_{\min} and α_{\max} are vertical. If $f(\alpha)$ is C^2 , Eq. (19) implies that $d^2f/d^2\alpha < 0$ for all values of α , thus f is convex.

2.2.3. The multifractal formalism

The *multifractal formalism* is the framework in which we consider the $f(\alpha)$ singularity spectrum as the Legendre transform of the $\tau(q)$ spectrum. It is represented by Eqs. (15), (16), (17) and (20). In this context, it has been proved that $f(\alpha)$ has a generic single humped shape as shown in Fig. 3.

Let us illustrate this formalism on two specific examples.

Examples

- Let μ be the homogenous measure lying on the triadic Cantor set. We saw in the last section that the singularity spectrum of this measure is $f(\alpha) = \alpha = \ln 2/\ln 3$. The spectrum $\tau(q)$ can be easily obtained by considering the covering $K(\varepsilon)$ with intervals of size $\varepsilon = 3^{-n}$, corresponding to the step n of the construction process of the measure μ . From Eqs. (15) and (16), we get, in the limit $n \rightarrow +\infty$,

$$\tau(q, \varepsilon) = 2^{-n(q-1)} \sim 3^{-n\tau(q)}, \quad (25)$$

which yields $\tau(q) = (q-1)\ln 2/\ln 3$. The spectrum $\tau(q)$ is a linear function whose slope is the singularity exponent characterizing the homogeneous measure μ . Let us note that we could have obtained this result directly by Legendre transforming $f(\alpha)$. The spectrum of the generalized fractal dimensions is independent of q :

$$D_q = \frac{\tau(q)}{(q-1)} = d_C(\text{Supp } \mu) = \frac{\ln 2}{\ln 3}. \quad (26)$$

The fact that the generalized fractal dimensions are all equal to the box (or Hausdorff) dimension

[i.e., the $\tau(q)$ spectrum is linear] characterizes the homogeneity of the measure. Both $\tau(q)$ and D_q spectra are displayed in Figs. 4(a) and 4(b) respectively.

- Let us now consider a nonhomogeneous measure lying on the triadic Cantor set such as the binomial measure described in Sec. 2.2.1 (Fig. 2). It is characterized by two parameters p_1 and p_2 which represent the distribution factors of the weight at each step of the construction process. By considering again the same covering $K(\varepsilon)$ made of intervals of size $\varepsilon = 3^{-n}$, one gets

$$\begin{aligned} \mathcal{Z}(q, \varepsilon) &= (p_1^n)^q + C_n^1(p_1^{n-1}p_2)^q + \dots \\ &\quad + C_n^{n-1}(p_1p_2^{n-1})^q + (p_2^n)^q \\ &= (p_1^q + p_2^q)^n. \end{aligned} \quad (27)$$

The behavior of $\mathcal{Z}(q, \varepsilon)$ when ε goes to 0^+ (i.e., $n \rightarrow +\infty$) leads to the following expression for the exponents $\tau(q)$:

$$\tau(q) = \frac{\ln(p_1^q + p_2^q)}{\ln(1/3)}. \quad (28)$$

The $\tau(q)$ and D_q spectra are displayed in Figs. 4(a) and 4(b) respectively. Let us note that $\tau(q)$ is no longer linear and that D_q is a decreasing function from $D_{-\infty} = \alpha_{\max} = -\ln p_2 / \ln 3$ to $D_{+\infty} = \alpha_{\min} = -\ln p_1 / \ln 3$. The Legendre transform relation [Eq. (20)] between $\tau(q)$ and $f(\alpha)$ can be checked analytically for this particular example [Halsey *et al.*, 1986; Mandelbrot, 1988; Tél, 1988].

A definition of a fractal measure. Actually, there exists a deep analogy that links the multifractal formalism with that of thermodynamics [Badii, 1987; Collet *et al.*, 1987; Feigenbaum, 1987; Bohr & Tél, 1988; Rand, 1989]. The variables q and $\tau(q)$ play the same role as the inverse of temperature and the free energy in thermodynamics, while the Legendre transform [Eq. (20)] indicates that instead of energy and entropy, we have α and $f(\alpha)$ as the thermodynamics variables conjugate to q and $\tau(q)$. This thermodynamic formalism has been worked out in the context of dynamical system theory [Sinai, 1972; Bowen, 1975; Ruelle, 1978]. But rigorous proofs of the above connection have been limited to some restricted classes of singular measures, e.g., the invariant measures of some expanding Markov maps (“cookie-cutter” Cantor sets) on an interval or a circle and the invariant measures associated to the

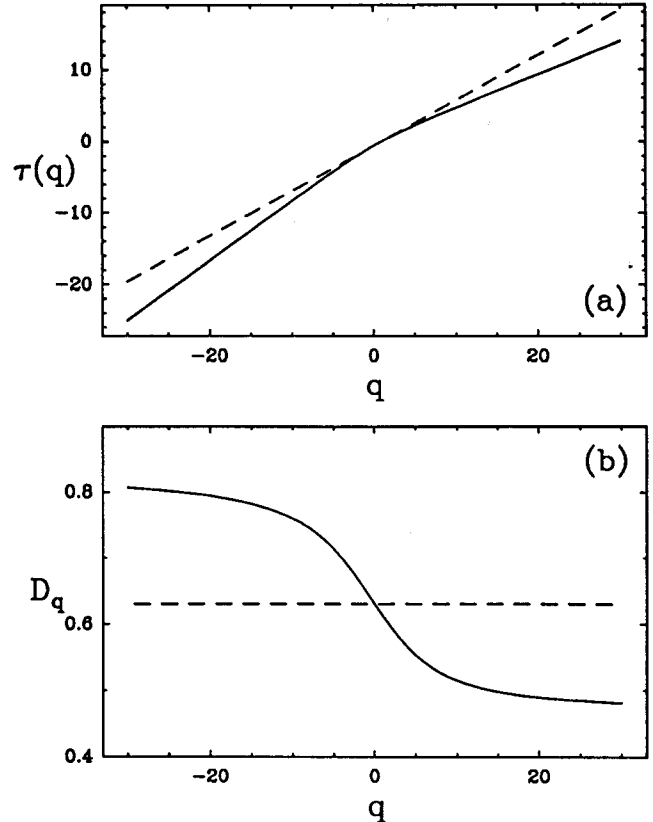


Fig. 4. $\tau(q)$ and D_q spectra for a homogeneous (---) and a binomial nonhomogeneous (—) measure lying on the triadic Cantor set. (a) $\tau(q)$ spectrum. (b) Generalized fractal dimensions D_q .

dynamical systems for period doubling and to critical circle mappings with golden rotation number [Collet *et al.*, 1987; Rand, 1989]. Nevertheless, successful applications of this thermodynamical formalism have been reported for singular measures which appear beyond the scope of dynamical systems [Paladin & Vulpiani, 1987; Feder, 1988; Vicsek, 1989]. Therefore, the generalized fractal dimensions D_q and the $f(\alpha)$ singularity spectrum are thermodynamical functions, i.e., statistical averages that provide macroscopic (global) information about the scaling properties of singular measures that are self-similar. In the same spirit as for fractal sets, we will thus define a *fractal measure* as a measure which is invariant (either in a deterministic or in a statistical sense) by the iterative action of some elementary similitudes. We will call a *multifractal measure* a fractal measure which is not homogeneous. Let us note that this analogy with thermodynamics provides a very attractive understanding of the phase transition phenomena sometimes observed in the scaling properties

of fractal measures [Badii, 1987; Cvitanovic, 1987; Grassberger *et al.*, 1988].

2.3. Fractal functions

2.3.1. The concept of self-affinity

Generically, the self-similarity properties of fractal sets and fractal measures induce some very intricate singular behavior. The spatial distribution of these singularities has been studied via the multifractal formalism. One could think of using the same kind of methods in order to study very irregular functions such as rough surfaces, stock exchange data, 1D component of the velocity in a turbulent flow, signals obtained from spectroscopy, $1/f$ noise ... [Mandelbrot, 1977, 1982; Pietronero & Tosatti, 1986; Stanley & Ostrowski, 1986, 1988; Feder, 1988; Aharony & Feder, 1989; Vicsek, 1989; Family & Vicsek, 1991], i.e., functions that do not have any characteristic scale and which are highly singular. These functions can be qualified as *fractal functions* in the sense that their graphs are fractal sets in \mathbb{R}^2 (we will only consider functions from \mathbb{R} to \mathbb{R}).

The *self-affinity property* characterizes the (fractal) sets which are invariant under affine transformations [Mandelbrot, 1982; Peitgen & Saupe, 1987; Voss, 1987, 1989; Dubuc *et al.*, 1989; Edgar, 1990]. In \mathbb{R}^2 , it means that the considered set is similar to itself when transformed by anisotropic dilations. A particular case of self-affinity is self-similarity which implies isotropic transformations. We will say that a function is self-affine when its graph is a self-affine set. We have displayed in Fig. 5(a) the graph of a Brownian motion $B_{1/2}(t)$ which is a typical self-affine function (in a statistical sense though) [Levy, 1965; Mandelbrot, 1982; Voss, 1987, 1989]. Figure 5(b) represents an isotropic zoom of a small part of Fig. 5(a); it is clearly not “similar” to the initial figure. On the other hand, Fig. 5(c) represents an anisotropic zoom by a factor of λ in the abscissa direction and of $\lambda^{-1/2}$ in the ordinate direction; the similarity with Fig. 5(a) appears clearly.

If $f(x)$ is a self-affine function then, $\forall x_0 \in \mathbb{R}$, $\exists H \in \mathbb{R}$ such that for any $\lambda > 0$, one has

$$f(x_0 + \lambda x) - f(x_0) \simeq \lambda^H (f(x_0 + x) - f(x_0)), \quad (29)$$

If f is a stochastic process, the identity holds in law for fixed λ and x_0 . The exponent H is called the *Hurst exponent* [Mandelbrot, 1977, 1982; Feder, 1988]. The graph of the function is self-similar only if the Hurst exponent is $H = 1$ (the graph is then

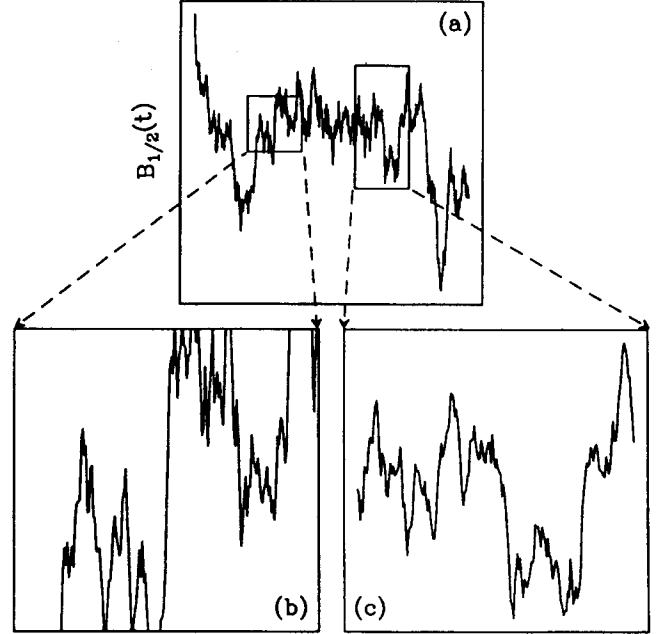


Fig. 5. Self affinity of the graph of a Brownian realization. (a) Graph of a realization of the Brownian motion $B_{1/2}(t)$. (b) Isotropic zoom of a part of the graph of $B_{1/2}(t)$. (c) Zoom with a factor λ in the t direction and with $\lambda^{-1/2}$ in the direction of $B_{1/2}(t)$.

invariant under some isotropic dilations). Let us note that if $H < 1$, then f is not differentiable and that the smaller the exponent H , the more singular f . The Hurst exponent indicates how irregular the function f is. Let us present some “classical” examples of self-affine functions.

Examples

- Let us consider the triadic Cantor set (introduced in Sec. 2.1) and μ the homogeneous measure on this set. We define $f : [0, 1] \rightarrow [0, 1]$ as the distribution function of μ , i.e.,

$$f(x) = \mu([0, x]) = \int_0^x d\mu, \quad x \in [0, 1]. \quad (30)$$

This function is displayed in Fig. 6(a). It is almost everywhere constant on $[0, 1]$ and looks like a staircase whose “steps” are uncountable and infinitely small. The so defined function f is called the *devil staircase* [Mandelbrot, 1977, 1982]. By definition, μ is invariant under the map $T(x)$ defined by $T|_{[0,1/3]}(x) = T_1(x) = 3x$ and $T|_{[2/3,1]}(x) = T_2(x) = 3x - 2$, i.e., for all interval A , $\mu(T^{-1}(A)) = \mu(A)$. Moreover $\mu(A) = 2\mu(T_1^{-1}(A)) = 2\mu(T_2^{-1}(A))$. Thus if $A = [0, x]$,

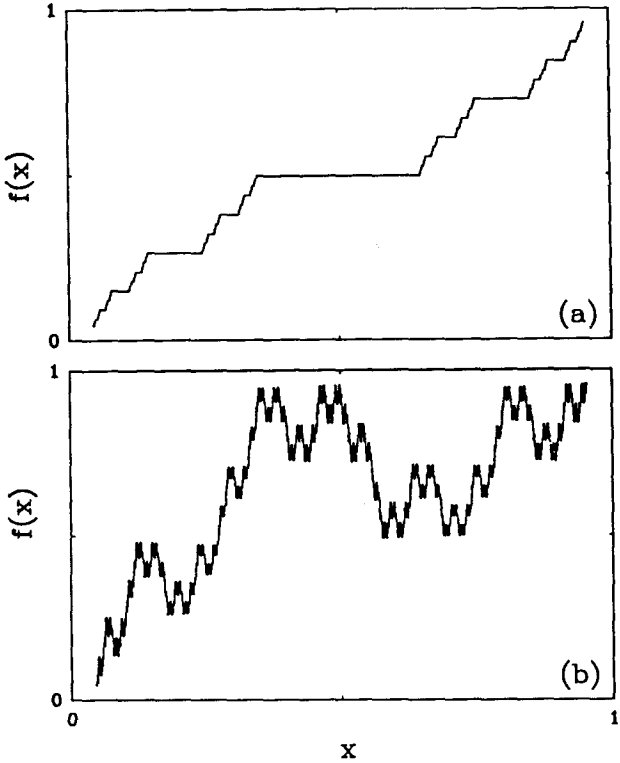


Fig. 6. Generalized devil staircases. (a) Devil staircase associated with the triadic Cantor set. (b) Distribution function of the signed measure recursively distributed on $[0, 1]$ with the weights $p_1 = p_2 = p_4 = -p_3 = 1/2$.

we get $f(x) = \mu(A) = 2\mu(T_1^{-1}(A)) = 2f(x/3)$ and then $f(\lambda x) = \lambda^{\ln 2/\ln 3} f(x)$. The Hurst exponent of f is the fractal dimension of the triadic Cantor set $H = \ln 2/\ln 3$.

- One can generalize the above construction to a nonhomogeneous measure lying on a “generalized” Cantor set. For instance, at the first step of construction, we divide the interval $[0, 1]$ into four subintervals of equal length but of different weights p_1, p_2, p_3 and p_4 . We then repeat the same operation recursively *ad infinitum*: at each step we distribute the former weights on four subintervals of the same size and using the same distribution weights p_i ($i = 1, 2, 3$ and 4). We can choose any real value for each p_i (positive or negative); the only constraint for convergence is that $\sum_i p_i = 1$. The so-obtained object is a “signed” measure μ whose distribution function $f(x) = \mu([0, x])$ is a self-affine function. This type of functions will be referred to as *generalized devil staircases*. We illustrate its construction for $p_1 = p_2 = p_4 = 1/2$ and $p_3 = -1/2$. The corresponding everywhere continuous but nowhere dif-

ferentiable function is displayed in Fig. 6(b). One can prove easily that for all x , $f(x/4) = f(x)/2$. The Hurst exponent is $H = \ln 2/\ln 4 = 1/2$. When the $|p_k|$ ’s are not equal, the Hurst exponent is much harder to get analytically. One can show that it is not unique; it actually depends on the point x_0 [Eq. (29)]. We will study this case in Sec. 2.3.2. Let us note that there exists a lot of different methods for constructing self-affine functions with deterministic rules. However, they are all based on the same process: the iteration of a multiplicative rule for distributing the weights at smaller and smaller scales [Peitgen & Saupe, 1987; Voss, 1987, 1989; Dubuc *et al.*, 1989; Edgar, 1990; Barabási & Vicsek, 1991].

- Originally introduced by Mandelbrot & Van Ness [1968], the *fractional Brownian motions* generalize the classical Brownian motion. They have been extensively used to model various physical phenomena [Mandelbrot, 1977, 1982; Feder, 1988; Stanley & Ostrowski, 1988; Vicsek, 1989; Family & Vicsek, 1991]. A fractional Brownian motion $B_H(t)$, indexed by $H \in]0, 1[$, is a Gaussian process of mean value 0 and whose correlation function is

$$\langle B_H(t)B_H(s) \rangle = \frac{\sigma^2}{2}(|t|^{2H} + |s|^{2H} - |t-s|^{2H}), \quad (31)$$

where $\langle \rangle$ represents the mean value. The variance of such a process is

$$\text{var}(B_H(t)) = \sigma^2|t|^{2H}. \quad (32)$$

The classical Brownian motion corresponds to $H = 1/2$ and to a variance $\text{var}(B_{1/2}(t)) = \sigma^2|t|$. One can easily show that the increments of a fractional Brownian motion, i.e., $\delta B_{H,l}(t) = B_H(t+l) - B_H(t)$ ($l \in \mathbb{R}^{+*}$ fixed), are stationary. Indeed, the correlation function $\langle \delta B_{H,l}(t), \delta B_{H,l}(s) \rangle = \sigma^2/2(|t-s+l|^{2H} + |t-s-l|^{2H} - 2|t-s|^{2H})$ depends only on $t-s$. For $H = 1/2$, we recover the fact that the increments of the classical Brownian motion are independent. For any other value of H , the increments are correlated. From Eq. (31), one gets

$$B_H(t + \lambda s) - B_H(t) \simeq \lambda^H(B_H(t+s) - B_H(t)), \quad (33)$$

where \simeq stands for the equality in law (for fixed t and λ). This means that fractional Brownian motions are self-affine processes and that the Hurst exponent is H . The higher the exponent H , the more regular the motion.

A definition of a fractal function. Along the same line as for sets and measures, we will define a fractal function as a self-similar function which is invariant (either in a deterministic or in a statistical sense) by the iterative action of some elementary similitudes. Let us anticipate that this definition extends quite naturally to fractal distributions.

2.3.2. A first step towards a multifractal formalism for fractal functions: the structure function method

In order to study fractal functions, one could just study their graphs as fractal sets in \mathbb{R}^2 . Basically, it would lead to computing the fractal dimension of a given graph in \mathbb{R}^2 . It would however be a very poor characterization as compared to the multifractal formalism for fractal measures which instead provides a continuous spectrum of fractal dimensions to account for the statistical contributions of singularities of various strengths. Could we not apply this formalism to study self-affine functions? For that purpose, we have to consider a self-affine function no longer as a geometric graph in \mathbb{R}^2 but as a function with local singular behavior. Let us change slightly the definition of the Hurst exponent of f so that it becomes a local quantity:

$$|f(x+l) - f(x)| \sim Cl^{h(x)}. \quad (34)$$

This “local Hurst exponent” $h(x)$ is generally called the *Hölder exponent* of f at the point x . In the next section, we will give a rigorous definition of this exponent; for now we will keep calling it the local Hurst exponent. This exponent characterizes the regularity of f at x ; the closer this exponent is to zero, the less regular is the function.

The way of adapting the multifractal formalism from fractal measures to fractal functions is clear when one compares Eq. (34) with Eq. (10). We just need to substitute the singularity exponent $\alpha(x)$ by the exponent $h(x)$. The balls of size ε that we used for covering the support of a measure are replaced by “increments” of the function over a distance l . In the same way we have defined the $f(\alpha)$ singularity spectrum of a measure μ , we will then define the $D(h)$ spectrum of local Hurst exponents of the function $f(x)$ by the function which associates to any h , the Hausdorff dimension of the set of points x which verify $h(x) = h$, i.e.,

$$D(h) = d_H(\{x, h(x) = h\}). \quad (35)$$

In the simple case where f is a devil staircase, i.e., $f(x) = \mu([0, x])$, let us note that the notions

of local Hurst exponent h and of $D(h)$ spectrum correspond respectively to the singularity exponent $\alpha(x)$ and the $f(\alpha)$ spectrum associated to the measure μ . The increments of f over a distance l can be computed as the measure in balls of size l .

These new concepts have been initially introduced by Frisch & Parisi [1985] for studying fully developed turbulent flows. In order to estimate the $D(h)$ singularity spectrum they have suggested considering the *structure functions* $S_p(l)$ [Monin & Yaglom, 1971] to replace the partition functions $\mathcal{Z}(q, \varepsilon)$ [Eq. (15)]. Their power law scaling behavior (when the scale l varies) defines the exponents ζ_p [to be compared to the exponents $\tau(q)$]:

$$S_p(l) = \int |f(x+l) - f(x)|^p dx \sim l^{\zeta_p}. \quad (36)$$

In the same way as we did for measures, a steepest descent argument shows that ζ_p and $D(h)$ are related [as $\tau(q)$ and $f(\alpha)$] by a *Legendre transform* [Frisch & Parisi, 1985]:

$$\zeta_p = 1 + \min_h (ph - D(h)). \quad (37)$$

This last equation completes the analogy with the multifractal formalism for fractal measures. It is clear that this new description gives a much richer characterization of self-affine functions than the one given by the fractal dimension of the graph [Frisch & Parisi, 1985; Barabási & Vicsek, 1991]. Indeed, it tells us whether the function is a homogeneous fractal function, i.e., $h(x_0) = H$, $\forall x_0$, or a *multifractal function* characterized by a nontrivial $D(h)$ spectrum.

Examples

- Let us consider the recursive fractal function which is the distribution function of a “generalized” Cantor measure, with the weights $p_1 = p_2 = -p_3 = p_4 = 1/2$ [same as in Fig. 6(b)]. If we choose $l = 4^{-n}$, then the structure functions are $S_p(4^{-n}) = 4^{-1}2^{-np}$. Thus the ζ_p spectrum is a linear function of p : $\zeta_p = p \ln 2 / \ln 4 = p/2 = pH$. The function is a homogeneous fractal function. The slope of ζ_p is the Hurst exponent which characterizes the function. We find $h(x) = H = 1/2$ and $D(H) = 1$.
- One can generalize the latter construction to any value for the weights p_i . One can prove that

$S_p(4^{-n}) = 4^{-1}(|p_1|^p + |p_2|^p + |p_3|^p + |p_4|^p)^n$ and thus $\zeta_p = \log_4(|p_1|^p + |p_2|^p + |p_3|^p + |p_4|^p)$. This function is generally nonlinear; the support of the $D(h)$ spectrum is the interval $[h_{\min}, h_{\max}]$ where $h_{\min} = \min_i(-\log_4 p_i)$ and $h_{\max} = \max_i(-\log_4 p_i)$. The function is multifractal.

Drawbacks of the structure function method. The structure function method is a first step in characterizing the singular structure of self-affine functions through a statistical description like the one used in the multifractal formalism for singular measures. However, this method has the main drawbacks which can basically be summarized as follows:

- Equation (36) involves a sum over the whole space. Generally, fractal functions are likely to have, at any scale, increments as close to zero as we want. It then appears clearly that $S_p(l)$ will diverge for $p < 0$. This means that the exponents ζ_p are only defined for positive values of p . Let us note also that ζ_0 is generically always equal to 0 and thus does not carry any information on the dimension of the set of all the singular points of f .
- If we analyze a signal which has some very strong singular behavior (e.g., Dirac distributions), the structure function method is extremely unstable. Indeed, the computation of the increments is very unstable. On the other hand, if the function is very smooth (i.e., more than C^1), then the ζ_p spectrum is trivially $\zeta_p = p$. In other words, it does not give any characterization of the singular behavior that could appear in the successive derivatives of f .

These drawbacks show that the structure function method does not provide a reliable generalization of the multifractal formalism to fractal functions and more generally to fractal distributions. In Sec. 3, we will try to analyze more deeply these problems and see how we can get rid of them. We will define a new method that will be a general unified multifractal formalism for fractal distributions (including measures and functions). This method is based on a very powerful tool for analyzing singular behavior which has been introduced in the early eighties: the *wavelet transform* [Combes *et al.*, 1989; Meyer, 1990, 1992; Lemarié, 1990; Daubechies, 1992; Ruskai *et al.*, 1992; Meyer & Roques, 1993].

3. Singularity Detection and Processing with Wavelets

The wavelet transform has been introduced about ten years ago by the geophysicist Morlet [1983]. While studying seismic signals for petroleum research, Morlet realizes that both the regular and the short term Fourier transforms are not adapted for analyzing signals with very different scales. In order to circumvent these difficulties, he builds a new transformation which provides a space-scale representation of a signal. This transformation basically consists in decomposing the signal in terms of some elementary functions $\psi_{b,a}$ obtained from a “mother” function ψ by dilations and translations: $\psi_{b,a}(x) = a^{-1/2}\psi((x - b)/a)$. In 1984, Grossmann, Morlet and their collaborators formalize this new transformation and show that it can be inverted if the “mother” function ψ is a *wavelet*, i.e., a function with some oscillations [Goupillaud *et al.*, 1984; Grossman & Morlet, 1984, 1985; Grossmann *et al.*, 1985, 1986]. Later on, Daubechies *et al.* [1986] find a way of discretizing the wavelet transform on “frames.” The frame theory is the foundation of all the work that has been done since on discrete wavelets. Lemarié & Meyer [1986], Meyer [1987] and Jaffard & Meyer [1989a, 1989b] construct some orthogonal wavelet bases. The multiresolution analysis discovered by Mallat [1989a, 1989b] and Meyer [1990] describes any orthogonal wavelet basis in terms of a common multiscale structure. It allows us to build a fast algorithm for computing wavelet transform. This fast algorithm combined with the compactly supported wavelet bases built by Daubechies [1988, 1992] makes the wavelet transform a very powerful tool for numerical applications. The wavelet theory has been applied recently to various domains such as functional analysis, theoretical physics, signal and image processing, partial differential equations and fractal theory [Combes *et al.*, 1989; Lemarié, 1990; Meyer, 1990, 1992; Daubechies, 1992; Ruskai *et al.*, 1992; Meyer & Roques, 1993].

3.1. The continuous wavelet transform

3.1.1. Definitions

In this section, we introduce the 1D continuous wavelet transform and some of the basic mathematical results. We consider a function $s(x)$ in the

Hilbert space $L^2(\mathbb{R}, dx)$. We are going to decompose this function s in terms of elementary functions obtained by dilations and translations of the real valued mother function $\psi(x)$. Let us define $\psi_{b,a}(x) = a^{-1/2}\psi((x-b)/a)$. We then define the *wavelet transform* (WT) of $s(x)$ by [Grossmann & Morlet, 1984, 1985]

$$\begin{aligned} T_\psi[s](b, a) &= \langle \psi_{b,a} | s \rangle_{L^2(\mathbb{R}, dx)} \\ &= a^{-1/2} \int \psi\left(\frac{x-b}{a}\right) s(x) dx, \end{aligned} \quad (38)$$

where $\langle \cdot | \cdot \rangle_{L^2(\mathbb{R}, dx)}$ is the scalar product in $L^2(\mathbb{R}, dx)$. The parameter b is a real valued space (or time) parameter whereas a is a scale parameter ($a \in \mathbb{R}^{+*}$). Thus the wavelet transform is basically the scalar product of the function with the mother function dilated by a and translated by b (Fig. 7).

In the Fourier domain, Eq. (38) can be rewritten in the following way:

$$T_\psi[s](b, a) = a^{1/2} \int \bar{\psi}(a\omega) \hat{s}(\omega) e^{ib\omega} d\omega, \quad (39)$$

where $\hat{s}(\omega) = \int e^{-i\omega x} s(x) dx$ represents the Fourier transform of $s(x)$. Thus at a fixed scale a , the wavelet transform corresponds to filtering the function s with the band-pass filter $\bar{\psi}(a\omega)$.

3.1.2. Inversion formula and reproducing kernel

In order to be able to reconstruct the original function $s(x)$ from its wavelet transform $T_\psi[s](b, a)$, we would like T_ψ to be an isometry, i.e., to verify for

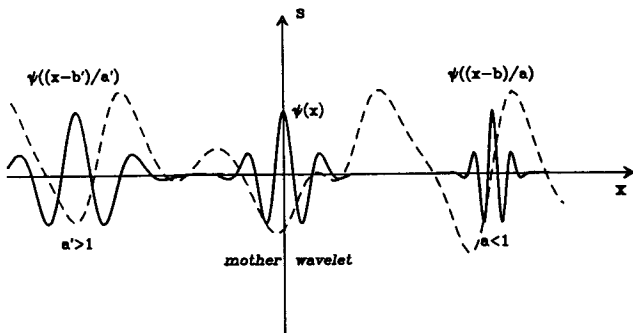


Fig. 7. The wavelet coefficients correspond to the scalar product of the given signal (—) with the wavelets $\psi_{b,a}(x)$ obtained by dilating and translating the mother function $\psi(x)$ (—).

any function s a relation of the type

$$\langle s | s \rangle_{L^2(\mathbb{R}, dx)} = C_\psi^{-1} \langle T_\psi[s] | T_\psi[s] \rangle_{L^2(\mathbb{R} \times \mathbb{R}^{+*}, d\mu(b, a))}, \quad (40)$$

where C_ψ is a constant and $d\mu(b, a)$ a measure in the space-scale half-plane. The wavelet transform is invariant under dilations and translations in the sense that [Goupillaud *et al.*, 1984; Grossmann & Morlet, 1984, 1985; Grossmann *et al.*, 1985]

$$\begin{aligned} T_\psi[s(x-x_0)](b, a) &= T_\psi[s(x)](b-x_0, a), \\ T_\psi\left[\lambda^{-1/2}s\left(\frac{x}{\lambda}\right)\right] &= T_\psi[s(x)]\left(\frac{b}{\lambda}, \frac{a}{\lambda}\right). \end{aligned} \quad (41)$$

Thus, according to Eq. (40), $d\mu(b, a)$ must be invariant under the transformation $(b, a) \rightarrow (b-x_0, a)$ and $(b, a) \rightarrow (b/\lambda, a/\lambda)$. It is then natural to choose $d\mu(b, a) = dbda/a^2$. By using this expression of $d\mu$ one can prove, using the Plancherel formula, that the relation (40) holds if ψ satisfies

$$C_\psi = \int_0^{+\infty} \frac{|\hat{\psi}(\omega)|^2}{\omega} d\omega < +\infty. \quad (42)$$

This relation is generally referred to as the *admissibility condition*. Let us note that it implies that $\hat{\psi}(0) = 0$ and therefore, if $\psi \in L^1(\mathbb{R})$,

$$\int_{-\infty}^{+\infty} \psi(x) dx = 0. \quad (43)$$

A mother function ψ which satisfies Eq. (42) will be called an *analyzing wavelet*. For such a mother function, the wavelet transform is an isometry (up to the factor C_ψ) and we have the following reconstruction formula [Grossmann & Morlet, 1984, 1985; Grossmann *et al.*, 1985, 1986; Meyer, 1990; Daubechies, 1992]:

$$s(x) = C_\psi^{-1} \int a^{-1/2} \psi\left(\frac{x-b}{a}\right) T_\psi[s](b, a) db da / a^2. \quad (44)$$

Let us note that the relation (42) is not a necessary condition and that one could choose a slightly different admissibility condition [Grossmann & Morlet, 1985; Daubechies, 1992].

Actually, one can obtain a much more general reconstruction formula. Indeed, it is possible to reconstruct s by using a mother function ψ^r different from the function ψ used to compute the wavelet transform [Holschneider & Tchamitchian,

1990]. The reconstruction formula then becomes

$$s(x) = C_{\psi, \psi^r}^{-1} \int a^{-1/2} \psi^r \left(\frac{x-b}{a} \right) \times T_\psi[s](b, a) db da / a^2, \quad (45)$$

where ψ^r and ψ are two mother functions satisfying the new admissibility condition

$$\begin{aligned} C_{\psi, \psi^r} &= \int_0^{+\infty} \frac{\hat{\psi}(\omega) \bar{\hat{\psi}}^r(\omega)}{\omega} \\ &= \int_0^{+\infty} \frac{\hat{\psi}(-\omega) \bar{\hat{\psi}}^r(-\omega)}{\omega} < +\infty. \end{aligned} \quad (46)$$

Let us note that if $\psi^r = \psi$, then we recover Eqs. (42) and (44). The new admissibility condition (46) is very “weak” and allows a very large choice for the reconstructing wavelet ψ^r . One interesting choice is the dirac distribution $\psi^r(x) = \delta(x)$. It leads to a very simple inversion formula [Holschneider, 1990]:

$$s(x) = C_{\psi, \delta}^{-1} \int T_\psi[s](x, a) \frac{da}{a^{3/2}}. \quad (47)$$

By taking the scalar product of the inversion formula (44) with the wavelet $\psi_{b', a'}$ one can easily get the interpolation formula [Grossmann & Morlet, 1984, 1985; Grossmann *et al.*, 1985; Daubechies *et al.*, 1986]

$$\begin{aligned} T_\psi(b', a') &= C_\psi^{-1} \int K_\psi \left(\frac{b-b'}{a'}, \frac{a}{a'} \right) \\ &\times T_\psi(b, a) da db / a^2, \end{aligned} \quad (48)$$

where $K_\psi(b, a)$ is the scalar product $\langle \psi_{b, a} | \psi \rangle$. The function $K_\psi(b, a)$ is called the *reproducing kernel* associated to the analyzing wavelet ψ . Equation (48) means that the wavelet coefficients are correlated and thus that a given function $S(b, a)$ is the wavelet transform of a function s iff it satisfies some correlation properties. For a given analyzing wavelet, the correlation “length” depends linearly on the scale a . That means that the value of the function s at a point x_0 will “influence” the values of the wavelet transform $T_\psi[s](b, a)$ for (b, a) in a domain of the form

$$|b - x_0| \leq \sigma_\psi a, \quad (49)$$

where σ_ψ^2 is the variance of the analyzing wavelet ψ . This domain is a cone which “points” to x_0 on

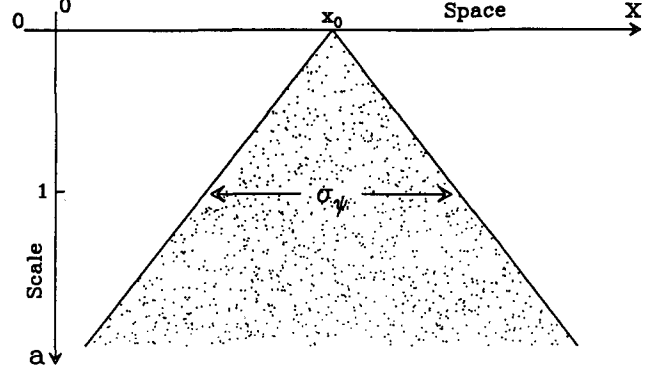


Fig. 8. The cone of influence associated with the point x_0 . ψ is the analyzing wavelet of variance σ_ψ^2 .

the space axis. This *cone of influence* is illustrated in Fig. 8.

3.1.3. Some examples of analyzing wavelets

There are almost as many analyzing wavelets as applications of the wavelet transform. The first one that Morlet [1983] used when he first developed the wavelet transform is a complex valued function referred to as the Morlet wavelet. It is a Gaussian function which is modulated so that its mean value is close to zero [Eq. (43)]. A very important class of wavelets are the ones that can be associated to orthonormal bases of $L^2(\mathbb{R})$. It is the case, for instance, of the Meyer wavelet [Meyer, 1987; Meyer, 1990], the spline wavelets built by Lemarié & Meyer [1986] and the compactly supported wavelets of Daubechies [1988, 1992]. When one uses these wavelets, the wavelet transform is performed only on a dyadic grid of the space-scale half-plane corresponding to a wavelet basis of $L^2(\mathbb{R})$. One generally refers to this method as the orthogonal (discrete) wavelet transform. However, for the study of fractals, we will need to compute the wavelet transform on a continuous (b, a) grid, i.e., we will perform a continuous wavelet transform. Since there is no point in using orthogonal wavelets, we will use the wavelets corresponding to the successive derivatives of the Gaussian function.

Let us define $\psi^{(N)}$ as

$$\psi^{(N)}(x) = \frac{d^N}{dx^N} e^{-\frac{x^2}{2}}. \quad (50)$$

Its Fourier transform is

$$\hat{\psi}^{(N)}(\omega) = (i\omega)^N e^{-\frac{\omega^2}{2}}. \quad (51)$$

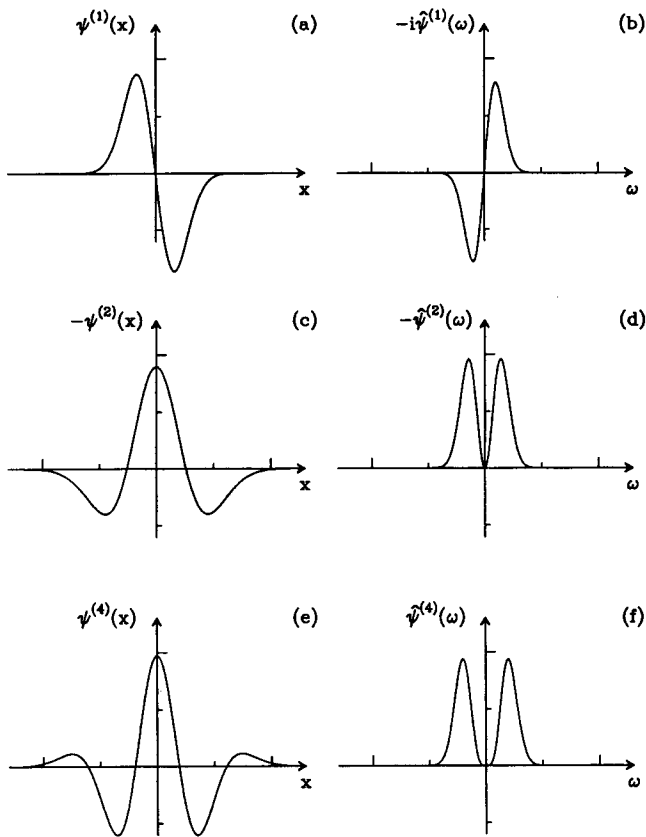


Fig. 9. Some analyzing wavelets of the class of the successive derivatives of the Gaussian function: (a) $\psi^{(1)}(x)$, (b) $\hat{\psi}^{(1)}(\omega)$, (c) $\psi^{(2)}(x)$, (d) $\hat{\psi}^{(2)}(\omega)$, (e) $\psi^{(4)}(x)$, (f) $\hat{\psi}^{(4)}(\omega)$.

These functions are C^∞ and are well localized both in space and frequency. The wavelet $\psi^{(2)}$ is a very “classical” wavelet and it is generally referred to as the “mexican hat” (Fig. 9). Let us note that the first N moments of $\psi^{(N)}$ are vanishing:

$$\int \psi^{(N)}(x) x^q dx = 0, \quad 0 \leq q < N. \quad (52)$$

As we will see in the next section, this property is fundamental for analyzing singular behavior. In Fig. 9 are displayed $\psi^{(N)}(x)$ and $\hat{\psi}^{(N)}(\omega)$ for $N = 1, 2$ and 4 .

3.2. Analysis of singularities with the continuous wavelet transform

3.2.1. Local regularity and Hölder exponents of a distribution

In Sec. 2.3.2, we have seen how the “strength” of a singularity can be described by an exponent called local Hurst exponent or Hölder exponent [Eq. (34)].

Let us give a more rigorous definition of a Hölder exponent.

Definition 2. The *Hölder exponent* $h(x_0)$ of a distribution f at the point x_0 is the greatest h so that f is *Lipschitz* h at x_0 , i.e., there exists a constant C and a polynomial $P_n(x)$ of order n so that for all x in a neighborhood of x_0 we have

$$|f(x) - P_n(x - x_0)| \leq C|x - x_0|^h. \quad (53)$$

If $h(x_0) \in]n, n + 1[$ one can easily prove that f is n times but not $n + 1$ times differentiable at the point x_0 . The polynomial $P_n(x)$ in Eq. (53) corresponds to the Taylor series of f around $x = x_0$ up to the order n . Thus $h(x_0)$ measures how irregular the distribution f is at the point x_0 . The higher the exponent $h(x_0)$, the more regular the distribution f .

Let us note that if f has a Hölder exponent $h(x_0) = h$ at the point x_0 , then the primitive of f corresponds to a Hölder exponent $h(x_0) \geq h + 1$. Actually, in most cases, $h(x_0) = h + 1$ for the primitive of f . This is not true however if the singularity of f at x_0 is an *oscillating singularity* [Mallat & Hwang, 1992]. Indeed, for instance, the Hölder exponent of $f(x) = \sin(1/x)$ at $x_0 = 0$ is $h(0) = 0$, whereas its primitive $F(x)$ verifies $|F(x) - F(0)| = O(x^2)$ in the neighborhood of 0, thus its Hölder exponent at $x_0 = 0$ is greater than 2! *In the following, we will only consider distributions whose singularities are not oscillating.* Basically, when one differentiates (integrates) such a distribution, the Hölder exponent is decreased (increased) by 1. Thus, for instance, the Heaviside function $H(x) = \chi_{[0,+\infty]}(x)$ corresponds to $h(0) = 0$ and its derivative, the Dirac distribution $\delta(x)$, corresponds to $h(0) = -1$. The function \sqrt{x} has a Hölder exponent $h(0) = 1/2$ and its derivative, the distribution $1/(2\sqrt{x})$, a Hölder exponent $h(0) = -1/2$.

Remark. In order to characterize the regularity of a distribution f , one generally studies the behavior of its Fourier transform \hat{f} at infinity. However, this method characterizes the global regularity of f and does not give any information on how regular f is around a given point x_0 . We will see that the wavelet transform is able to do so.

3.2.2. Wavelet analysis of local Hölder regularity

Let us suppose that the Hölder exponent of a distribution $f(x)$ around the point $x = x_0$ is $h(x_0) \in$

$]n, n + 1[$ and that the behavior of $f(x)$ around $x = x_0$ is given by

$$\begin{aligned} f(x) &= c_0 + c_1(x - x_0) + \cdots + c_n(x - x_0)^n \\ &\quad + C|x - x_0|^{h(x_0)}. \end{aligned} \quad (54)$$

The wavelet transform of f is the scalar product of f with the wavelets $\psi_{b,a}(x) = a^{-1/2}\psi((b - x)/a)$ [Eq. (38)]. Thus, if we suppose that the analyzing wavelet $\psi(x)$ has $n_\psi > n$ vanishing moments [Eq. (52)], then it means that ψ is orthogonal to polynomials up to order n (included). One can derive from Eq. (54) the expression of the wavelet transform of f at x_0 , when the scale a goes to 0:

$$\begin{aligned} T_\psi[f](x_0, a) &= Ca^{1/2} \int \psi(x)|ax|^{h(x_0)}dx, \\ &= a^{h(x_0)+1/2}CT_\psi[f](x_0, a). \end{aligned} \quad (55)$$

For the sake of simplicity, we slightly change the definition of the wavelet transform by multiplying its expression (Eq. 38) by the factor $a^{-1/2}$:

$$T_\psi[f](b, a) = \frac{1}{a} \int \psi\left(\frac{x-b}{a}\right)f(x)dx. \quad (56)$$

In this definition, we assume that f is no longer restricted to $L^2(\mathbb{R}, dx)$; it can be any distribution. The relation (55) then becomes

$$T_\psi[f](x_0, a) \sim a^{h(x_0)}, \quad a \rightarrow 0^+. \quad (57)$$

Thus, the local singular behavior $C|x - x_0|^{h(x_0)}$ of f around $x = x_0$ is characterized by a power law scaling exponent $h(x_0)$ of the wavelet transform of f at the point x_0 when the scale a goes to 0. On the other hand if f were C^∞ at x_0 , one could prove that we would get a power law scaling exponent n_ψ , i.e.,

$$T_\psi[f](x_0, a) \sim a^{n_\psi}, \quad a \rightarrow 0^+. \quad (58)$$

Thus, around a given point x_0 , the faster the wavelet decreases when the scale a goes to 0, the more regular f is around that point. This result can be summed up in a single theorem which has been proved independently by Jaffard [1989] and by Holschneider & Tchamitchian [1990].

Theorem 1. *Let ψ be an analyzing wavelet with n_ψ vanishing moments and let f be a bounded function.*

(a) *If f is Lipschitz $\gamma \leq n_\psi$ at x_0 , then the wavelet transform of f satisfies:*

$$|T_\psi[f](x, a)| = O(a^\gamma + |x - x_0|^\gamma). \quad (59)$$

- (b) *Reciprocally, let $\gamma < n_\psi$ and let us suppose that*
- (i) $\exists \nu > 0$, $|T_\psi[f](x, a)| = O(a^\nu)$ uniformly in x ,
 - (ii) $|T_\psi[f](x, a)| = O(a^\gamma + |x - x_0|^\gamma / |\ln |x - x_0||)$,
- then f is Lipschitz γ at x_0 .*

This theorem is the “rigorous” version of Eqs. (57) and (58). The greatest value of γ corresponds to the Hölder exponent $h(x_0)$.

Let us note that the necessary condition [Eq. (59)] is not sufficient: one has to add a logarithmic correction by replacing $|x - x_0|^\gamma$ in (a) by $|x - x_0|^\gamma / |\ln |x - x_0||$. However, from a numerical point of view, a logarithmic correction does not make any difference, and the condition (a) can be considered as a necessary and sufficient condition. Moreover for nonoscillating singularities, one can prove that the behavior of the wavelet transform inside the cone $|x - x_0| \leq Ca$ is enough to recover the Hölder exponent $h(x_0)$ [Mallat & Hwang, 1992]. The Hölder exponent $h(x_0)$ ($\leq n_\psi$) is thus the greatest exponent so that

$$\max_{|x-x_0| \leq Ca} |T_\psi[f](x, a)| = O(a^{h(x_0)}). \quad (60)$$

3.2.3. Detection and identification of singularities with the wavelet transform. Wavelet transform modulus maxima and maxima lines

As just explained, in order to recover the Hölder exponent $h(x_0)$ of a distribution f at the point x_0 , we need to study the behavior, when a goes to 0, of its wavelet transform inside a cone $|x - x_0| \leq Ca$. For that purpose, we just need to look (at each scale a) at the “maximum” values of the wavelet transform inside the cone, and to study how these “maximum” values vary when a goes to 0 [Eq. (60)]. In order to do so Mallat & Zhong [1992] have introduced the notions of *modulus maxima* and of *maxima lines* of the wavelet transform [Mallat & Hwang, 1992; Mallat & Zhong, 1992].

Definition 3

- We call *modulus maximum* of the wavelet transform $T_\psi[f]$, any point (x_0, a_0) of the space-scale half-plane which corresponds to a local maximum of the modulus of $T_\psi[f](x, a_0)$ considered as a function of x , i.e., $|T_\psi[f](x_0, a_0)| > |T_\psi[f](x, a_0)|$

for all x in a right neighborhood of x_0 and $|T_\psi[f](x_0, a_0)| \geq |T_\psi[f](x, a_0)|$ for all x in a left neighborhood of x_0 . Thus, $\partial|T_\psi[f]|/\partial x(x_0, a_0) = 0$.

- We call *maxima line*, any connected curve in the space-scale half plane made of modulus maxima.

We illustrate these definitions in Fig. 10. The considered function is $f(x) = k_0|x - x_0|^{0.4} + k_1 e^{-(x-x_1)^2/2}$. This function is C^∞ everywhere but

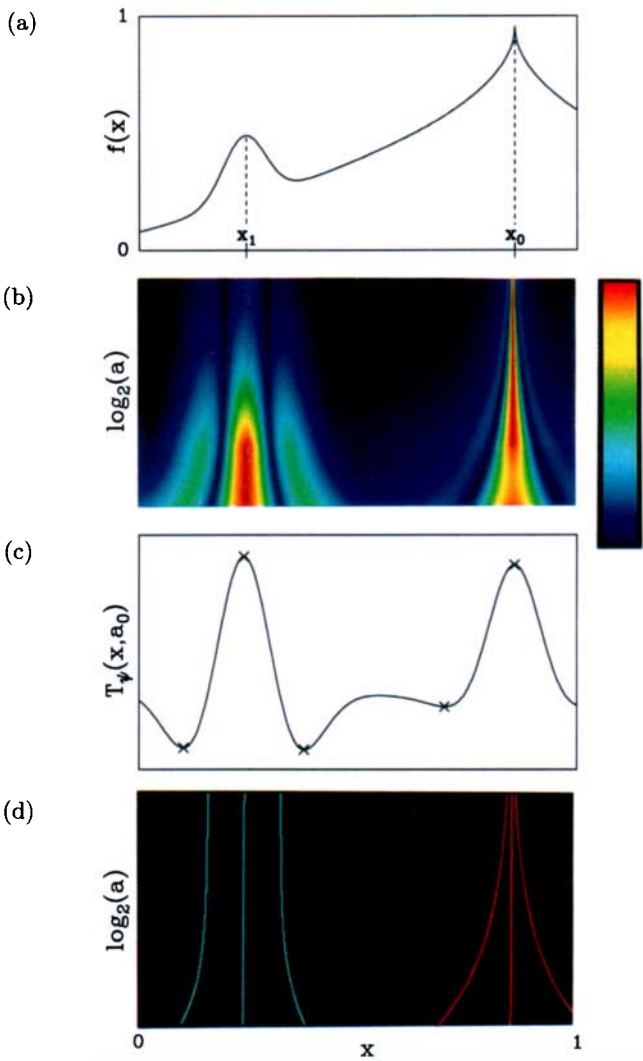


Fig. 10. Modulus maxima of the wavelet transform of the function $f(x) = k_0|x - x_0|^{0.4} + k_1 e^{-(x-x_1)^2/2}$. (a) Graph of $f(x)$. (b) The wavelet transform of $f(x)$ coded, independently at each scale a , according to the natural order of the light spectrum from black ($T_\psi \leq 0$) to red ($\max_x T_\psi > 0$); the small scales are at the top. (c) Horizontal section of the wavelet transform $T_\psi[f](x, a)$ at $a = a_0$; the symbols (\times) represent the modulus maxima. (d) Maxima lines of the wavelet transform in the (x, a) half-plane. The analyzing wavelet is the Mexican hat $\psi = \psi^{(2)}$ [Eq. (50)].

at $x = x_0$ where f is singular with $h(x_0) = 0.4$. Its wavelet transform is shown in Fig. 10(b); it is coded at each scale a from black ($T_\psi[f] < 0$) to red ($\max_x T_\psi[f](x, a)$). Figure 10(c) represents an horizontal section of the wavelet transform at some given coarse scale a_0 . The modulus maxima at this scale are marked on the same figure using the symbol (\times). The set of all the modulus maxima lies on maxima lines in the space-scale half-plane (b, a); they are displayed in Fig. 10(d). The analyzing wavelet is the Mexican hat $\psi^{(2)}$ ($n_\psi = 2$).

Mallat & Hwang [1992] have shown that a singular behavior of a distribution around a point x_0 implies that there exist maxima lines converging (when a goes to 0) towards the point x_0 on the space axis. Then, if there are no such lines, the distribution is uniformly Lipschitz n_ψ in a neighborhood of x_0 [i.e., $h(x) \geq n_\psi$ in a neighborhood of x_0]. Thus the modulus maxima lines of the wavelet transform provide information on the location of the singularities of a distribution f . One can check in Fig. 10(d), that on any interval which does not contain, at small scales, any modulus maximum, the function f is uniformly Lipschitz $n_\psi = 2$, whereas some maxima lines are converging towards the points $x = x_0$ (which is singular). Let us note that it does not exclude the possibility that there could be maxima lines on an interval where f is not singular. Indeed, in Fig. 10(d), some maxima lines are converging towards the point $x = x_1$ where f is not singular.

From Eq. (60) one can expect that by looking at the value of the wavelet transform along a maxima line $l_i(x_0)$ converging to a given point x_0 , one can estimate $h(x_0)$ ($\leq n_\psi$) as the greatest exponent so that

$$|T_\psi[f](x, a)| = O(a^{h(x_0)}), \quad (x, a) \in l_i(x_0), \quad (61)$$

in the limit $a \rightarrow 0^+$. Thus the maxima line allows us to locate and to estimate local singular behavior.

In Figure 10(d), we see that the maxima lines converge towards four different points. By looking at the power law scaling of $|T_\psi[f]|$ along these lines, one can recover that only the point $x = x_0$ corresponds to a singular behavior. Indeed, the exponent which characterizes the power law scaling of the other three points is $h = n_\psi$, whereas the exponent corresponding to x_0 is $h(x_0) < n_\psi$. In Fig. 11, we show log-log plots of the wavelet transform respectively along a maxima line which con-

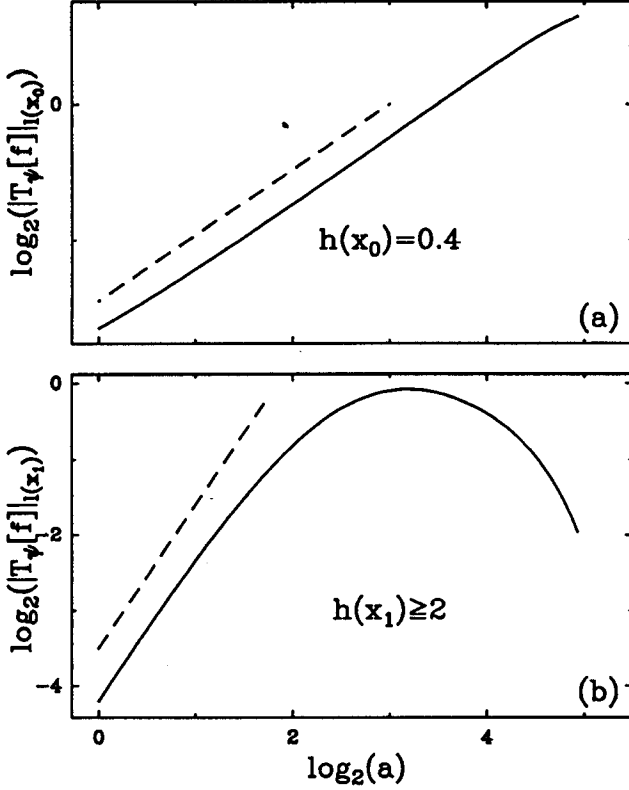


Fig. 11. Estimating the Hölder exponent from the behavior of the wavelet transform along the maxima lines. The slope of the curve $\log_2(|T_\psi[f](x, a)|)$ versus $\log_2(a)$ along a maxima line which converges towards a given point provides an estimate of the Hölder exponent at that point [Eq. (61)]. (a) Measurement for a line converging towards x_0 in Fig. 10(d). (b) Measurement for a maxima line converging towards the point x_1 of the same figure. The analyzing wavelet is the Mexican hat $\psi = \psi^{(2)}$.

verges towards x_0 and along a maxima line which converges towards $x = x_1$. According to Eq. (61), the slope of these curves gives an estimate of $\hat{h}(x) = \min(h(x), n_\psi = 2)$. By a linear regression fit we obtain $\hat{h}(x_0) \simeq 0.4$ and $\hat{h}(x_1) \simeq 2$; thus f is singular at $x = x_0$ with Hölder exponent $h(x_0) = \hat{h}(x_0) = 0.4$ but it is not singular at $x = x_1$ [it is at least once differentiable and the Hölder exponent is $h(x_1) \geq \hat{h}(x_1) = n_\psi = 2$].

Thus the modulus maxima of the wavelet transform allows us to study in a very efficient way the isolated singularities of a distribution f . In the case of fractal distributions, these singularities are not isolated. However, as we will see in the next sections, in most cases, the same analysis can be carried out.

4. A Multifractal Formalism for Distributions Based on Wavelets

4.1. Wavelet transform of multifractal measures

4.1.1. Wavelet analysis of the local scaling properties of singular measures

The singularity behavior of a measure at a given point x_0 is generally characterized by the exponent $\alpha(x_0)$ which satisfies the relation [Eq. (10)] [Farmer *et al.*, 1983; Halsey *et al.*, 1986; Grassberger *et al.*, 1988]:

$$\mu(B_{x_0}(\varepsilon)) \sim \varepsilon^{\alpha(x_0)}, \quad \varepsilon \rightarrow 0^+ \quad (62)$$

where $B_{x_0}(\varepsilon)$ is an interval of size ε , centered at x_0 . Let us note that this definition is very close to the definition (34) of the local Hurst exponent $h(x_0)$ introduced in Sec. 2.3.2. Indeed, if Eq. (62) holds and if $s(x)$ is the distribution function associated to μ ($s(x) = \mu([0, x])$), then one can prove that $h(x_0) = \alpha(x_0)$, where $h(x_0)$ is the local Hurst exponent of s at x_0 . Thus, in the same spirit in which we derived Eq. (57) from Eq. (54) in the case of Hölder exponents, one can derive from Eq. (62) a formula which shows that the wavelet transform of μ behaves like $a^{\alpha(x_0)}$ in the limit of the scale a going to 0 [Arneodo *et al.*, 1988, 1989a, 1989b, 1990; Grasseau, 1989]:

$$T_\psi[\mu](x_0, a) \sim a^{\alpha(x_0)}, \quad a \rightarrow 0^+, \quad (63)$$

where the wavelet transform of the measure μ is defined by [Arneodo *et al.*, 1988; Holschneider, 1988b]

$$T_\psi[\mu](b, a) = \int \psi\left(\frac{x-b}{a}\right) d\mu. \quad (64)$$

Let us note that this latter definition is nothing but the definition (56) of the wavelet transform of a distribution except for the $1/a$ factor that we have removed so that T_ψ scales exactly like $a^{\alpha(x_0)}$ (and not like $a^{\alpha(x_0)-1}$).

Remark. In Sec. 2, we have pointed out that the definition of the scaling exponent α [Eq. (62)] is not appropriate to account for singularities of strength $\alpha > 1$ in the presence of some density component. This is the main reason why we have introduced in Sec. 3 the wavelet transform. Actually, this transformation is a mathematical tool which is well suited

to detect and measure local Hölder exponents which are in fact a generalization of both the α scaling exponents of measures and the local Hurst exponents of functions. Indeed the wavelet transform can detect Hölder exponents up to $h \leq n_\psi$, where n_ψ is the number of vanishing moments of the analyzing wavelet ψ . However, the multifractal measures we will consider in this section are “purely” singular, i.e., they do not have any density component. Thus, there is *a priori* no point in using a function ψ with some vanishing moments (i.e., $n_\psi \geq 1$). Using a Gaussian function ψ or any function localized in space, in Eqs. (63) and (64), is sufficient since, in this case, measuring α is equivalent to measuring the Hölder exponent h [Bacry, 1992; Ghez & Vaienti, 1992; Muzy, 1993]. Indeed, if we use the “box function” $\psi = \chi_{[0,1]}$ (i.e., the characteristic function of the interval $[0, 1]$) as the analyzing wavelet, then $T_\psi[\mu](x_0, \varepsilon) = \mu(B_{x_0}(\varepsilon))$ and Eq. (63) is nothing but the definition (62) of the exponent $\alpha(x_0)$.

Figure 12 displays $\log_2 |T_\psi[\mu](x_0, a)|$ as a function of $\log_2 a$ at three different points x of the triadic Cantor set on which a nonuniform measure has been distributed with the weights $p_1 = 0.6$ and $p_2 = 0.4$ (Fig. 2). One can see in Fig. 12(a) that when x corresponds either to the sequence $LLL\ldots LL\ldots$ or to the sequence $RRR\ldots RR\ldots$, the log-log plot displays a clear linear behavior (the oscillations are due to the fact that μ is invariant under discrete dilations of a factor 3^n , $n > 0$) whose slope gives, with a very good precision, the expected values $\alpha(x) = \alpha_{\min} = \ln 0.6 / \ln 1/3$ and $\alpha_{\max} = \ln 0.4 / \ln 1/3$ respectively. But when x corresponds to the sequence $LLLLRRRR$, Fig. 12(b) displays a crossover from α_{\min} to α_{\max} and thus, measuring the exponent $\alpha(x)$ becomes inaccurate and somehow inappropriate. In fact, the exponent α , obtained from a linear regression fit on the entire available range of scales, corresponds to the strength of the singularity with periodic symbolic sequence of period $LLLLRRRR$. The singularities associated to nonperiodic sequences are not amenable to such a local scaling behavior analysis [Arneodo *et al.*, 1989b, 1990].

We understand now why Eq. (63), in the same way as Eq. (62), cannot be used for systematically “counting” the number of points x corresponding to the same value $\alpha(x) = \alpha$ and thus for computing the singularity spectrum of a measure. For that purpose, we need to use a “global” method (which goes beyond local estimates) and which is based

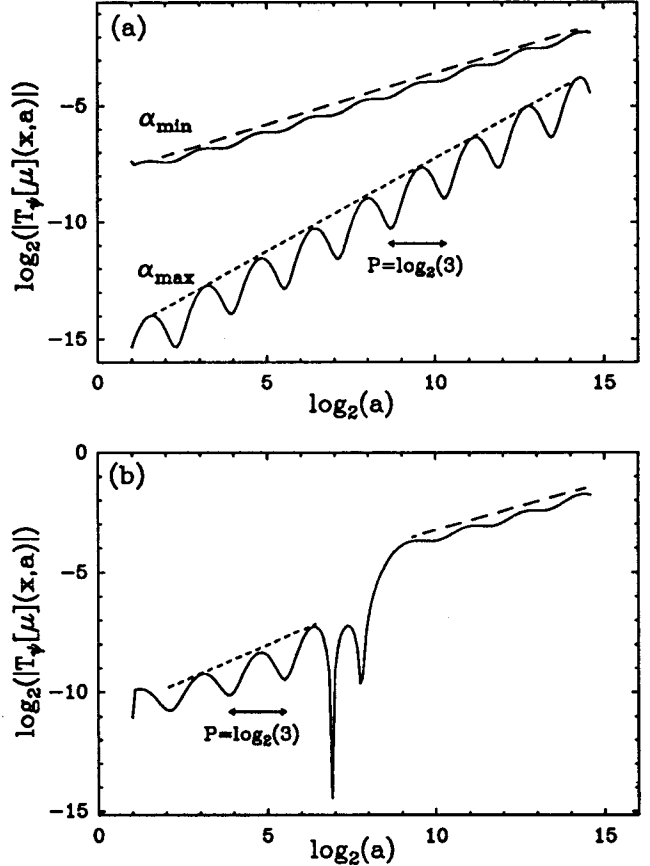


Fig. 12. $\log_2 |T_\psi[\mu](x, a)|$ as a function of $\log_2 a$ at three different points x of the triadic Cantor which supports a Bernoulli measure associated to the weights $p_1 = 0.6$ and $p_2 = 0.4$. (a) $x = x_1$ and $x = x_2$ where x_1 and x_2 correspond respectively to the kneading sequences $LLLLLLL$ ($\alpha = \alpha_{\min} = -\ln p_1 / \ln 3$) and $RRRRRRRR$ ($\alpha = \alpha_{\max} = -\ln p_2 / \ln 3$). (b) $x = x_3$ which corresponds to the kneading sequence $LLLLRRRR$. The analyzing wavelet is the Mexican hat $\psi = \psi^{(2)}$

on the computation of partition functions from the continuous wavelet analysis.

Furthermore, there is a major argument in favor of using the wavelet transform for studying fractal objects. The wavelet transform is a space-scale analysis; it actually plays the role of a “mathematical microscope” whose enlargement factor is $1/a$ and whose optics is defined by the shape of the analyzing wavelet ψ . As we will illustrate in the next section, this microscope provides some unfolding, in the space-scale half-plane, of the hierarchical structure of the analyzed fractal object; this unfolding can eventually “reveal” the underlying construction process [Arneodo *et al.*, 1988, 1989a, 1989b, 1990; Holschneider, 1988a, 1988b; Grasseau, 1989]. It is thus tempting to develop a multifractal analysis

relying on such a tool which is likely to capture the main structural ingredients to make this analysis optimal in the way that it will converge faster than any other analysis.

4.1.2. Wavelet transform and renormalization

In this section, we will show on three examples how the wavelet transform unfolds the hierarchical structure of a fractal measure by revealing the corresponding “renormalization operations” [Arneodo *et al.*, 1990].

Uniform measure on the triadic Cantor set.

Let μ be the uniform measure on the triadic Cantor set (Fig. 1). The self-similarity properties of this measure are mathematically described by saying that it is invariant under the application T (i.e., $\mu(T^{-1}(A)) = \mu(A), \forall A$) defined as follows:

$$T(x) = \begin{cases} T|_{[0,1/3]}(x) = T_1(x) = 3x, \\ T|_{[2/3,1]}(x) = T_2(x) = 3x - 2. \end{cases} \quad (65)$$

Let us recall that the wavelet transform of μ is defined by Eq. (64):

$$T_\psi[\mu](b, a) = \int_{A=[0,1]} \psi\left(\frac{x-b}{a}\right) d\mu. \quad (66)$$

Let $x' = T_k^{-1}(x)$ where $k = 1$ or 2 , we thus obtain

$$T_\psi[\mu](b, a) = 2 \int_{T_k^{-1}(A)} \psi\left(\frac{T_k(x) - b}{a}\right) d\mu. \quad (67)$$

Then, by using the fact that T_k is linear, we get

$$T_\psi[\mu](b, a) = 2 \int_{T_k^{-1}(A)} \psi\left(\frac{x - T_k^{-1}(b)}{3^{-1}a}\right) d\mu. \quad (68)$$

However, if we suppose that ψ has a compact support, then for a small enough

$$\begin{aligned} & \int_{T_k^{-1}(A)} \psi\left(\frac{x - T_k^{-1}(b)}{3^{-1}a}\right) d\mu \\ &= \int_A \psi\left(\frac{x - T_k^{-1}(b)}{3^{-1}a}\right) d\mu, \end{aligned} \quad (69)$$

and thus

$$T_\psi[\mu](b, a) = 2T_\psi[\mu](T_k^{-1}(b), 3^{-1}a). \quad (70)$$

This relation shows how the self-similarity of the measure μ is reproduced in the space-scale representation given by its wavelet transform. The color pictures in Figs. 13(a) and 14(a) represent the wavelet transform of μ using the analyzing wavelets $\psi^{(0)}$ and $\psi^{(2)}$ respectively. The amplitude is coded using 256 colors from black ($T_\psi \leq 0$) to red [$\max_x T_\psi(x, a)$]. The coding is defined, independently at each scale, according to the maximum value of the wavelet transform at this scale. The construction process is clearly revealed through the relation (70) for both $k = 1$ and $k = 2$ [Arneodo *et al.*, 1988, 1989a, 1989b, 1990]. Indeed, the “structure” at any scale a_* is exactly reproduced at the scale $a = a_*/3$ in two similar structures reduced by a factor of 3. Thus, in both Figs. 13(a) and 14(a) (independently of the analyzing wavelet) the original portion of the space-scale half-plane can be uncovered in the two symmetric dashed rectangles obtained from the original (large scale) picture by applying the two *renormalization operations*:

$$\begin{aligned} R_1 : \mathbb{R} \times \mathbb{R}^{+*} &\rightarrow \mathbb{R} \times \mathbb{R}^{+*}, \\ (b, a) &\rightarrow \left(\frac{b}{3}, \frac{a}{3}\right), \\ R_2 : \mathbb{R} \times \mathbb{R}^{+*} &\rightarrow \mathbb{R} \times \mathbb{R}^{+*}, \\ (b, a) &\rightarrow \left(\frac{b}{3} + \frac{2}{3}, \frac{a}{3}\right). \end{aligned} \quad (71)$$

Figure 15 illustrates the wavelet transform computed with the Mexican hat [Fig. 14(a)] using a three-dimensional representation. To make the singularities easy to visualize, T_ψ is normalized by the factor a^{-2} so that it diverges ($\sim a^{\ln 2/\ln 3-2}$), when a goes to 0, at each point of the triadic Cantor set. Figure 15 illustrates the fact that the singularities can be tracked in a very efficient way with the wavelet transform microscope. Indeed, the lines formed by the highest wavelet coefficients are converging towards the support of μ . These lines correspond to the maxima lines made of maxima of the function $|T_\psi[\mu](x, a)|$ considered as a function of x . They are pointing towards the singularities of the measure. Moreover they follow the same renormalization rules R_1 and R_2 as the wavelet transform itself. Thus the behavior of the wavelet transform along these lines is of the same type as the one described by Eq. (63). According to Eq. (71) (which transforms a maxima line into another maxima line), dilating the scales a by a factor 3^{-1} corresponds to a multiplication of the wavelet coefficients by a factor 2^{-1} ; thus, along these lines

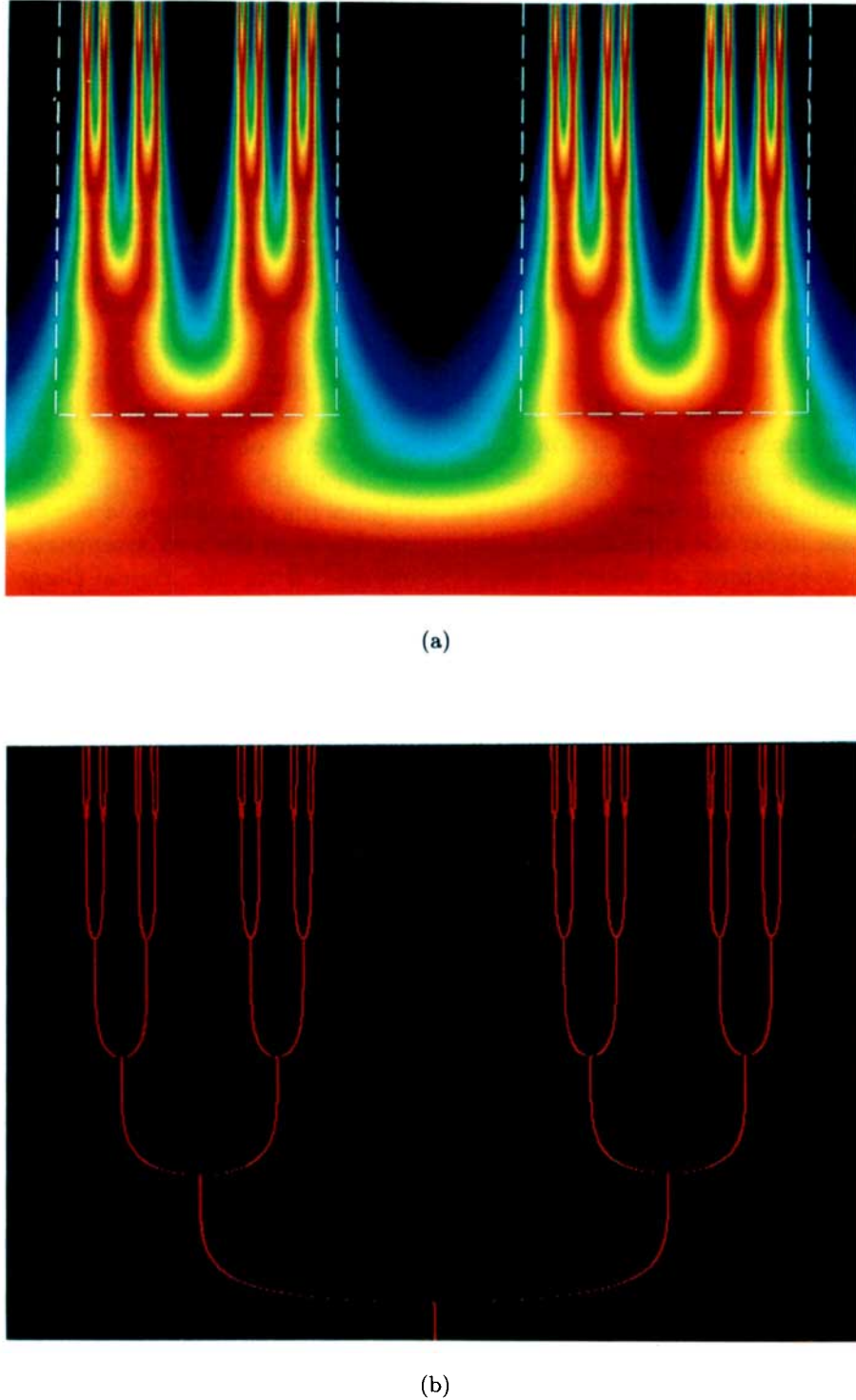
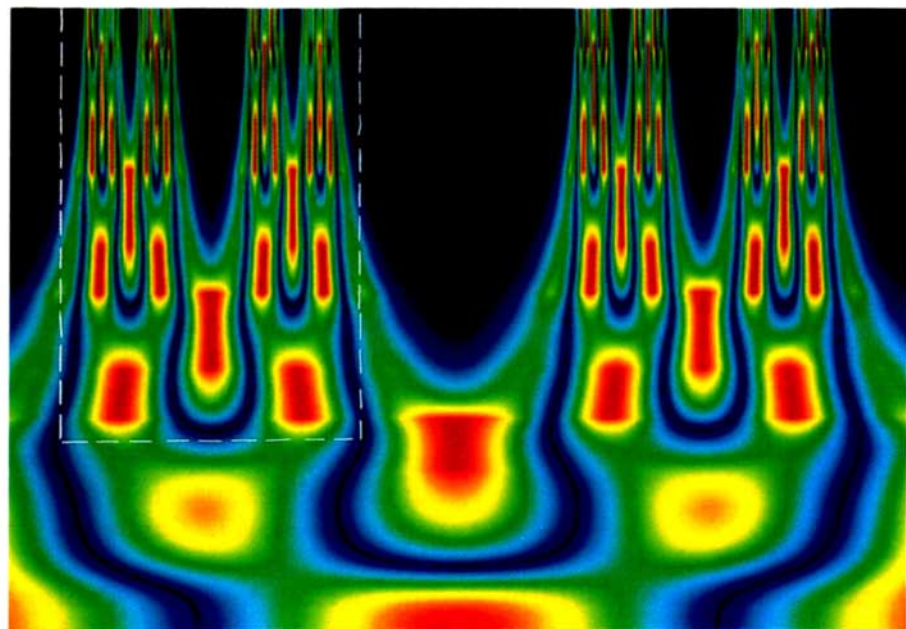
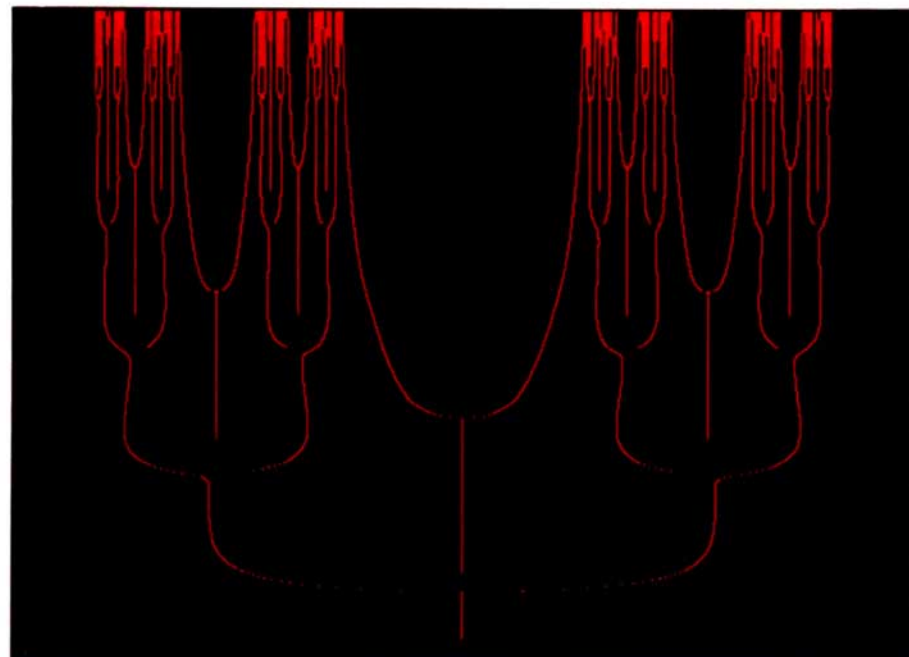


Fig. 13. Continuous wavelet transform of the uniform measure on the triadic Cantor set. (a) Wavelet transform $T_\psi[\mu](b, a)$ in the (b, a) half-plane; a logarithmic scale is used for a , the small scales are at the top. The amplitude of the wavelet transform is coded (256 colors), independently at each scale a , according to the natural order of the light spectrum from black ($T_\psi \leq 0$) to red ($\max T_\psi > 0$). The left (right) dashed rectangle illustrates the renormalization operation R_1 (R_2) (Eq. (71)). (b) Position in the space-scale half-plane of the local maxima of $|T_\psi[\mu]|$. The analyzing wavelet is the Gaussian function $\psi^{(0)}$.



(a)



(b)

Fig. 14. Continuous wavelet transform of the uniform measure on the triadic Cantor set. Same calculation as in Fig. 13 except that the analyzing wavelet is the mexican hat $\psi^{(2)}$ [Eq. (50)].

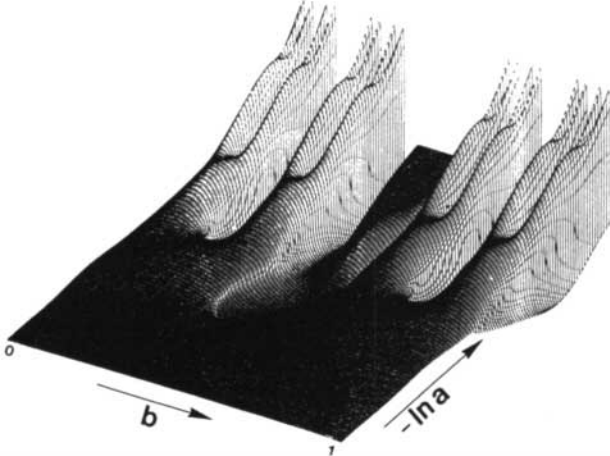


Fig. 15. 3D representation of the continuous wavelet transform ($a^{-2}T_\psi[\mu](b, a)$) of the uniform measure on the triadic Cantor set. The analyzing wavelet is the mexican hat $\psi^{(2)}$.

$T_\psi(b, a) \sim a^{\ln 2 / \ln 3}$ [Arneodo *et al.*, 1991; Bacry *et al.*, 1993]. As illustrated in Figs. 13(b) and 14(b), the maxima lines of the wavelet transform defines a tree whose branching process contains all the information concerning the hierarchical structure of the triadic Cantor set and thus its construction process. This explain why such a *skeleton* is a “key” tool in processing fractal measures and detecting singularities. As we will see in the next section, this wavelet transform skeleton will play a very important role in the definition of the new multifractal formalism based on wavelets.

Nonuniform measure on the triadic Cantor set. We can perform the same kind of analysis on a Bernoulli measure distributed nonuniformly (e.g., $p_1 = 0.6$ and $p_2 = 0.4$) on the triadic Cantor set [Arneodo *et al.*, 1988, 1989a, 1989b, 1990]. One can easily prove that the self-similarity of μ is reproduced on its wavelet transform according to the following rule [corresponding to Eq. (70)]:

$$T_\psi[\mu] \circ R_k = p_k T_\psi[\mu], \quad (72)$$

where R_k for $k = 1$ or 2 are the renormalization operations defined in Eq. (71). The color picture in Fig. 16(a) displays the wavelet transform of μ ; the coding is the same as the one used for the former color figures. The analyzing wavelet is the Gaussian function $\psi^{(0)}$. The two renormalization operations are once again illustrated by two small dashed rectangles reproducing the structure of the original picture at smaller scales. But this time the reproduction is “attenuated” by 2 different amplitude

factors (p_1 and p_2) depending upon which rectangle is considered. A 3D representation of this image is displayed in Fig. 17. Again the maxima lines are converging towards the singularities of the measure, i.e., towards the triadic Cantor set, and they reproduce its hierarchical structure. Moreover, the behavior of the wavelet transform along these lines characterizes the strength α of the singularity it is pointing to (even though, as noted before, this value cannot be reliably computed by this local method). The fact that the wavelet transform displays different scaling behavior in Fig. 17 indicates that the measure is not homogeneous. Let us note that the symmetric “forking” process in Fig. 15 has disappeared; this comes from the fact that the symmetry of the uniform Cantor set is broken by the nonuniform weights $p_1 \neq p_2$. This measure is multifractal; the scaling exponent α fluctuates from point to point on the triadic Cantor set.

The period-doubling Cantor set. As a first step towards fully developed turbulence, the transition to chaos in dissipative systems [Eckmann, 1981; Ott, 1981; Cvitanovic, 1984; Guckenheimer & Holmes, 1984] presents a strong analogy with second-order phase transitions [Hu, 1982; Crutchfield *et al.*, 1982; Coullet, 1984; Argoul & Arneodo, 1986]. Among the different scenarios from ordered to disordered temporal patterns, the most popular is undoubtedly the cascade of period-doubling bifurcations [Coullet & Tresser, 1978; Feigenbaum, 1978, 1979; Tresser & Coullet, 1978] and the transition to chaos from quasiperiodicity with irrational winding numbers [Feigenbaum *et al.*, 1982; Ostlund *et al.*, 1982, 1983; Shenker, 1982]. In this section, we will focus on the period-doubling scenario and we refer the reader to our original work for a similar analysis of the scenario from quasiperiodicity with golden mean winding number [Arneodo *et al.*, 1988, 1989a, 1989b, 1990].

Dissipative dynamical systems that exhibit the cascade of period-doubling bifurcations are in practice well modelled by one-dimensional maps with a single quadratic extremum such as the map [Coullet & Tresser, 1978; Feigenbaum, 1978, 1979; Tresser & Coullet, 1978; Collet & Eckmann, 1980]

$$x_{n+1} = \Phi_R(x_n) = 1 - Rx_n^2, \quad (73)$$

or quadratics maps of the form $\Phi_R(x) = Rx(1-x)$, $R \sin \pi x \dots$ As one increases the parameter R which determines the height of the maximum of Φ_R at $x = x_c = 0$, one observes an infinite sequence of subhar-

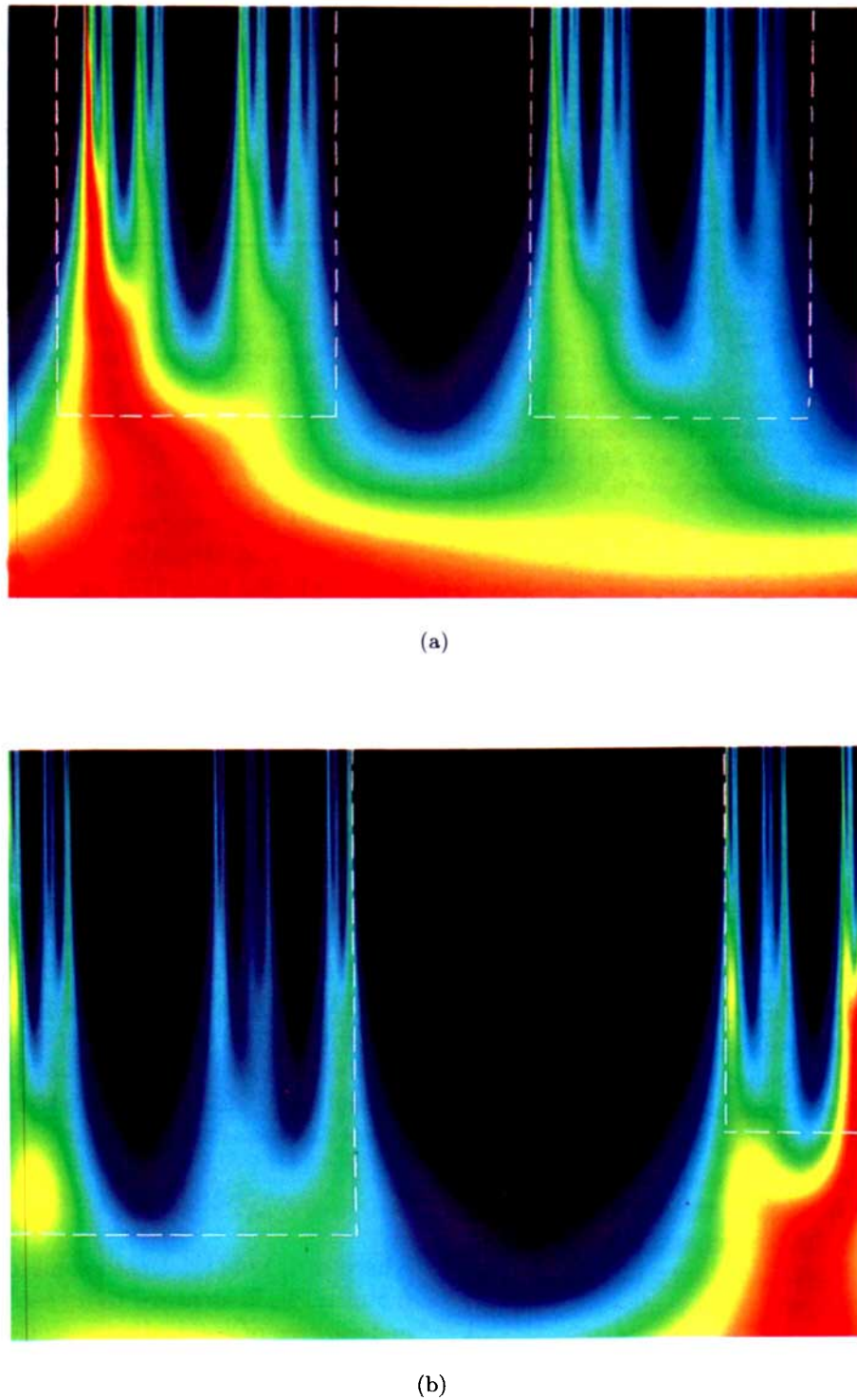


Fig. 16. Continuous wavelet transform of (a) a multifractal measure distributed nonuniformly on the triadic Cantor set with the weights $p_1 = 0.6$ and $p_2 = 0.4$ and (b) the natural measure of the period-doubling quadratic map $\Phi_*(x)$ [Eq. (75)]. The color coding is the same as in Fig. 13. The left (right) dashed rectangle corresponds to the renormalization operation R_1 (R_2) discussed in the text. The analyzing wavelet is the Gaussian function $\psi^{(0)}$.

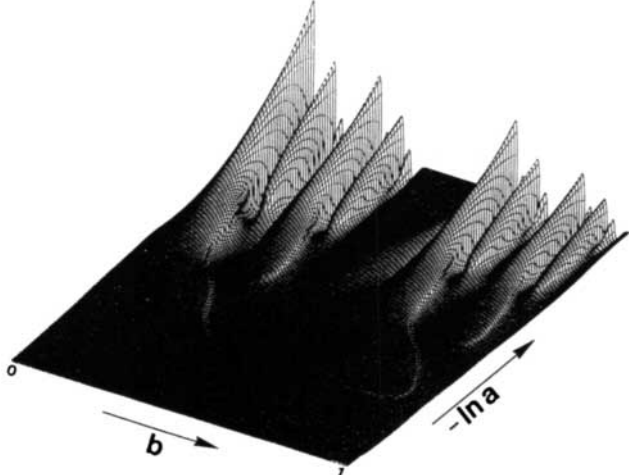


Fig. 17. 3D representation of the continuous wavelet transform ($a^{-2}T_\psi[\mu](b, a)$) of a multifractal measure distributed nonuniformly on the triadic Cantor set with the weights $p_1 = 0.6$ and $p_2 = 0.4$. The analyzing wavelet is the Mexican hat $\psi^{(2)}$.

monic bifurcations at each stage of which the period of the limit cycle is doubled. This period-doubling cascade accumulates at $R_c = 1.40115\dots$ where the system possesses a 2^∞ -orbit that displays scale invariance (Fig. 18). Beyond this critical value, the attractor becomes chaotic, even though there still exist parameter windows of periodic behavior. As originally emphasized by Coullet & Tresser [1978], Feigenbaum [1978, 1979] and Tresser & Coullet [1978], this scenario presents strong analogy with second-order phase transition in critical phenomena. Above criticality ($R > R_c$), the envelop of the Lyapunov characteristic exponent (which provides a quantitative estimate of chaos) displays a universal “order parameter” like behavior $\bar{L}(R) \sim (R - R_c)^\nu$, where ν is a universal exponent in the sense that it does not depend on the explicit form of the map but only on the quadratic nature of its maximum. Below criticality ($R < R_c$), the period of the bifurcating cycles is a “characteristic time” which diverges at the transition according to the scaling law $P(R) \sim (R_c - R)^{-\nu}$, with the same critical exponent $\nu = \ln 2 / \ln \lambda$ as for the Lyapunov exponent. This universal behavior results from the observation that the bifurcation parameter values R_n from an orbit of period 2^n to an orbit of period 2^{n+1} , converge to $R_c = R_\infty$ according to the geometric law $(R_c - R_n) \sim \lambda^{-n}$, where $\lambda = 4.669\dots$ for quadratic maps. Very much like the case in critical phenomena, Coullet & Tresser [1978], Feigenbaum [1978, 1979] and Tresser & Coullet [1978] have demon-

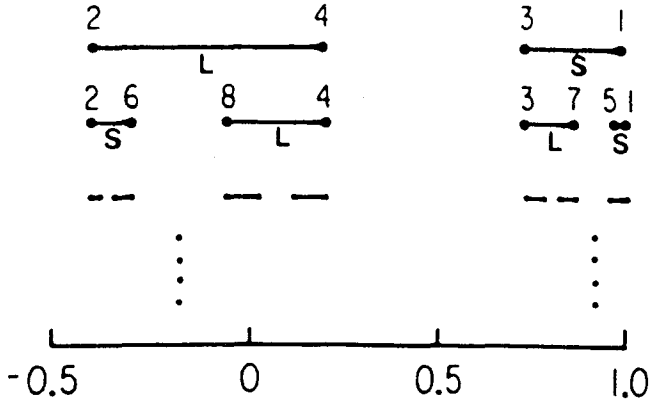


Fig. 18. The construction rule of the period-doubling Cantor set; the indices refer to the number n of the iterate $\Phi_{R_c}^{(n)}(0)$ of the critical point $x_c = 0$ of the map defined in Eq. (75).

strated that these universal properties can be understood using renormalization group techniques.

Indeed, at criticality $R = R_c$, the attractor of the quadratic map (73) exhibits scale invariance: the adherence of the asymptotic orbit of almost all initial conditions in the invariant interval is a Cantor set. As sketched in Fig. 18, the iterates of the critical point $x_c = 0$ form this Cantor set, with half of the iterates falling between $\Phi_{R_c}^{(3)}(0)$ and $\Phi_{R_c}^{(4)}(0)$, and the other half between $\Phi_{R_c}^{(2)}(0)$ and $\Phi_{R_c}^{(3)}(0)$. At the next stage of the construction process, each subinterval is again divided in two subintervals with equal probability and so on. Consequently, the visiting probability measure is symmetrically distributed with the weights $p_1 = p_2 = 1/2$. Actually, the critical map Φ_{R_c} belongs to the stable manifold of the fixed point Φ_* of the renormalization operation [Coullet & Tresser, 1978, 1981; Feigenbaum, 1978, 1979; Tresser & Coullet, 1978; Collet & Eckmann, 1980]:

$$\mathcal{R}(\Phi) = \alpha \Phi \circ \Phi \left(\frac{x}{\alpha} \right), \quad (74)$$

where $\alpha = 1/\Phi(1)$. Up to some dilation by a scale factor α , Φ_* is identical to its second iterate. In the generic case of quadratic maps, the functional equation $\Phi_* = \mathcal{R}(\Phi_*)$ was solved using truncated recursion formula [Derrida et al., 1979] and numerical algorithms [Coullet & Tresser, 1978; Feigenbaum, 1978, 1979; Tresser & Coullet, 1978]:

$$\Phi_*(x) = 1 - 1.5276\dots x^2 + 0.1048\dots x^4 + \dots \quad (75)$$

with $\alpha = -2.5029\dots$. Later on, rigorous mathematical proofs were carried out by Campanino &

Epstein [1980], Epstein & Lascoux [1981], Campanino *et al.* [1982], Lanford [1982, 1984] and Epstein [1986]. Since Φ_{R_c} belongs to the stable manifold of Φ_* , their respective invariant measures display similar multifractal characteristics. In particular, it was shown that the $f(\alpha)$ singularity spectrum of the invariant measure of Φ_* is universal [Halsey *et al.*, 1986; Collet *et al.*, 1987]. Moreover Ledrappier & Misiurewicz [1985] succeeded in proving that this measure can be considered as the invariant measure obtained by iterating backward the following dynamical system defined on the interval $A = [\Phi_*(1), 1]$:

$$T(x) = \begin{cases} T_1(x) = x/\Phi_*(1) & \text{if } x \in [\Phi_*(1), x^*], \\ T_2(x) = \Phi_*(x)/\Phi_*(1) & \text{if } x \in [x^*, 1], \end{cases} \quad (76)$$

where x^* is the fixed point of Φ_* in A [$\Phi_*(x^*) = x^*$]. The construction rule of the period-doubling Cantor set $J^* = \cap_{n=0}^{+\infty} T^{-n}(A)$ is illustrated in Fig. 19.

Let us point out that, as compared to the Bernoulli measures distributed on generalized Cantor sets, the self-similarity properties of the invariant measure of critical period-doubling dynamical systems depend dramatically on the fact that one branch of $T(x)$, i.e., $T_2(x) = \Phi_*(x)/\Phi_*(1)$ is nonlinear. Nevertheless, if one supposes again that the analyzing wavelet has a compact support, one can

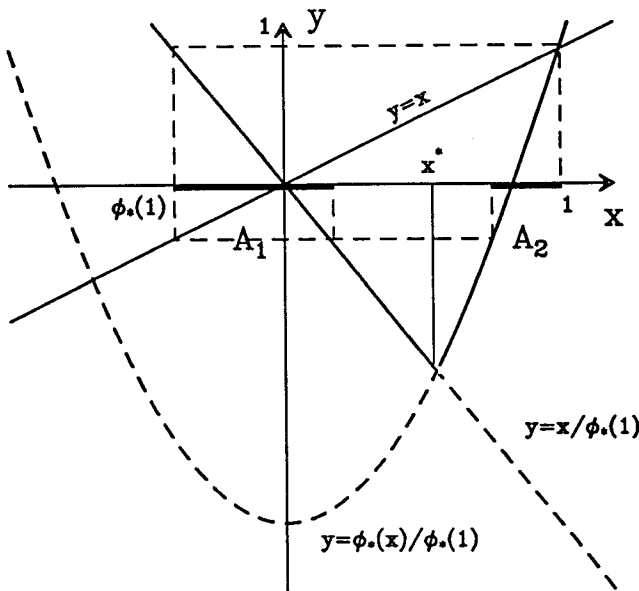


Fig. 19. The natural measure of the critical quadratic map $\Phi_*(x)$ [Eq. 75] as “seen” as the invariant measure of the hyperbolic mapping $T(x)$ defined in Eq. (76).

investigate the self-similarity properties of the wavelet transform in the same way as for invariant measures of piece-wise linear maps:

$$\begin{aligned} T_\psi[\mu](b, a) &= \int_A \psi\left(\frac{x-b}{a}\right) d\mu, \\ &= 2 \int_{A_k} \psi\left(\frac{T(x)-b}{a}\right) d\mu, \end{aligned} \quad (77)$$

where $A_1 = A \cap T_1^{-1}(A)$ and $A_2 = A \cap T_2^{-1}(A)$ (Fig. 19). Now using the fact that $|T'|$ is bounded on A by two constants larger than 1, for a small enough the above integral can be restricted to a subinterval of the form $[b' - c_1 a, b' + c_2 a]$, where $b' = T_k^{-1}(b)$. Then, after expanding $T(x) - T(b')$ at first order, one can rewrite Eq. (77) in the following form:

$$\begin{aligned} T_\psi[\mu](b, a) &= 2 \int_{A_k} \psi\left(\frac{x-b'}{a} T'(b') + O(a)\right) d\mu, \\ &= 2T_\psi[\mu](T_k^{-1}(b), T_k^{-1}'(b)a)[1 + O(a)], \end{aligned} \quad (78)$$

where we have implicitly assumed that $T_\psi[\mu](b, a) = O(T_\psi[\mu](b, a))$. This relation accounts for the self-similarity properties of the wavelet transform of the natural measure associated to the critical quadratic map Φ_* [Eq. (75)], in the limit $a \rightarrow 0^+$. Let us note that the main difference between this new relation and Eq. (70), is the fact that the dilation factor in the right-hand side of Eq. (78) depends explicitly on the point b as a direct consequence of the nonlinearity of T . A color coding of $T_\psi[\mu](b, a)$ is shown in Fig. 16(b), in comparison with the wavelet transform of a nonuniform measure distributed on the triadic Cantor set [Fig. 16(a)] [Arneodo *et al.*, 1988, 1989a, 1989b, 1990, 1992a]. The analyzing wavelet is the Gaussian function $\psi^{(0)}$. The two dashed rectangles illustrate the two renormalization operations R_1 and R_2 associated respectively to the two branches T_1^{-1} and T_2^{-1} of the inverse mapping T^{-1} [Muzy, 1993]:

$$\begin{aligned} R_1 : \mathbb{R} \times \mathbb{R}^{+*} &\rightarrow \mathbb{R} \times \mathbb{R}^{+*}, \\ (b, a) &\rightarrow (T_1^{-1}(b), aT_1^{-1}'(b)), \\ R_2 : \mathbb{R} \times \mathbb{R}^{+*} &\rightarrow \mathbb{R} \times \mathbb{R}^{+*}, \\ (b, a) &\rightarrow (T_2^{-1}(b), aT_2^{-1}'(b)). \end{aligned} \quad (79)$$

The self-similarity of the wavelet transform in the space-scale half-plane observed in Fig. 16(b) is thus contained in Eq. (78). The multifractality of the invariant measure of the critical quadratic map $\Phi_*(x)$

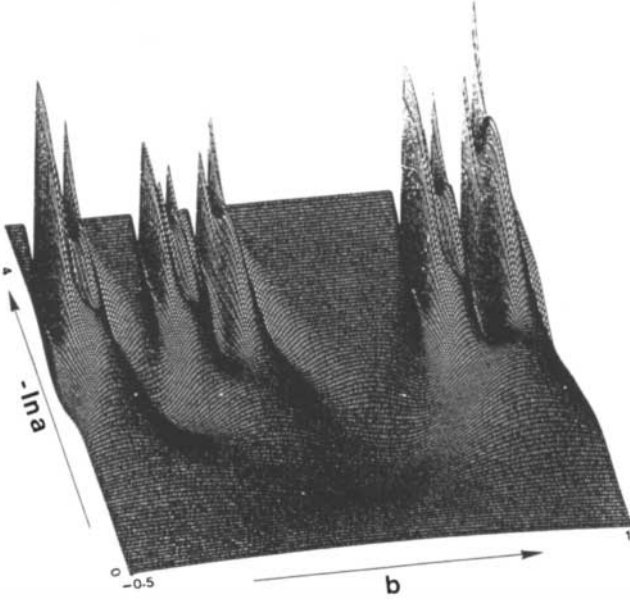


Fig. 20. 3D representation of the continuous wavelet transform ($a^{-1}T_\psi[\mu](b, a)$) of the invariant measure of the critical quadratic map $\Phi_*(x)$ [Eq. (75)]. The analyzing wavelet is the Mexican hat $\psi^{(2)}$.

is conspicuous in the 3D representation of the wavelet transform shown in Fig. 20. The singularity exponent $\alpha(x)$ clearly fluctuates from point to point on the period-doubling Cantor set. In the concluding section, we will elaborate on a very promising attempt to solve the inverse fractal problem, taking advantage of the self-similarity properties of the wavelet transform in the space-scale half-plane [Eqs. (70) and (78)].

4.2. The multifractal formalism for singular measures revisited with wavelets

In Sec. 4.1, we already pointed out that if one takes an analyzing wavelet ψ which is the box function $\chi_{[0,1]}$ (i.e., the characteristic function of the interval $[0, 1]$), then Eqs. (62) and (63) become the same. Indeed, $\mu(B_{x_0}(\varepsilon))$ is nothing but the wavelet transform of μ using $x[0, 1]$ as the analyzing wavelet. In this way, Eq. (63) can be seen as a “generalization” of Eq. (62). However, it is a generalization not only because it holds for any wavelet ψ but also because it still holds when “perturbing” μ with regular behavior (provided n_ψ is large enough). As we have emphasized at the end of Sec. 4.1.1, this last point is the main reason why we advocate the use of wavelets instead of “boxes”: our goal is to get rid of

possible smooth behavior that could mask the singularities or perturb the estimate of their strength α and would thus lead to dramatic errors in the computation of the singularity spectrum (as an exercise just consider that μ is “perturbed” by a uniform measure on $[0, 1]$ and try to apply Eq. (62)...). Our aim is to revisit the multifractal formalism in substituting the box functions by wavelets. Let μ be a “purely” singular measure. A “naive” way to proceed would be to define the new following partition functions [Holschneider, 1988b; Arneodo et al., 1991, 1992b; Muzy et al., 1991, 1992; Bacry et al., 1993]:

$$K(q, a) = \int |T_\psi[\mu](x, a)|^q dx, \quad (80)$$

where $q \in \mathbb{R}$. One can prove that this definition would lead to a consistent multifractal formalism for positive values of q only [Bacry et al., 1993; Muzy, 1993]. Indeed, nothing prevents $T_\psi[\mu](b, a)$ from vanishing at some points (b, a) of the space-scale half-plane (even for b in the support of μ). The function $K(q, a)$ would then diverge for $q < 0$; thus, Eq. (80) is not a good definition of a partition function.

In order to avoid these divergencies, we could change the continuous sum over space in Eq. (80) into a discrete sum over the maxima of $|T_\psi[\mu](x, a)|$ (considered as a function of x). As seen in Sec. 4.1.2, the maxima lines satisfy two main properties [Muzy et al., 1991, 1993a, 1993b; Mallat & Hwang, 1992; Bacry et al., 1993]:

- (i) They follow the same renormalization rules as the wavelet transform itself and thus, reproduce the hierarchical structure of the fractal measure μ (see Figs. 13 and 14).
- (ii) Each line $l = \{b_l(a), a\}$ is pointing (when a goes to 0) towards a point $b_l(0)$ which corresponds to a singularity of μ ; moreover, along such a line the wavelet transform behaves like

$$T_\psi[\mu](b_l(a), a) \sim a^{\alpha(b_l(0))}. \quad (81)$$

[The maxima line l is then said to be *associated* with the exponent $\alpha(b_l(0))$].

Let $N_\alpha(a)$ be the number of maxima lines, at the scale a , associated with the same exponent α . From (i) and (ii), one can prove that $N_\alpha(a)$ scales like

$$N_\alpha(a) \sim a^{-f(\alpha)}. \quad (82)$$

This result has been proved rigorously by Bacry et al. [1993] in the case of Bernoulli measures. It

can be intuitively understood by saying that the maxima lines reproduce the hierarchical structure of μ , i.e., when a goes to 0, the rate of multiplication (when constructing μ) of singularities corresponding to the exponent α (which is by definition $a^{-f(\alpha)}$) is given by the rate of multiplication of maxima lines (in the wavelet transform skeleton) associated to the exponent α .

Example

- Let us illustrate this result with a very simple case: the uniform measure lying on the triadic Cantor set. From Sec. 2.2.1, we know that this measure is homogeneous and that its singularity spectrum is represented by a single point $f(D_H) = D_H$ where $D_H = \ln 2 / \ln 3$ is the Hausdorff dimension of the support of μ . Then, according to Eq. (82), $N(a) = N_{D_H}(a) \sim a^{-D_H}$. In Figs. 13(b) and 14(b) are displayed the maxima lines (in the space-scale half-plane) of μ computed with the analyzing wavelet $\psi^{(0)}$ (Gaussian function) and $\psi^{(2)}$ (Mexican hat) respectively. Both figures reveal clearly the hierarchical structure of μ . One can “read” the self-similarity of μ in these perfect symmetric “forkings” which look exactly the same at any scale. One can estimate easily the multiplication rate of the maxima lines: each of the $N(a)$ maxima lines at the scale a is going to give birth to two maxima lines at the scale $a/3$. Thus we found the expected result $N(a) = N_0 a^{-\ln 2 / \ln 3}$. Let us note that the constant N_0 depends basically on the shape of the analyzing wavelet we use; it is generally proportional to the number of vanishing moments n_ψ of ψ [Muzy *et al.*, 1991, 1993a, 1993b; Bacry *et al.*, 1993].

Let us come back to the original purpose: the definition of wavelet based partition functions. As suggested before, in order to avoid the divergence of the partition functions for $q < 0$, we could change the continuous sum in Eq. (80) into a discrete sum over the maxima of $|T_\psi[\mu](x, a)|$ (considered as a function of x) only. We then obtain the following partition function [Arneodo *et al.*, 1991; Muzy *et al.*, 1991, 1993a, 1993b; Bacry *et al.*, 1993]:

$$\mathcal{Z}(q, a) = \sum_{l \in \mathcal{L}(a)} |T_\psi[\mu](b_l(a), a)|^q, \quad (83)$$

where $\mathcal{L}(a)$ is the set of all the maxima lines l existing at the scale a , and $b_l(a)$ is the position, at the scale a , of the maximum belonging to the line

l . Then by using Eq. (81), the partition function $\mathcal{Z}(q, a)$ becomes

$$\mathcal{Z}(q, a) \sim \sum_{\alpha} N_{\alpha}(a) (a^{\alpha})^q, \quad (84)$$

and by substituting the expression of N_{α} given in Eq. (82), one gets

$$\begin{aligned} \mathcal{Z}(q, a) &\sim \sum_{\alpha} a^{(q\alpha - f(\alpha))}, \\ &\sim a^{\min_{\alpha} (q\alpha - f(\alpha))}. \end{aligned} \quad (85)$$

Thus, if $\tau(q)$ is the scaling exponent characterizing the power-law behavior of $\mathcal{Z}(q, a)$:

$$\mathcal{Z}(q, a) \sim a^{\tau(q)}, \quad (86)$$

we then obtain

$$\tau(q) = \min_{\alpha} (q\alpha - f(\alpha)) = \tau_B(q), \quad (87)$$

where $\tau_B(q)$ is the exponent defined in Eq. (16) corresponding to the “standard box-counting” multifractal formalism. It means that the newly defined multifractal formalism is consistent with the classical formalism originally introduced for singular measures: it allows us to obtain the $f(\alpha)$ singularity spectrum of a multifractal measure μ as the Legendre transform of the $\tau(q)$ function. However, the definition (83) is not quite convenient since it is unstable for negative values of q , very much like fixed-size box-counting algorithms. Indeed, let us suppose that along a maxima line the value of the wavelet transform goes from positive to negative values; then there is a scale where the maximum of $|T_\psi[\mu]|$ is 0! It corresponds to an inflection point of the wavelet transform (considered at a fixed scale a). So we need to change slightly the definition of the partition function by replacing the value of the wavelet transform modulus at each maximum by the supremum value along the corresponding maxima line at scales smaller than a [Arneodo *et al.*, 1991; Muzy *et al.*, 1991, 1993a, 1993b; Bacry *et al.*, 1993]:

$$\mathcal{Z}(q, a) = \sum_{l \in \mathcal{L}(a)} \left(\sup_{a' \leq a} |T_\psi[\mu](b_l(a'), a')| \right)^q \sim a^{\tau(q)}. \quad (88)$$

We have proved rigorously, that for any Bernoulli measure μ and for a large class of analyzing wavelets ψ , the Legendre transform of the so defined $\tau(q)$

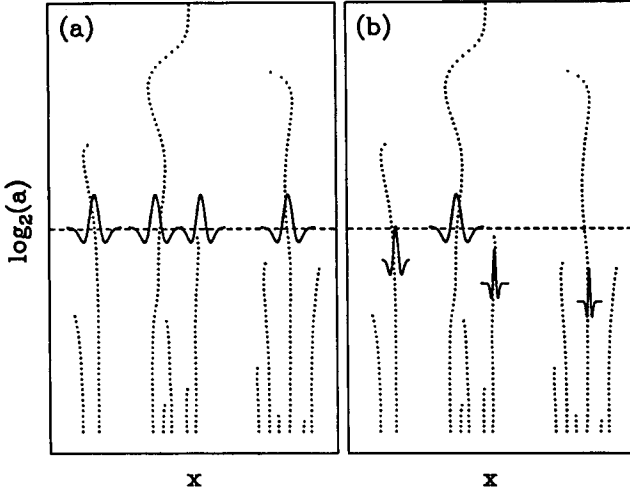


Fig. 21. Representation of the uniform [Eq. (83)] and scale-adapted [Eq. (88)] partitions. (a) Uniform partition: $\mathcal{Z}(q, a)$ involves wavelets of the same size a . (b) Scale-adapted partition: $\mathcal{Z}(q, a)$ involves wavelets of different sizes $a' \leq a$.

function is the $f(\alpha)$ singularity spectrum of μ [Bacry et al., 1993]. Numerical examples are given in Sec. 5.

Let us note that this new definition of $\mathcal{Z}(q, a)$ corresponds to a “scale-adapted” partition with wavelets at different sizes (smaller than a) whereas the former definition (83) uses a uniform partition [Arneodo et al., 1991; Muzy et al., 1991; 1993a, 1993b; Bacry et al., 1993]. This is illustrated in Fig. 21 where the support of the measure is covered with wavelets centered at the maxima positions (instead of covering the support with boxes along the line of the “standard” multifractal formalism).

4.3. Generalization of the multifractal formalism to fractal distributions: the wavelet transform modulus maxima method

Before describing how this new multifractal formalism can be used to analyze any fractal distribution, we need to define the notion of singularity spectrum of a distribution. The Hölder exponent $h(x_0)$ [Eq. (53)] provides a quantitative characterization of the degree of regularity of a distribution s at the point x_0 . It is thus natural to use it in order to define the singularity spectrum of a distribution.

Definition 4. Let s be a distribution and S_h the set of all the points x_0 so that the Hölder exponent of s in x_0 is h . The singularity spectrum $D(h)$ of

s is the function which associates with any h the Hausdorff dimension of S_h :

$$D(h) = d_H(\{x_0 \in \mathbb{R}, h(x_0) = h\}). \quad (89)$$

Let us note that when the distribution s is a singular measure with no density component, the exponent $\alpha(x_0)$ defined in Eq. (62) is related to the Hölder exponent $h(x_0)$ according to

$$h(x_0) = \alpha(x_0) - 1. \quad (90)$$

Therefore the $D(h)$ spectrum of Hölder exponents is obtained by just translating $f(\alpha)$ by 1 [Muzy, 1993]:

$$D(h = \alpha - 1) = f(\alpha). \quad (91)$$

This comes from the fact that instead of considering μ as a measure, we consider it as a distribution. In the following, we will only talk about distributions and the term *singularity spectrum* will always refer to $D(h)$.

As in Eq. (88), let us define the partition function for any $q \in \mathbb{R}$ [Bacry et al., 1993; Muzy et al., 1993a, 1993b]:

$$\mathcal{Z}(q, a) = \sum_{l \in \mathcal{L}(a)} \left(\sup_{a' \leq a} |T_\psi[s](b_l(a'), a')| \right)^q. \quad (92)$$

The exponent $\tau(q)$ is then given by

$$\mathcal{Z}(q, a) \sim a^{\tau(q)}, \quad (93)$$

in the limit $a \rightarrow 0^+$. We then suggest the following theorem:

Theorem 2. *The $D(h)$ singularity spectrum of the distribution s is obtained by Legendre transforming the function $\tau(q)$ defined in Eq. (93):*

$$D(h) = \min_q (qh - \tau(q)). \quad (94)$$

Both the $D(h)$ and $\tau(q)$ spectra involved in this new multifractal formalism are much more general than the ones defined in the “standard” multifractal formalism described in Sec. 2.2. The above theorem is likely to hold for a very large class of fractal objects. For rigorous results concerning this new formalism we refer the reader to the work of Bacry et al. [1993] and Jaffard [1993].

Remark. In Sec. 5, we will present some numerical applications of this wavelet based multifractal formalism. From a numerical point of view, in order

to compute $D(h)$ we will either directly perform the Legendre transform of $\tau(q)$ [Eq. (94)] or calculate two intermediate partition functions:

$$h(q, a) = \sum_{l \in \mathcal{L}(a)} \tilde{T}_\psi[f](q, l, a) \times \ln \left| \sup_{a' \leq a} T_\psi[f](b_l(a'), a') \right|, \quad (95)$$

and

$$D(q, a) = \sum_{l \in \mathcal{L}(a)} \tilde{T}_\psi[f](q, l, a) \ln \tilde{T}_\psi[f](q, l, a), \quad (96)$$

from which we will extract the scaling exponents

$$h(q) = \lim_{a \rightarrow 0^+} \frac{1}{\ln a} h(q, a), \quad (97)$$

and

$$D(q) = \lim_{a \rightarrow 0^+} \frac{1}{\ln a} D(q, a), \quad (98)$$

and in turns $D(h)$. This alternative method is inspired from the so-called canonical method [Badii, 1987; Jensen *et al.*, 1987; Chhabra & Jensen, 1989; Chhabra *et al.*, 1989], which requires first the computation of the “Boltzmann probability measure” from the wavelet transform modulus maxima:

$$\tilde{T}_\psi[f](q, l, a) = \left| \sup_{a' \leq a} T_\psi[f](b_l(a'), a') \right|^q / \mathcal{Z}(q, a), \quad (99)$$

where $\mathcal{Z}(q, a)$ is the partition function defined in Eq. (88). In the following, both methods will be referred to as the wavelet transform modulus maxima (WTMM) method [Arneodo *et al.*, 1991; Muzy *et al.*, 1991, 1993a, 1993b; Bacry *et al.*, 1993]. Generally, they will give consistent results and robust estimates of the $D(h)$ singularity spectrum.

Interpretation of $\tau(q)$ for some values of q .

- For $q = 0$, one can see from Eqs. (92) and (93) that the exponent $\tau(0)$ accounts for the divergence of the number of maxima lines in the limit $a \rightarrow 0^+$. This number basically corresponds to the number of wavelets of size a required to cover the set of singularities of the distribution. In full analogy with standard box-counting arguments, $-\tau(0)$ can be identified to the fractal dimension (capacity) of this set:

$$-\tau(0) = d_C(\{x, h(x) < +\infty\}). \quad (100)$$

- For $q = 1$, one can prove that the value of the exponent $\tau(1)$ is related to the capacity of the graph \mathcal{G} of the considered distribution (provided \mathcal{G} is well defined). More precisely,

$$d_C(\mathcal{G}) = \max(1, 1 - \tau(1)). \quad (101)$$

- For $q = 2$, if β is the scaling exponent of the spectral density $\hat{S}(k) = |\hat{s}(k)|^2 \sim k^{-\beta}$, then one can show that

$$\tau(2) = \beta - 2. \quad (102)$$

5. Numerical and Experimental Applications of the Wavelet Transform Modulus Maxima Method

5.1. Generalized devil staircases

5.1.1. Deterministic and stochastic signals

Before applying the WTMM method to the analysis of experimental signals, it is important to test it on “simple” functions for which the singularity spectra can be computed analytically. In the former sections, we introduced the class of self-similar measures lying on “generalized” Cantor sets. These measures are constructed using some very basic recursive rules which make the analytic computation of their singularity spectra particularly easy. The corresponding distribution functions (i.e., $f(x) = \mu([0, x])$) are self-affine and are thus particularly “good” functions for testing numerically the WTMM method. Moreover, their singular behavior is exactly given by the singularities of their associated fractal measures. Therefore one can prove easily that the $D(h)$ singularity spectra of these functions are equal to the $f(\alpha)$ singularity spectra of μ [Arneodo *et al.*, 1991; Muzy *et al.*, 1991]:

$$D(h) = f(\alpha = h). \quad (103)$$

In this section, we illustrate the WTMM method on three such distribution functions and we compare the so-obtained singularity spectra to the theoretical spectra. Let us note that it has been proved that for any distribution function of a self-similar measure μ lying on a generalized Cantor set and for a large class of analyzing wavelets, the WTMM method converges to the singularity spectrum of μ . This is equivalent to saying that for these particular functions both Eqs. (93) and (94) hold. For the

proof of this theorem we refer the reader to Bacry *et al.* [1993].

Examples

- Let μ be the uniform measure lying on the triadic Cantor set ($p_1 = p_2 = 1/2$), and $f(x) = \mu([0, x])$ the so-called devil staircase. The function f is shown in Fig. 22(a). Figure 22(b) illustrates its wavelet transform coded, independently at each scale, using 32 grey levels. The analyzing wavelet is $\psi^{(1)}$ the first derivative of the Gaussian function. Figure 22(c) represents an horizontal cross section of $|T_\psi[f](x, a_0)|$ at a fixed scale a_0 corresponding to the dashed line in Fig. 22(b); the modulus maxima are marked by the symbols (\times). The skeleton of the wavelet transform is shown in Fig. 22(d). It is on these maxima lines that the partition function $Z(q, a)$ is computed according to Eq. (92). Let us note that the perfect similitude of the skeletons in Fig. 22(d) (the maxima lines of $T_{\psi^{(1)}}[f]$) and Fig. 13(b) (the maxima lines of $T_{\psi^{(0)}}[\mu]$) comes from the fact that the two wavelet transforms are proportional at every scale:

$$T_{\psi^{(1)}}[f] = -a T_{\psi^{(0)}}[\mu]; \quad (104)$$

this relation is simply derived by integrating Eq. (56) by parts. Figure 23(a) displays some

plots of $\log_2 Z(q, a)$ versus $\log_2 a$ for different values of q . Apart from the presence of the periodic oscillations of period $\log_2 3$ which reflects the invariance of the Cantor set under discrete dilations by a factor 3, these plots clearly display a linear behavior on the whole range of scales and this for any q . Using a linear regression fit, we then obtain the slopes $\tau(q)$ of these graphs. As illustrated in Fig. 23(b), $\tau(q)$ follows a linear curve, the slope of which provides an accurate estimate of the unique Hölder exponent $h = \ln 2 / \ln 3$ which characterizes the uniform triadic Cantor set. Actually, the data in Fig. 23(b) fit perfectly the theoretical curve $\tau_{th}(q) = (q - 1) \ln 2 / \ln 3$. This result is corroborated in Fig. 23(c) where $h(q)$ is determined, for different values of q , by plotting $h(q, a)$ versus $\log_2 a$ [Eq. (97)]. The slope of these graphs is $h = \ln 2 / \ln 3$, independently of q . Then by Legendre transforming $\tau(q)$ [Eq. (94)], one gets, up to the experimental uncertainty, that the singularity spectrum reduces to a single point $D(h = \ln 2 / \ln 3) = \ln 2 / \ln 3$, i.e., the Hausdorff dimension of the triadic Cantor set [Fig. 23(d)] [Arneodo *et al.*, 1991; Muzy *et al.*, 1991; Bacry *et al.*, 1993].

Let us note that although this example could seem too “simple,” it is a basic example for which

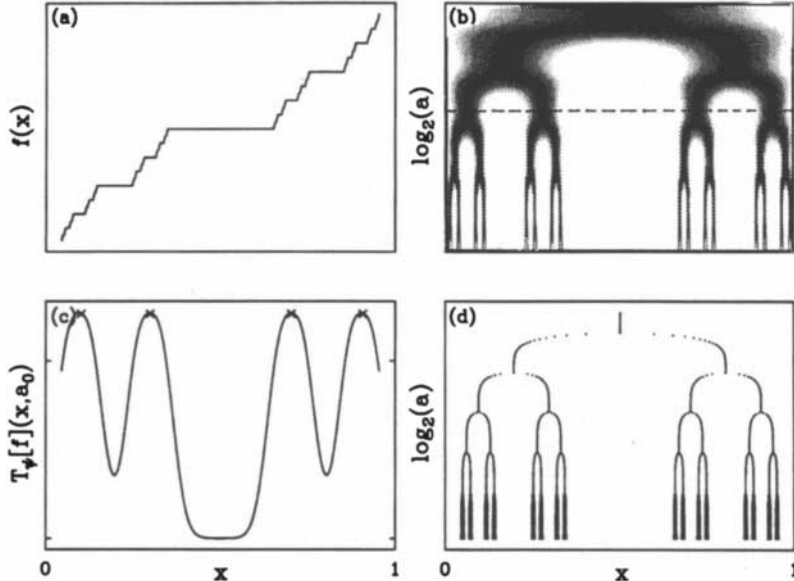


Fig. 22. Continuous wavelet transform of the devil staircase corresponding to the uniform triadic Cantor set. (a) Graph of the function. (b) Wavelet transform computed with the analyzing wavelet $\psi^{(1)}$; the amplitude is coded, independently at each scale a , using 32 grey levels from white ($T_\psi[f](x, a) < 0$) to black ($\max_x T_\psi[f](x, a)$). (c) Definition of the modulus maxima at a given scale a_0 corresponding to the dashed line in figure (b). (d) The skeleton of the wavelet transform, i.e., the set of all the maxima lines. In (b) and (d) the large scales are at the top.

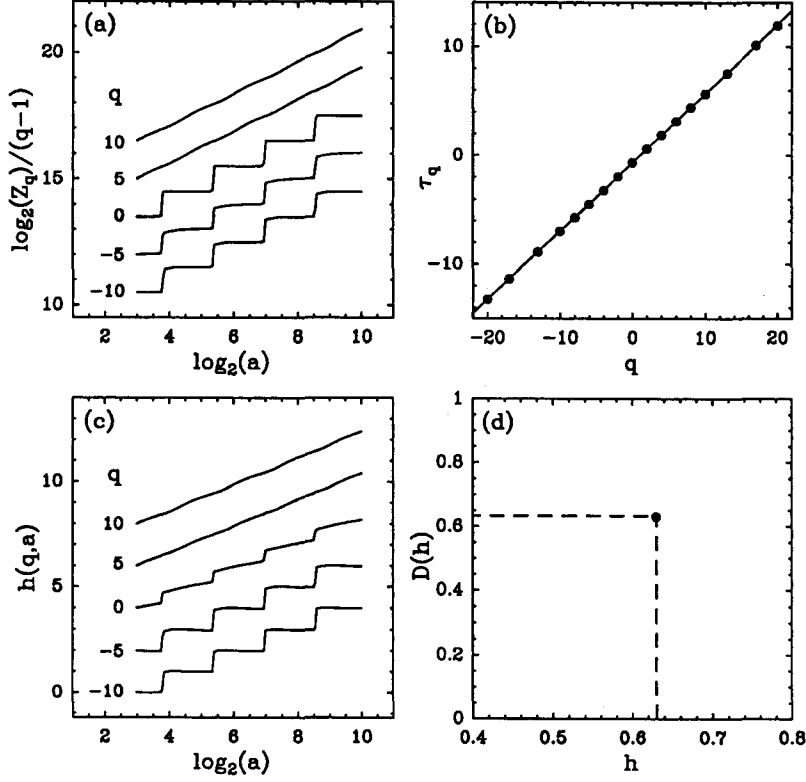


Fig. 23. Determination of the multifractal spectra of the devil staircase associated with the uniform triadic Cantor set using the WTMM method. (a) $\log_2 Z(q, a)/(q - 1)$ versus $\log_2 a$. (b) $\tau(q)$ versus q ; the solid line corresponds to the theoretical curve $\tau(q) = (q - 1) \ln 2 / \ln 3$. (c) Determination of the exponents $h(q)$; $h(q, a)$ is plotted versus $\log_2 a$ according to Eq. (97). (d) $D(h)$ versus h . The analyzing wavelet is $\psi^{(1)}$.

the use of the WT maxima lines to partition the signal is crucial. Indeed, as the singularities of f are lying on a set which is of Lebesgue measure 0, a continuous sum over the whole domain $[0, 1]$ would lead to drastic errors [Muzy *et al.*, 1993a].

- Let f be the generalized devil staircase associated to the self-similar measure μ constructed recursively as follows: each interval at each step of the construction is divided into four subintervals of the same length on which we distribute respectively the weights $p_1 = 0.69$, $p_2 = -p_3 = 0.46$ and $p_4 = 0.31$. One of the weights has been chosen negative so that the so-obtained measure is signed. This definition is consistent as far as the relation $p_1 + p_2 + p_3 + p_4 = 1$ holds. Let us note that in the case of a distribution function of a signed measure, the relation $\tau(1) = 0$ does not hold *a priori* since the “norm” $\sum_{L(a)} |T_\psi(b_l(a), a)|$ is no longer conserved through the scales; it diverges when a goes to 0. Actually, one can prove that in this particular case, $\tau(q)$ is given by the relation [Arneodo *et al.*, 1991; Muzy *et al.*, 1991]

$$\tau(q) = -\ln_4(|p_1|^q + |p_2|^q + |p_3|^q + |p_4|^q). \quad (105)$$

Figure 24(a) displays the distribution function $f(x) = \mu([0, x])$, whereas Fig. 24(b) shows the

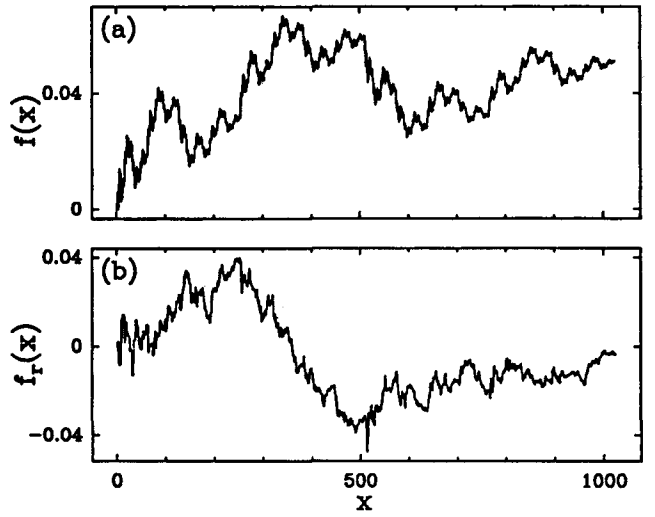


Fig. 24. Graphs of the generalized devil staircases. (a) Deterministic signal $f(x) = \mu([0, x])$. (b) Random signal $f_r(x) = \mu_r([0, x])$. μ and μ_r are signed measures.

distribution function $f_r(x) = \mu_r([0, x])$ which is constructed exactly in the same way as f except that, at each step of the construction, the order of the weights is chosen randomly. Their wavelet transforms are illustrated in Figs. 25(a) and 25(b) respectively. In the case of the random distribution function f_r , the partition function is averaged

over the realizations of the random process, i.e.,

$$\mathcal{Z}_r(q, a) = \langle \mathcal{Z}(q, a) \rangle_{\text{real.}} \sim a^{\tau_r(q)}. \quad (106)$$

Clearly, as the analytical expression (105) of $\tau(q)$ does not depend on the specific order of p_1, p_2, p_3 and p_4 , one deduces easily that $\tau_r(q) = \tau(q)$.

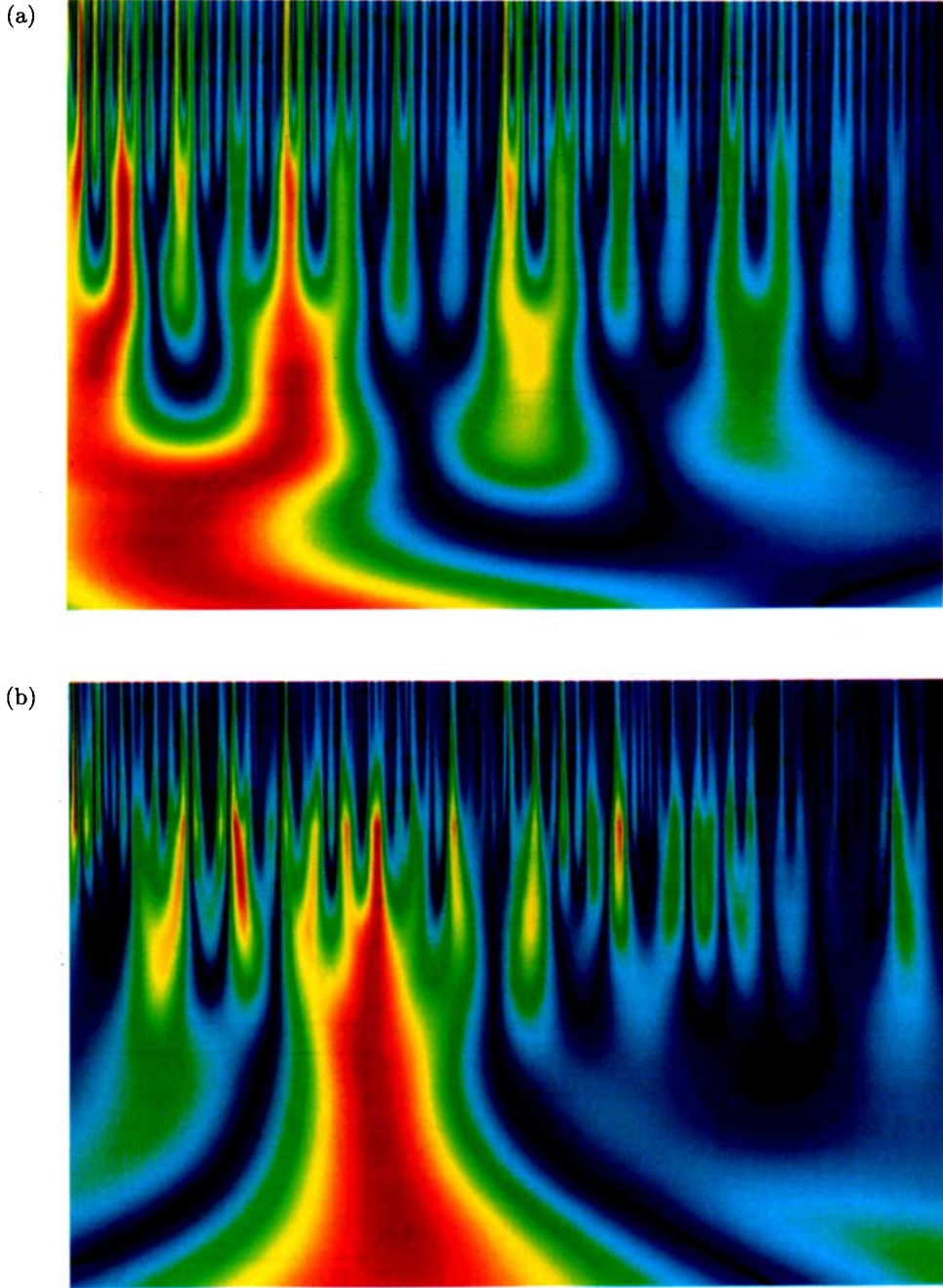


Fig. 25. Continuous wavelet transforms of (a) the deterministic devil staircase f shown in Fig. 24(a), and (b) the random devil staircase f_r shown in Fig. 24(b). The analyzing wavelet is $\psi^{(1)}$. Same color coding as in Fig. 13. The small scales are at the top.

The results of the multifractal analysis of f and f_r using the WTMM method are reported in Fig. 26 [Arneodo *et al.*, 1991; Muzy *et al.*, 1991]. As shown in Fig. 26(b), the functions $\tau(q)$ and $\tau_r(q)$ are nonlinear convex increasing functions. The numerical data both for the deterministic signal (\bullet) and the random signal (\blacktriangle) match perfectly the theoretical prediction given by Eq. (105). The corresponding $D(h)$ singularity spectra obtained by Legendre transforming $\tau(q)$ and $\tau_r(q)$ are displayed in Fig. 26(d); their single humped shapes are characteristic of multifractal signals. The support of $D(h)$ extends over a finite interval $h_{\min} \leq h \leq h_{\max}$. This nonuniqueness of the Hölder exponent is confirmed in Fig. 26(c), where the exponent $h(q)$, computed directly from Eq. (97), clearly evolves from the value $h_{\min} \simeq 0.28$ to $h_{\max} \simeq 0.82$ when q varies from $q = 10$ to $q = -10$. The maximum of the $D(h)$ curve is obtained for $q = 0$: $D(h(q = 0)) = -\tau(0) = D_F = 1$. The generalized devil staircases in Fig. 24 are thus everywhere singular signals that display

multifractal properties; the fractal dimension of the support of the set of singularities of these distribution functions is $D_F = 1$.

5.1.2. The structure function approach versus the wavelet transform modulus maxima method

The efficiency of the WTMM method comes from two basic points [Arneodo *et al.*, 1991; Muzy *et al.*, 1991]. First, it is based on the wavelet transform of the signal; thus it can be adjusted easily (mainly by changing the analyzing wavelet) to the particular singular behavior involved in the analyzed signal. Furthermore, it uses the modulus maxima of the wavelet transform so that the partition automatically covers only the points where the signal is singular. These two capital features are clearly missing to the structure function (SF) method introduced by Frisch & Parisi [1985]. However, this method has been playing a very important role in the context of fully developed turbulence and it constitutes

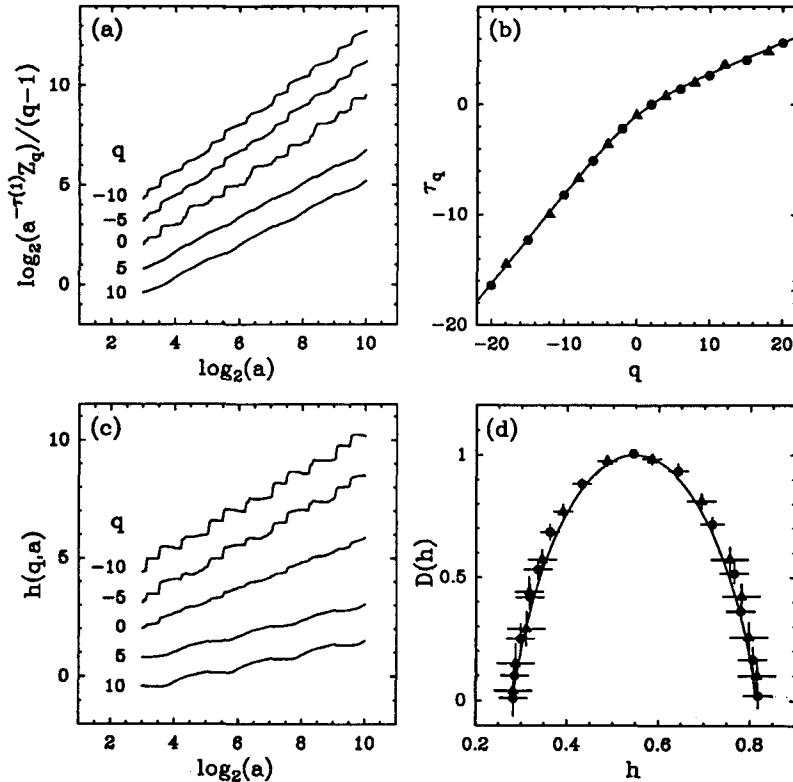


Fig. 26. Determination of the multifractal spectra of the devil staircases displayed in Fig. 24 using the WTMM method. (a) $\log_2 a^{-\tau^{(1)}Z_q}/(q-1)$ versus $\log_2 a$. (b) τ_q versus q ; the solid line corresponds to the theoretical curve given by Eq. (105). (c) Determination of the exponents $h(q)$; $h(q, a)$ is plotted versus $\log_2 a$ according to Eq. (97). (d) $D(h)$ versus h ; the solid line corresponds to the theoretical spectrum. The analyzing wavelet is $\psi^{(2)}$. In (b) and (d) the symbols correspond to the data obtained for the deterministic (\bullet) and the random (\blacktriangle) signal.

historically a first step towards a multifractal formalism for fractal signals [Frisch & Orszag, 1990; Barabási & Vicsek, 1991; Family & Vicsek, 1991]. It has been applied and is still very often used to analyze experimental fractal signals. A direct comparison of the SF and WTMM methods when applied on specific examples is thus of great interest for future analysis.

In this subsection we review the main situations where the SF method leads to drastic bias whereas the WTMM method provides reliable results. We illustrate these bias on simple numerical examples. The very interesting case of the influence of C^∞ behavior on the computation of the $D(h)$ singularity spectrum will be studied in Sec. 5.2.

Divergencies for negative values of q . Let us recall that in the definition initially proposed by Frisch & Parisi [1985], the structure functions $S_p(l)$ [Eq. (36)] are not defined for negative values of p . Indeed, there is no reason *a priori* that the probability density of the increments δf_l of a function f should vanish around 0. Consequently, the Legendre transform [Eq. (37)]

$$D_{SF}(h) = \min_q (qh - \zeta_q) + 1 \quad (107)$$

is valid only for $q \geq 0$. Therefore, if the singularity spectrum is a single humped function [Fig. 26(d)], only the increasing part of $D(h)$ corresponding to the strongest singularities is accessible to the SF method.

Let us note that in order to circumvent this difficulty, Barabási & Vicsek [1991] have used a slightly different SF method for studying the multifractal properties of some rough interfaces in nonequilibrium growth phenomena. They defined the following “correlation functions of order q ”:

$$C_q(l) = \langle |f(x+l) - f(x)|^q \rangle \sim l^{\zeta_q}, \quad (108)$$

where the spatial average is performed only on the terms so that $\delta f_l(x) = |f(x+l) - f(x)| \neq 0$. Then $C_q(l)$ can be defined for any values of q . However, this definition is totally artificial and does not cure at all the divergency problems encountered for $q < 0$. Practically, this method consists in not taking into account the increments which are smaller than a given threshold. Since this artificial “cut-off” is scale independent; the self-similarity is broken locally where the increments of the signal are small; note that the small increments are dominating in Eq. (108) for $q < 0$. This will lead in most cases to

a phase transition phenomenon in the ζ_q spectrum. This is exactly what Barabási & Vicsek [1991] did observe when studying a fractional Brownian motion. Indeed, let B_H be a fractional Brownian motion of parameter H [Eq. (31)]. The corresponding increments δB_H are Gaussian and stationary. Thus their spatial averages can be computed using an ergodic formula [Azencott & Dacunha-Castelle, 1984]. The spatial average of $C_q(l)$ is given by [Muzy et al., 1993a]:

$$\langle C_q(l) \rangle = \frac{l^{-H}}{2\sqrt{2\pi}} \int_c^\infty e^{-b^2/4l^{2H}} b^q db, \quad (109)$$

where $c > 0$ is the cut-off. When l is large enough one gets

$$\begin{aligned} \langle C_q(l) \rangle &\sim l^{qH} \int_c^\infty e^{-x^2} x^q dx, \\ &\sim l^{qH} (Cst + l^{-(q+1)H}), \\ &\sim l^{qH} + l^{-H}. \end{aligned} \quad (110)$$

One thus obtains the following expression for the exponent ζ_q

$$\zeta_q = \begin{cases} qH & \text{if } q > -1, \\ -H & \text{if } q < -1, \end{cases} \quad (111)$$

which differs from the theoretical prediction for a homogeneous fractal signal which is almost everywhere singular with a unique Hölder exponent $h = H$:

$$\zeta_q = qH. \quad (112)$$

The nonanalyticity of ζ_q for $q = -1$ in Eq. (111), can be understood as a phase transition in the scaling properties of the signal which results from an artefact of the method proposed by Barabási & Vicsek [1991].

This example clearly demonstrates that the divergencies encountered in the structure function method for negative values of q are really intrinsic to the method and generally cannot be avoided by using some numerical “tricks.” Therefore, only the increasing part of the singularity spectrum (corresponding to the strongest singularities) is potentially accessible to the SF method, whereas, in the case of the WTMM method, the use of the modulus maxima makes consistent the definition of the exponent $\tau(q)$ for any value of q . This will be illustrated in Sec. 5.3.1 where a detailed analysis of the $D(h)$

singularity spectrum of fractional Brownian motion using the WTMM method will be reported.

Limitations on the range of accessible Hölder exponents

(a) Singularities with negative Hölder exponents

The increments used in the SF method can be seen as wavelet coefficients using the analyzing wavelet $\Delta^{(1)} = \delta(x - 1) - \delta(x)$:

$$\begin{aligned} \delta f_l(x_0) &= T_{\Delta^{(1)}}[f](x_0, l) \\ &= l^{-1} \int_{-\infty}^{\infty} \Delta^{(1)}\left(\frac{x-x_0}{l}\right) f(x) dx. \end{aligned} \quad (113)$$

In the wavelet jargon, this wavelet is generally referred to as the “poor man’s wavelet” [Vergassola

& Frisch, 1991; Muzy *et al.*, 1993a]. Its extreme irregularity makes it a very unpleasant wavelet to work with. Indeed, $T_{\Delta^{(1)}}[f](b, a) = \langle f, \Delta_{b,a}^{(1)} \rangle$ is generally not defined when f is a distribution! In the particular case f has some singular behavior corresponding to negative Hölder exponents, Eq. (113) is theoretically not defined and the computation of the SF is numerically unstable. Thus using the SF method to analyze a signal which has discontinuities or stronger singularities may lead to unexpected results as a consequence of intrinsic drawbacks of this poor man’s wavelet based approach.

In Fig. 27, we show the results of both the SF and the WTMM analysis of a signal that possesses some singularities of negative Hölder exponents [Muzy *et al.*, 1993a]. The signal is a

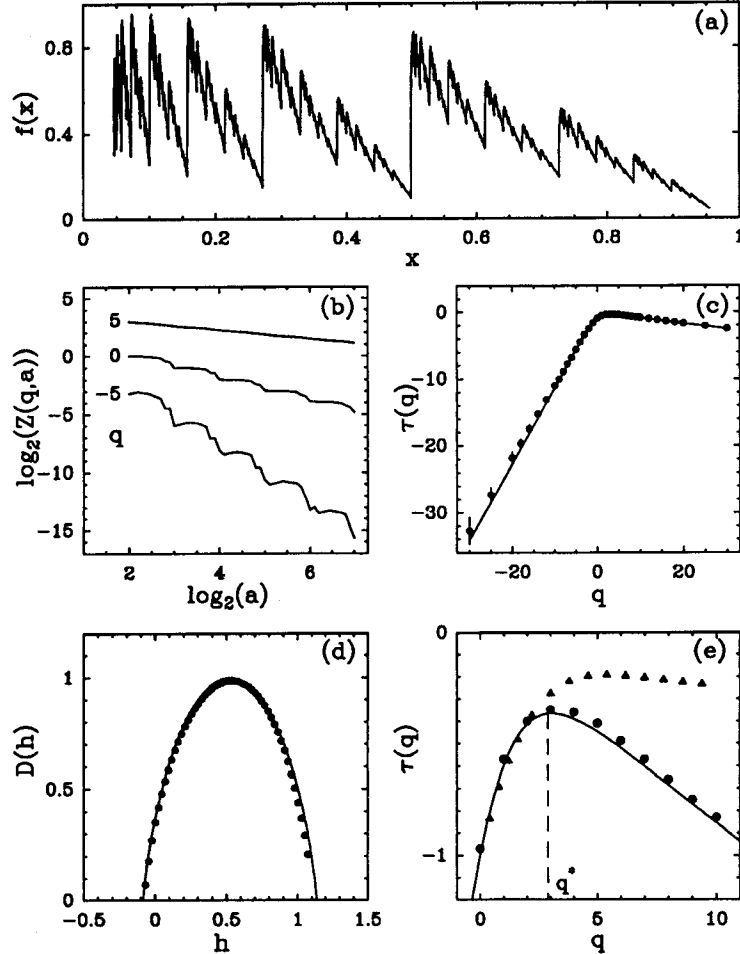


Fig. 27. WTMM and SF analysis of a multifractal signal with negative Hölder exponents. (a) Graph of the signal. This signal is a generalized devil staircase constructed from the recursive signed measure involving the weights $p_1 = 0.69$, $p_2 = -p_3 = 0.46$ and $p_4 = 0.31$; it has been fractionally differentiated with a coefficient $\beta = 0.6$. (b) $\log_2(Z(q, a))$ versus $\log_2 a$ for some values of q . (c) $\tau(q)$ spectrum obtained with the WTMM method; the analyzing wavelet is $\psi^{(2)}$. (d) $D(h)$ singularity spectrum obtained by Legendre transforming the numerical $\tau(q)$ data in (c). (e) Comparison of the $\tau(q)$ spectra obtained with the WTMM (\bullet) and the SF (\blacktriangle) methods. In (c), (d) and (e), the solid lines correspond to the theoretical spectra.

generalized devil staircase similar to the one illustrated in Fig. 24(a) (the weights are $p_1 = 0.69$, $p_2 = 0.46$, $p_3 = -0.46$ and $p_4 = 0.31$), but it has been fractionally differentiated with a coefficient $\beta = 0.6$ so that a part of the support of the $D(h)$ singularity spectrum is below 0 (a fractional derivation of a signal with a coefficient β induces a translation of the singularity spectrum to the left by a factor β [Schertzer & Lejevov, 1987]). In Fig. 27(a), one can notice the “jumps” in the signal which correspond to negative Hölder exponents. The theoretical singularity spectrum is represented by the solid line in Fig. 27(d); it extends over the range $[-0.1, 1.36]$. The analyzing wavelet is the mexican hat $\psi^{(2)}$. The results obtained when using the WTMM method are reported in Figs. 27(b), 27(c) and 27(d). As illustrated in Fig. 27(c), the numerical data for $\tau(q)$ fall on a convex nonlinear curve which is particularly well fitted by the theoretical $\tau(q)$ spectrum. Its Legendre transform $D(h)$ in Fig. 27(d) is a single humped curve characteristic of a multifractal signal; it is also in remarkable agreement with the theoretical $D(h)$ spectrum. The comparison of the SF and WTMM methods is reported in Fig. 27(e). As expected theoretically, the SF method gives a correct $\tau(q)$ spectrum for $q < q^*$ only. The value $q = q^*$ corresponds to the point until which $\tau(q)$ starts to decrease, i.e., until the corresponding Hölder exponents become negative [from the properties of the Legendre transform, h corresponds to the derivative of $\tau(q)$]. Beyond that point, the $\tau(q)$ spectrum is significantly different from the theoretical curve since negative Hölder exponents become dominating in the behavior of the partition functions. Consequently, the analyzing wavelet $\Delta^{(1)}$ implicitly used in the SF method, is clearly not well adapted for analyzing signals with negative Hölder exponents. The WTMM method uses very smooth wavelets and leads to robust and accurate results.

(b) Singularities with Hölder exponents $h > 1$

As we have just pointed out, the increment $\delta f_l(x_0)$ of size l , at a point x_0 , can be seen as the wavelet transform $T_{\Delta^{(1)}}[f](x_0, l)$ of f , at the scale $a = l$ and at the point $b = x_0$, using the analyzing wavelet $\Delta^{(1)}$ [Eq. (113)]. However, $\Delta^{(1)}$ is orthogonal to polynomials of order 0 (i.e., constant terms) only. Thus, as discussed in Sec. 3.2.2, the increments will be blind to any Hölder exponent greater than 1, since only the first moment of $\Delta^{(1)}$ vanishes ($n_{\Delta^{(1)}} = 1$). If we suppose that $h(x_0) > 1$ at a given point x_0 ,

the increment $\delta f_l(x_0)$ will be generically dominated by a term of the form $f'(x_0)l$ (i.e., the first term in the Taylor series of f which is not constant). Each time the Hölder exponent is greater than 1, the increments measure the exponent $h = 1$. Thus, for $h > 1$, the SF method leads to a degenerate singularity spectrum $D(h = 1) = 1$ corresponding to $\tau(q) = q - 1$. Actually, it is even worse: one can prove that, in most cases, there exists h^{**} verifying $h^{**} = 1 - [1 - D(h^{**})]/D'(h^{**}) < 1$ (respectively q^{**}) so that $D(h)$ [respectively $\tau(q)$] is degenerate for any $h > h^{**}$ (respectively $q < q^{**}$) [Muzy et al., 1993a]. Let us note that these problems do not exist when using the WTMM method since the wavelet is always chosen so that the number of vanishing moments n_ψ is large enough ($n_\psi \geq \max_h\{h, D(h)\} \neq -\infty\}$).

These considerations are illustrated on a specific example in Fig. 28 [Muzy et al., 1993a]. The analyzed function is a generalized devil staircase similar to the one shown in Fig. 24(a) (the weights are $p_1 = 0.84$, $p_2 = -p_3 = 0.36$, $p_4 = 0.16$), but it has been fractionally integrated with $\beta = 0.7$ so that the support of the $D(h)$ singularity spectrum contains 1 (a fractional integration of a signal with a coefficient β induces a translation of the singularity spectrum to the right by a factor β). The function is represented in Fig. 28(a). The theoretical $D(h)$ singularity spectrum of this function is represented by a solid line in Fig. 28(d); it lies on the interval $[0.83, 2.04]$. The results obtained using the WTMM method are represented in Figs. 28(b), 28(c) and 28(d). We used the fourth derivative $\psi^{(4)}$ of the Gaussian as the analyzing wavelet. The so-obtained $D(h)$ and $\tau(q)$ spectra are in excellent agreement with the theoretical spectra. The $\tau(q)$ spectrum obtained for $q > 0$ using the SF method is shown in Fig. 28(e) for comparison. Along the lines of the above theoretical discussion, below some critical value $q < q^{**}$, the data corresponding to the SF method systematically deviate from the analytical $\tau(q)$ curve and follow the trivial behavior $\tau(q) = q - 1$. In the range $q < q^{**}$, the scaling behavior of the structure functions is dominated by the weakest singularities which are misleadingly identified with $h = 1$. For $q > q^{**}$, the WTMM and SF methods converge to a unique $\tau(q)$ spectrum, in good agreement with the analytical curve.

Remark: Would a higher order SF method work? We have just seen in the last paragraph that since the SF method uses explicitly the analyzing

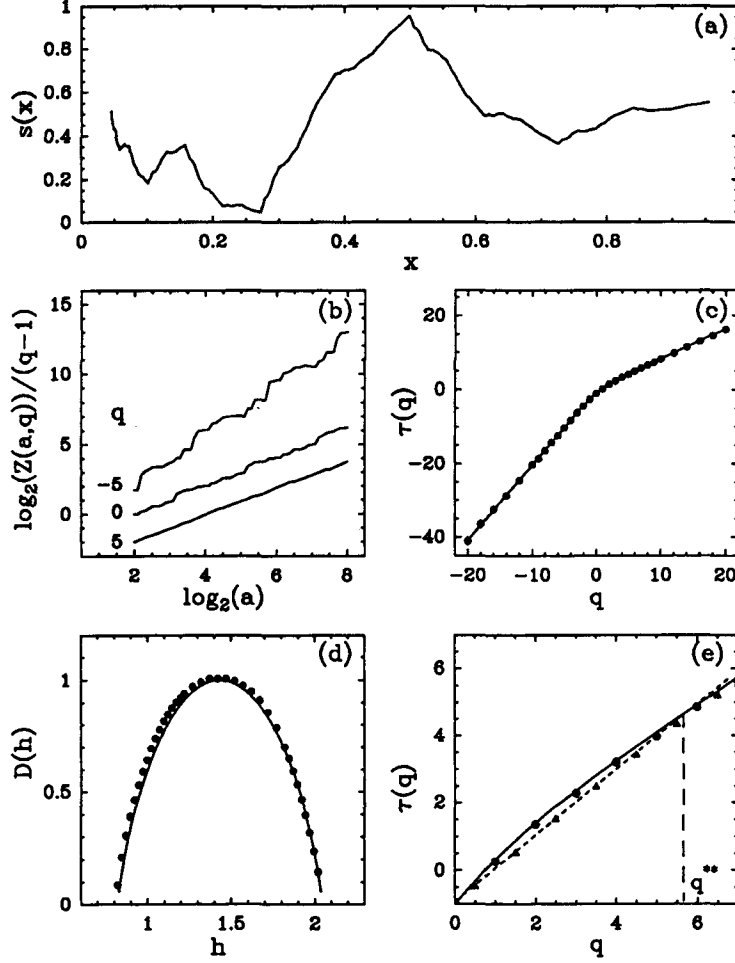


Fig. 28. WTMM and SF analysis of a multifractal signal that possesses some singularities of Hölder exponents $h > 1$. (a) Graph of the signal. This signal is a generalized devil staircase constructed from the recursive signed measure involving the weights $p_1 = 0.84$, $p_2 = -p_3 = 0.36$ and $p_4 = 0.16$; it has been fractionally integrated with a coefficient $\beta = 0.7$. (b) $\log_2(Z(q, a))$ versus $\log_2 a$ for some values of q . (c) $\tau(q)$ spectrum obtained with the WTMM method; the analyzing wavelet is $\psi^{(4)}$. (d) $D(h)$ singularity spectrum obtained by Legendre transforming the numerical $\tau(q)$ data in (c). (e) Comparison of the $\tau(q)$ spectra obtained with the WTMM (●) and the SF (▲) methods. The dashed line corresponds to the degenerate spectrum $\tau(q) = q - 1$. In (c), (d) and (e), the solid lines correspond to the theoretical spectra.

wavelet $\Delta^{(1)}$, it basically restricts the study of the singularity behavior to Hölder exponents $h \in [0, 1]$. However, one could try to generalize this technique to “higher” or “lower” SF approaches which would allow us to capture other Hölder exponents. For example, in Sec. 4.1, we took the “box function” $\Delta^{(0)}(x) = \chi_{[0,1]}(x)$ as analyzing wavelet in order to characterize multifractal measures. The corresponding Hölder exponents were then found in the range $[-1, 0]$; indeed we saw that $h = \alpha - 1$ with $\alpha \in [0, 1]$ [Eq. (90)]. In the same way one could use the wavelet $\Delta^{(-1)} = x\chi_{[0,1]}(x)$ to study the Hölder exponents in the range $[-2, -1]$ as well as the wavelet $\Delta^{(2)}(x) = \delta(x+1) - 2\delta(x+1/2) + \delta(x)$ for Hölder exponents in $[1, 2]$ and so on. Thus one

could imagine combining the singularity spectra obtained for each of the wavelets $\Delta^{(-1)}, \Delta^{(0)}, \Delta^{(1)}, \Delta^{(2)} \dots$ in order to get the entire $D(h)$ singularity spectrum. Besides the fact that such a method would be numerically very “heavy,” it clearly would not work because of what we could call “border effects.” Indeed, we know from the former paragraphs that when using the wavelet $\Delta^{(1)}(x)$, the Hölder exponents are actually restricted to an interval $[h^*, h^{**}]$ which is strictly included in $[0, 1]$. Therefore one cannot really hope to combine all the “sub” spectra (obtained with the different $\Delta^{(i)}$ analyzing wavelets) into a whole $D(h)$ spectrum without expecting some drastic bias around all the integer values of h [Muzy *et al.*, 1993a].

5.2. Non-everywhere-singular fractal functions

Smooth behavior induced phase transition in the singularity spectrum of multifractal functions. In Sec. 5.1, we have pointed out that the WTMM method is very efficient as long as we use an analyzing wavelet with a number of vanishing moments n_ψ which is greater than $h_{\max} = \max_h\{h, D(h) \neq -\infty\}$. Let us see what happens when this is not possible, i.e., if $h_{\max} = +\infty$. It would mean that the analyzed function is C^∞ at some points. As we have just discussed, the structure function method would fail, in this situation, since the increments are unable to detect any Hölder exponent greater than 1. Therefore let us concentrate on the influence of such C^∞ behavior on the singularity spectrum obtained with the WTMM method.

For the sake of simplicity, we will consider that the fractal function $f(x) = s(x) + r(x)$ is the sum of a multifractal singular part $s(x)$ (whose maximum Hölder exponent h_{\max} is strictly smaller than $+\infty$) and a C^∞ regular part $r(x)$. Typically, s can be a generalized devil staircase, then h_{\max} corresponds to the largest Hölder exponent found on the support of the multifractal measure. The other points are not important since the wavelet transform at these points is 0 at any scale a small enough; in other words, these points do not contribute to the partition functions $\mathcal{Z}(q, a)$. Let $\tau_s(q)$ and $D_s(h)$ be the multifractal spectra which characterize the function $s(x)$. We will use an analyzing wavelet ψ with a number of vanishing moments n_ψ greater than the greatest Hölder exponent h_{\max} of $s(x)$. Thus as $r(x)$ is C^∞ , the wavelet transform of r is uniformly of the order of a^{n_ψ} when a is small enough [Eq. (58)]. On the other hand, as h_{\max} is the maximum Hölder exponent involved in s , wherever the wavelet transform of s is not 0, it is of an order which is uniformly larger than $a^{h_{\max}}$. As illustrated in Fig. 29, the wavelet transform $T_\psi[f]$ is basically equal to either $T_\psi[r] (\sim a^{n_\psi})$, at the points where $T_\psi[s] = o(a^{n_\psi})$, or $T_\psi[s] (\sim a^h)$ anywhere else. Thus the set $\mathcal{L}_f(a)$ of the maxima lines of f can be decomposed, at any scale a , into two subsets: the subset $\mathcal{L}_s(a)$ of the maxima lines of s [slightly perturbed by a term of the order of a^{n_ψ} due to the presence of $r(x)$] and the subset $\mathcal{L}_r(a)$ of the maxima lines of r around which $T_\psi[s] = o(a^{n_\psi})$ (e.g., the maxima lines which lie outside of the support of the multifractal measure associated with the devil staircase). Thus the

partition function of f splits into two parts [Bacry et al., 1993; Muzy et al., 1993a]:

$$\mathcal{Z}_f(q, a) = \mathcal{Z}_s(q, a) + \mathcal{Z}_r(q, a) \sim a^{\tau_s(q)} + a^{qn_\psi}, \quad (114)$$

where \mathcal{Z}_s and \mathcal{Z}_r are the partition functions corresponding respectively to summing over the maxima lines in \mathcal{L}_s and \mathcal{L}_r . Thus one deduces easily that there exists a critical value $q_{\text{crit}} < 0$ so that

$$\begin{aligned} q > q_{\text{crit}} &\Rightarrow \tau(q) = \tau_s(q), \\ q < q_{\text{crit}} &\Rightarrow \tau(q) = qn_\psi. \end{aligned} \quad (115)$$

One thus predicts the existence of a singularity in the $\tau(q)$ spectrum. This nonanalyticity in the function $\tau(q)$ expresses the breaking of the self-similarity of the singular signal $s(x)$ by the C^∞ perturbation $r(x)$. In the context of the thermodynamical analogy, this phenomenon defines a phase transition [Badii, 1987; Cvitanovic, 1987; Grassberger et al., 1988]. Below the critical value q_{crit} (which is the analog of the inverse of the transition temperature) one observes a regular phase, whereas for $q > q_{\text{crit}}$ one switches to the multifractal phase. Let us note that this phenomenon is “meaningful” (as compared to the spurious phase transitions previously obtained with the modified SF method); indeed, it really detects the fact that there is a smooth behavior superimposed to the multifractal function. Moreover, Eq. (115) indicates that the $\tau(q)$ spectrum in the “ C^∞ phase” is governed by the number n_ψ of vanishing moments of the analyzing wavelet. Therefore, checking whether $\tau(q)$ is sensitive to some change in the order n_ψ of the analyzing wavelet constitutes a very good test for the presence of a highly regular part in the signal.

This phenomenon is illustrated in Fig. 29. The analyzed function $f(x)$ is the sum of $r(x) = R \sin(8\pi x)$ and $s(x)$ a generalized devil staircase which is the distribution function of a measure nonuniformly distributed on the triadic Cantor set with the weights $p_1 = 0.6$ and $p_2 = 0.4$. The function $f(x)$ is represented in Fig. 29(a). The $\tau(q)$ and $D(h)$ spectra obtained with the WTMM method are displayed in Figs. 30(a) and 30(b) respectively. Two different analyzing wavelets $\psi^{(1)}$ ($n_{\psi^{(1)}} = 1$) and $\psi^{(2)}$ ($n_{\psi^{(2)}} = 2$), namely the first and the second derivative of the Gaussian function, were used to compute the wavelet transform.

For $q > 0$, these two wavelets lead to the same numerical estimate for $\tau(q)$ in perfect agreement with the theoretical curve. However, for $q < 0$,

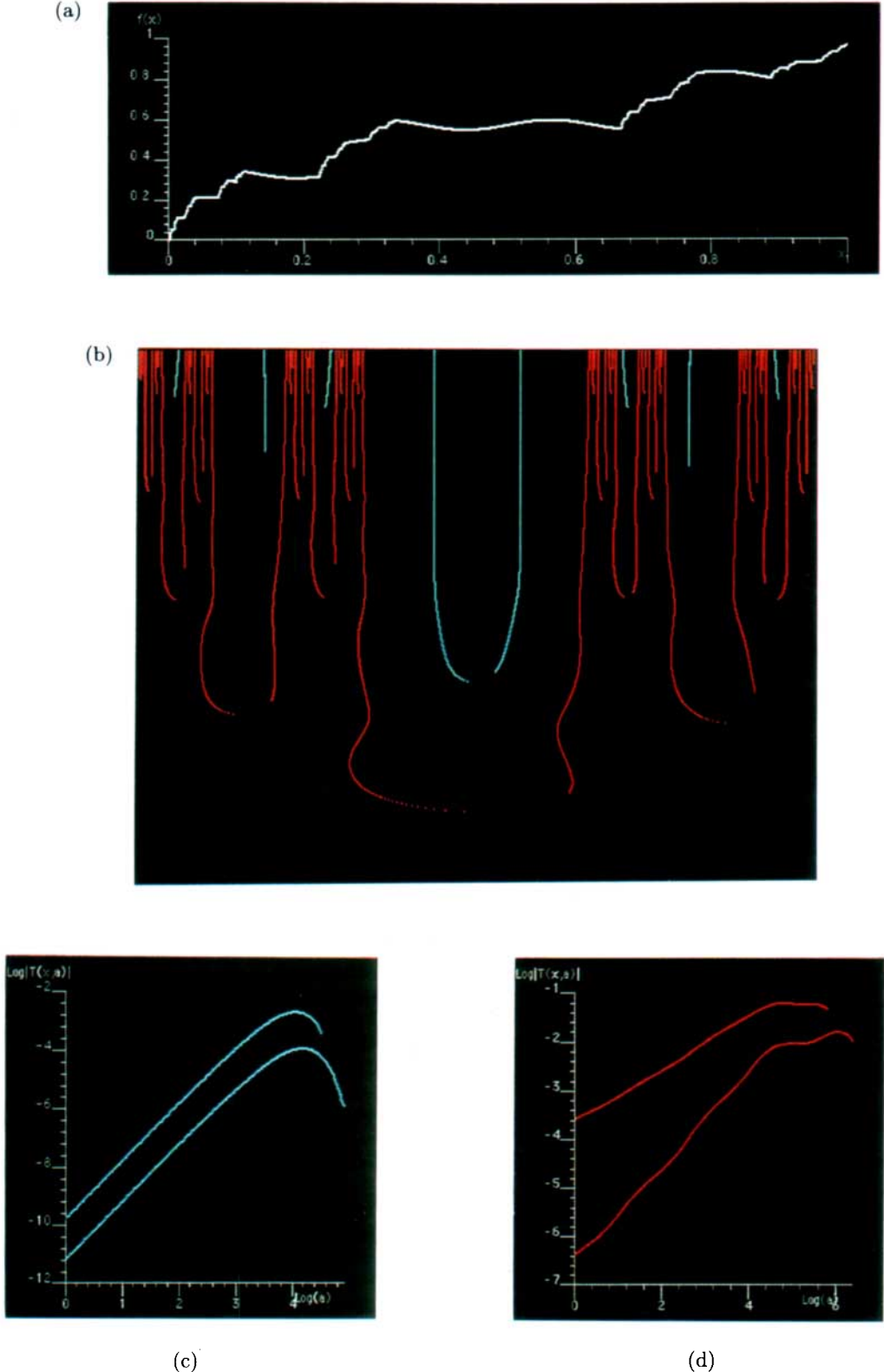


Fig. 29. Processing the singularities of a fractal signal perturbated by a C^∞ function. (a) Graph of the signal $f(x) = s(x) + r(x)$, with $r(x) = R \sin(8\pi x)$ and $s(x)$ is the devil staircase constructed from the recursive measure distributed on the triadic Cantor set with the weights $p_1 = 0.6$ and $p_2 = 0.4$. (b) WTMM skeleton computed with the mexican hat $\psi^{(2)}$; the small scales are at the top. The sets $\mathcal{L}_s(a)$ and $\mathcal{L}_r(a)$ of maxima lines are coded in red and blue respectively. (c) Along the maxima lines in $\mathcal{L}_r(a)$, $T_\psi[f] \sim a^{n_\psi}$ ($n_\psi = 2$). (d) Along the maxima lines in $\mathcal{L}_s(a)$, $T_\psi[f] \sim a^h$ where h fluctuates from line to line ($h \in [h_{\min}, h_{\max}]$).

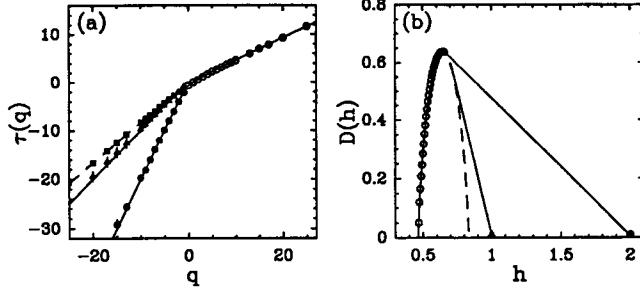


Fig. 30. Phase transition phenomenon in the $\tau(q)$ and $D(h)$ spectra of the fractal signal perturbed by a C^∞ function shown in Fig. 29(a). (a) $\tau(q)$ spectrum obtained by the WTMM method using the analyzing wavelet $\psi^{(1)}$ [(\circ) and (\blacktriangle)], $\psi^{(2)}$ [(\circ) and (\bullet)] and $\psi^{(4)}$ [(\circ) and (\blacksquare)]; the solid lines correspond to the theoretical curves [Eq. (115)]; the dashed line corresponds to $\tau_s(q)$ for $q < q_{\text{crit}}$. (b) $D(h)$ versus h from the Legendre transform of $\tau(q)$.

the results obtained with $\psi^{(1)}$ and $\psi^{(2)}$ are different; they consist of two lines of respective slopes 1 and 2. This corresponds to the phase transition predicted by the above theoretical speculations; the data for $\tau(q)$ depend on n_ψ : $\tau(q) = n_\psi q$ [Eq. (115)]. The Legendre transform, $D(h)$, of these two curves are represented in Fig. 30(c). One can check that they perfectly fit the predicted curve for $q > q_{\text{crit}}(n_\psi)$. For $q \leq q_{\text{crit}}(n_\psi)$, however, $D(h)$ displays a linear fall off towards the limiting value $h = 1$ for $\psi^{(1)}$ and $h = 2$ for $\psi^{(2)}$ (actually $h = N$ for $\psi^{(N)}$) where $D(h)$ vanishes. This linear part is tangent to the theoretical $D(h)$ spectrum (dashed line) and has a slope equal to $q_{\text{crit}}(n_\psi)$. This is the signature of the phase transition phenomenon described above [Bacry et al., 1993; Muzy et al., 1993a].

Remark. We have shown that a C^∞ component superimposed on a distribution that is not singular everywhere manifests in a phase transition phenomenon that masks the weakest singularities. However, since the wavelet coefficients behave like a^{n_ψ} along the maxima lines created by the C^∞ function, by choosing n_ψ large enough and/or choosing a numerical threshold below which any local maximum is not considered, one can remove all the C^∞ maxima lines in $\mathcal{L}_r(a)$ and thus “numerically restore” the self-similarity of $s(x)$. The whole $\tau_s(q)$ and $D_s(h)$ spectra can then be estimated.

To show that this procedure is actually operational, we have reproduced the WTMM analysis on the same signal but with the fourth derivative of the Gaussian function ($\psi^{(4)}(x)$) as analyzing wavelet.

The faster decrease of the wavelet coefficients along the maxima lines of \mathcal{L}_r ($(T_\psi[f](., a))_{a \in \mathcal{L}_r} \sim a^4$) makes more efficient the threshold discrimination of the maxima lines emanating from the singular part $s(x)$. The so-obtained $\tau(q)$ spectrum is shown in Fig. 30(a). Now the theoretical spectrum of the singular measure is recovered and no phase transition phenomenon is observed. Let us point out that the choice of such a threshold (or analyzing wavelet) is somewhat uncertain and strongly depends on various parameters like the number of sampling points, the relative amplitudes of $r(x)$ and $s(x)$ in the signal, etc. Indeed, a more reliable way to proceed consists in choosing n_ψ large enough [as compared to the largest Hölder exponent of $s(x)$] so that the maxima lines induced by the regular part of the signal becomes easily distinguishable from the anomalously stiff decrease of the wavelet coefficients on the range of scale used to estimate the scaling exponents $\tau(q)$.

5.3. Brownian and turbulent signals

5.3.1. Fractional Brownian motions

As seen in Sec. 2.3.1, the fractional Brownian motions (fBm) $B_H(x)$ are Gaussian stochastic processes of zero mean; they are indexed by a parameter H ($0 < H < 1$) [Mandelbrot & Van Ness, 1968]. Their correlation function is given by

$$\langle B_H(x)B_H(y) \rangle = |x|^{2H} + |y|^{2H} - |x - y|^{2H}. \quad (116)$$

Thus their increments are stationary Gaussian processes whose variance is

$$\langle (\delta B_H(l))^2 \rangle = \langle (B_H(x+l) - B_H(x))^2 \rangle = l^{2H}. \quad (117)$$

The classical Brownian motion is obtained for the value $H = 1/2$. The fractional Brownian motions are statistically self-similar in the sense that

$$B_H(t+\lambda l) - B_H(t) \simeq \lambda^H (B_H(t+l) - B_H(t)), \quad (118)$$

where \simeq means that the two processes are equal in law (for fixed t and λ). Thus, the exponent H is directly related to the Hölder exponent which characterizes the realizations of the Brownian processes. One can prove that almost all the realizations are continuous, everywhere nondifferentiable and characterized by a single Hölder exponent $h = H$ [Levy, 1965]. In the multifractal formalism framework we

will say that the fBm's are homogeneous, i.e., their singularity spectrum reduces to a single point

$$D(h = H) = 1, \quad (119)$$

[$D(h) = -\infty$ if $h \neq H$].

There have been previous attempts to analyze fBm with the wavelet transform [Argoul *et al.*,

1989b; Everson *et al.*, 1990; Bacry *et al.*, 1991]. When using a color coding similar to the one used in the previous sections, the wavelet representation in the space-scale half-plane of a fBm clearly displays some kind of fractal branching [Fig. 31(a)] as observed in the analysis of generalized devil staircases (Fig. 25). Recently, Vergassola & Frisch [1991]

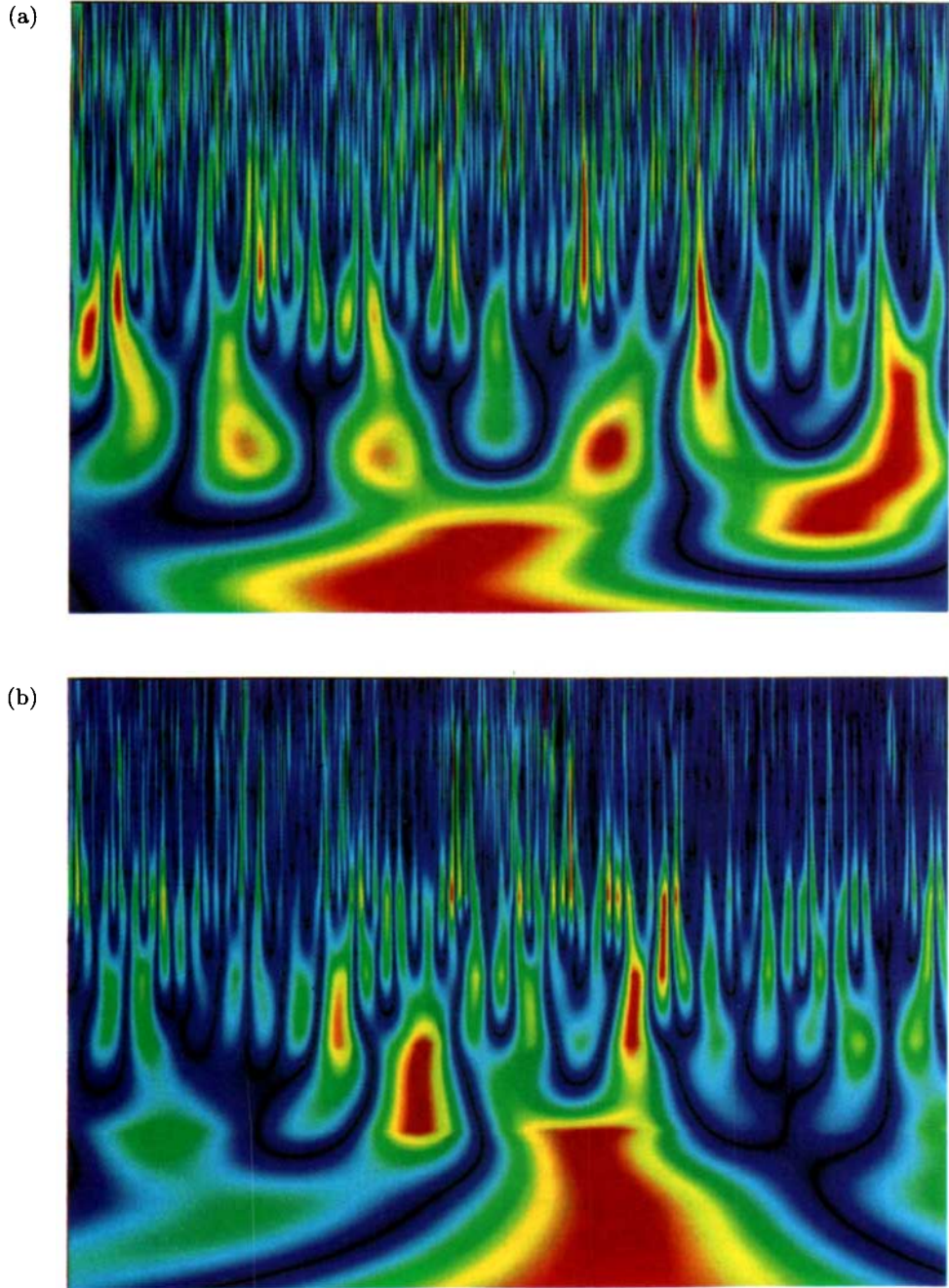


Fig. 31. Continuous wavelet transform of (a) a fractional Brownian signal $B_{1/3}(t)$ [Fig. 32(a)] and (b) a turbulent velocity signal recorded in the Modane wind tunnel [Fig. 34(a)]. The analyzing wavelet is the Mexican hat $\psi^{(2)}$. Same color coding as in Fig. 13. The small scales are at the top.

and Vergassola *et al.* [1991] have tried to pursue this analysis on a more quantitative basis, using the wavelet analysis to characterize the local Hölder regularity of these random signals. But they have been facing the presence of random fluctuations, superimposed on the pertinent power-law behavior of the wavelet transform at small scales [Eq. (57)], that makes quite uncertain the estimate of the local scaling exponents. In order to circumvent this difficulty, they have established an ergodic formula from which one can extract the Hölder exponents from zoom-averagings over logarithmically varying scales. In fact, this ergodic formula indicates that in principle, Hölder exponent measurement of fBm is possible. In practice, however, the available finite range of scales is not sufficient for the averaging process to converge and the above mentioned fluctuations result in an important scatter of the measured scaling exponents around the value $h = H$ [Vergassola *et al.*, 1991].

In Figs. 32 and 33, we report the results of a statistical analysis of the fBm using the WTMM method [Arneodo *et al.*, 1991; Muzy *et al.*, 1991]. We focus on the fBm $B_{1/3}$ since it has a $k^{-5/3}$ power spectrum similar to the spectrum of the turbulent velocity signal investigated in the next section. This will allow us to clearly discriminate between these two fractal signals. The numerical signal was generated by filtering uniformly distributed pseudo-random noise in Fourier space to have the required $k^{-5/3}$ spectral density [Peitgen & Saupe, 1987]. A $B_{1/3}$ fractional Brownian trail is shown in Fig. 32(a). The corresponding WTMM skeleton computed with the Mexican hat $\psi^{(2)}(x)$, is illustrated in Fig. 32(b). When plotted versus q , the exponents $\tau(q)$ extracted from the scaling behavior of the partition function $Z(q, a)$ [Eq. (92)], consistently fall on a line of slope $h = 0.33 \pm 0.01$. Moreover, Fig. 33(b) shows that the theoretical prediction

$$\tau(q) = \frac{q}{3} - 1 \quad (120)$$

provides a remarkable fit of the data. According to Eq. (120), $[a^{2/3} Z(q, a)]^{1/(q-1)}$ is expected to scale like $a^{1/3}$, independently of q . The data reported in Fig. 33(a) for different values of q are in good agreement with this general scaling law. The homogeneity of the fBm $B_{1/3}$ signal is confirmed in Fig. 33(c) where the direct estimate of the exponent $h(q)$ from Eq. (97), for different values of q , does not reveal any significant q -dependence of this ex-

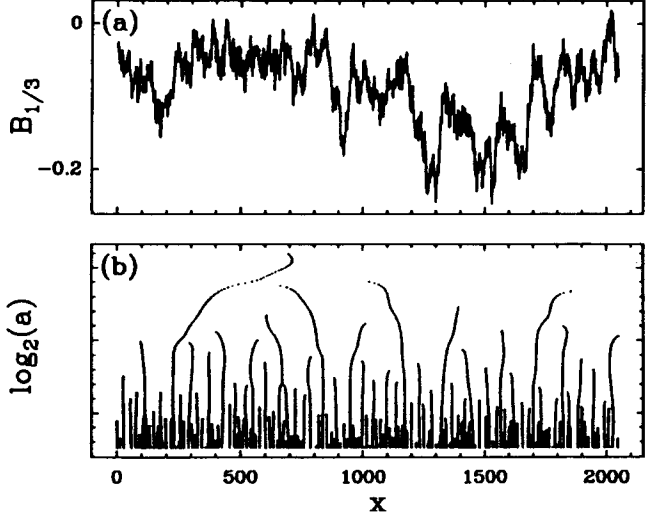


Fig. 32. WTMM skeleton of a Brownian signal. (a) A realization of the fractional Brownian motion $B_{1/3}$. (b) Wavelet transform maxima lines corresponding to the realization in (a). The analyzing wavelet is the Mexican hat $\psi^{(2)}$. The large scales are at the top.

ponent: $h(q) = 0.33 \pm 0.01$. Similarly, from Eq. (98) one gets $D(h) = 1.001 \pm 0.002$ for all considered q values. These numerical results are in remarkable agreement with the theoretical singularity spectrum [Eq. (119)]: $h = H = 1/3$; $D(h = 1/3) = 1$. As expected theoretically, we find that the fractional Brownian motion $B_{1/3}(x)$ is nowhere differentiable with a unique Hölder exponent $h = H = 1/3$.

5.3.2. Experimental velocity signals from fully developed turbulence data

The central problem of three-dimensional fully developed turbulence is the energy cascading process. It has resisted all attempts at a full understanding or mathematical formulation. The main reasons for this failure are related to the large hierarchy of scales involved, the highly nonlinear character inherent in the Navier-Stokes equations and the spatial intermittency of the dynamical active regions [Monin & Yaglom, 1971; Frisch & Orszag, 1990]. In this context, statistical and scaling properties have been the basic concepts used to characterize turbulent flows [Frisch, 1985, 1991]. One of the striking signatures of the so-called intermittency phenomenon, is the non-Gaussian statistics at small scales. The energy transfer towards small scales is related to the nonzero skewness of the probability distribution function (PDF) of the velocity increments and the large flatness of the PDF

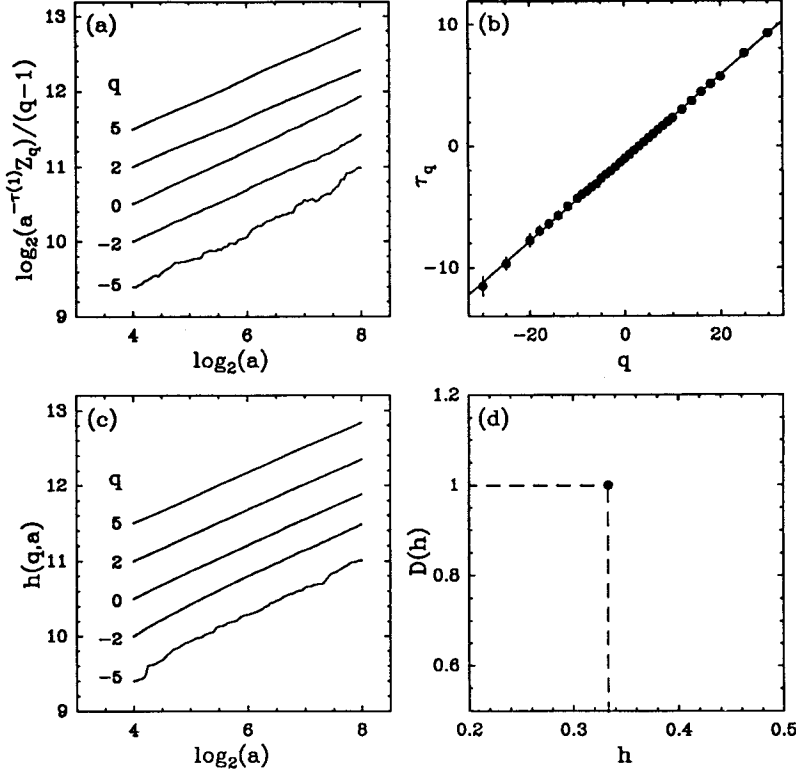


Fig. 33. Determination of the $\tau(q)$ and $D(h)$ spectra for a fractional Brownian motion $B_{1/3}$ using the WTMM method. (a) $\log_2(a^{-\tau(1)}Z(q, a))/(q - 1)$ versus $\log_2 a$. (b) $\tau(q)$ versus q . (c) Determination of the exponent $h(q)$ from Eq. (97). (d) $D(h)$ versus h . The analyzing wavelet is the Mexican hat $\psi^{(2)}$. In (b) the solid line represents the theoretical spectrum $\tau(q) = q/3 - 1$ [Eq. (120)].

(kurtosis) corresponds to the presence of strong bursts in the energy dissipation. This fine-scale intermittency is responsible for some departure to the classical $k^{-5/3}$ theory of Kolmogorov [1941] which neglects the presence of fluctuations in the energy transfer. Mandelbrot [1974] was the first one to advocate the use of fractals in turbulence. Some of his early multiplicative cascade models contained all the ingredients of the classical multifractal formalism described in Sec. 2.2.3. During the past few years, considerable effort has been devoted to the multifractal analysis of high Reynolds number turbulence [Frisch & Orszag, 1990]. But the problem of comparing the predictions of various multifractal cascade models [Novikov & Stewart, 1964; Mandelbrot, 1974, 1984; Frisch *et al.*, 1978; Benzi *et al.*, 1984; Nelkin, 1989] with experimental data comes from the fact that three-dimensional processing of turbulent flows is at the moment feasible only for numerical simulations which are unfortunately limited in Reynolds numbers to regimes where the scaling just begins to manifest itself. Present experimental techniques have access to the two-

dimensional structure of passive scalars [Prasad *et al.*, 1989; Miller & Dimotakis, 1991] and only to the one-dimensional structure of the velocity field [Anselmet *et al.*, 1984; Gagne, 1987; Gagne *et al.*, 1988; Castaing *et al.*, 1990; Meneveau & Sreenivasan, 1991]. Here, we will mainly elaborate on the statistical analysis of single-point data based on hot-wire techniques in the presence of a mean flow (wind tunnels, jets, etc.).

Very recently, there has been increasing interest in applying the wavelet analysis to turbulence data [Farge, 1992]. In this section, we report on the first such analysis performed on single point velocity data from high Reynolds number 3D turbulence [Argoul *et al.*, 1989b; Bacry *et al.*, 1991]. The data were obtained by Gagne and collaborators [Gagne, 1987; Gagne *et al.*, 1988; Castaing *et al.*, 1990] in the large wind tunnel S1 of ONERA at Modane. The Taylor scale based Reynolds number is $R_\lambda = 2720$ and the extent of the inertial range following approximately the Kolmogorov $k^{-5/3}$ law is almost three decades. The results reported here concern the analysis in the inertial range of about

100 integral length scales of the recorded turbulent signal.

Local scaling exponents of a turbulent velocity signal. The application of the continuous wavelet transform to investigate the local scaling exponent fluctuations that characterize the multi-fractal nature of a turbulent velocity field at inertial range scales has been initiated by Bacry *et al.* [1991]. Figure 31(b) illustrates the wavelet transform of a sample of the velocity signal of length of about one integral scale. The WTMM skeleton in Fig. 34(b) is actually hardly distinguishable from the WTMM arrangement obtained in Fig. 32(b) for a fractional Brownian signal $B_{1/3}(x)$ which has a similar $k^{-5/3}$ power spectrum. However, when using the additional information given by the WT amplitude [Fig. 31(b)], this discrimination becomes easier. By analyzing the behavior of $|T_\psi(x_0, a)|$ versus a along the WTMM lines, one can estimate the value of the local Hölder exponent $h(x_0)$ according to Eq. (61). Regardless some fluctuations due to finite size effects [Vergassola & Frisch, 1991], the Hölder exponent of the Brownian signal $B_{1/3}(x)$ does not depend on $x : h = H = 1/3$. In contrast, for the turbulent velocity signal, h is actually found to fluctuate in a wide range [Arneodo *et al.*, 1991; Bacry *et al.*, 1991] between -0.3 and 0.7 , thereby suggesting that the multifractal picture proposed by

Frisch & Parisi [1985] is appropriate. Statistically, the most frequent exponents are close to the Kolmogorov value $h = 1/3$. We believe that the data are statistically significant for negative exponents down to -0.1 and beyond. Negative exponents do not seem to have been previously reported in the literature. One possible interpretation tossed up by Bacry *et al.* [1991] is the occasional passage near the probe of slender vortex filaments of the sort observed in recent experiments [Douady *et al.*, 1991] and 3D numerical simulations [Siggia, 1981; Brachet *et al.*, 1983; Brachet, 1990, 1992; She *et al.*, 1990; Vincent & Meneguzzi, 1991].

Determination of the singularity spectrum of a turbulent velocity signal. In Fig. 35 are shown the results of the multifractal analysis of the Modane turbulent velocity signal performed with the WTMM method [Arneodo *et al.*, 1991; Muzy *et al.*, 1991, 1993b]. In contrast to the fractional Brownian motion (Fig. 33), the $\tau(q)$ spectrum obtained for the turbulent signal unambiguously deviates from a straight line. Let us note that the results obtained with the structure function method $\tau(q) = \zeta_q - 1$ (exclusively obtained for positive integer values of q) are in good agreement with the nonlinear behavior of $\tau(q)$ found with the WTMM method. The values of $h = \partial\tau(q)/\partial q$ when varying q from the -30 to 30 range in the interval $[0.10, 0.62]$. The corresponding $D(h)$ singularity spectrum is shown in Fig. 35(d). It displays the characteristic single-humped shape of multifractal signals. Its maximum $D(h(q=0)) = -\tau(0) = 1.000 \pm 0.001$ does not deviate substantially from $D_F = 1$. This strongly suggests that the turbulent signal is everywhere singular. This observation is corroborated by the robustness of the $D(h)$ data with respect to changes in the shape of the analyzing wavelet: similar quantitative estimates of the $\tau(q)$ and $D(h)$ spectra are obtained when using the first ($\psi^{(1)}$), the second ($\psi^{(2)}$) and the fourth ($\psi^{(4)}$) derivative of the Gaussian function and no wavelet dependent phase transition phenomenon of the type described in Sec. 5.2 is observed. In Fig. 35(d), the $D(h)$ singularity spectrum of the wind tunnel turbulent velocity signal is compared to a solid curve which actually corresponds to a common fit of dissipation field data at lower Reynolds number [Meneveau & Sreenivasan, 1991]. This curve has been deduced from the experimental average $f(\alpha)$ spectrum of the energy dissipation $\varepsilon(x) = (dv/dx)^2$ (considered as a measure) of laboratory and atmospheric turbulent flows by

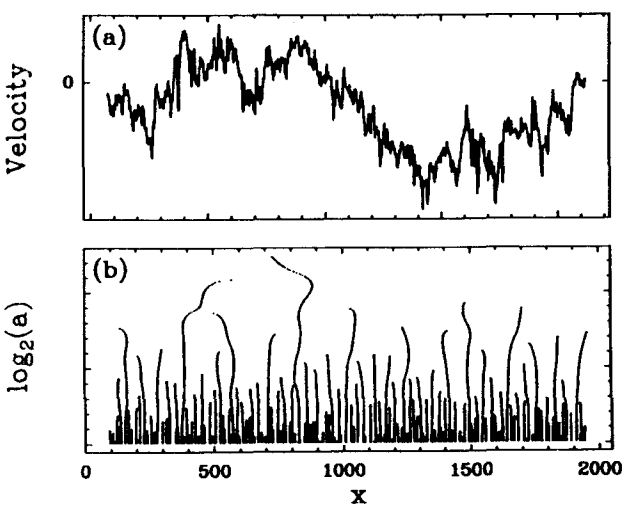


Fig. 34. WTMM skeleton of a turbulent velocity signal recorded in the wind tunnel S1 of the ONERA at Modane. (a) The velocity signal over about one integral scale. (b) WTMM skeleton defined by the maxima lines. The analyzing wavelet is the Mexican hat $\psi^{(2)}$. The large scales are at the top.

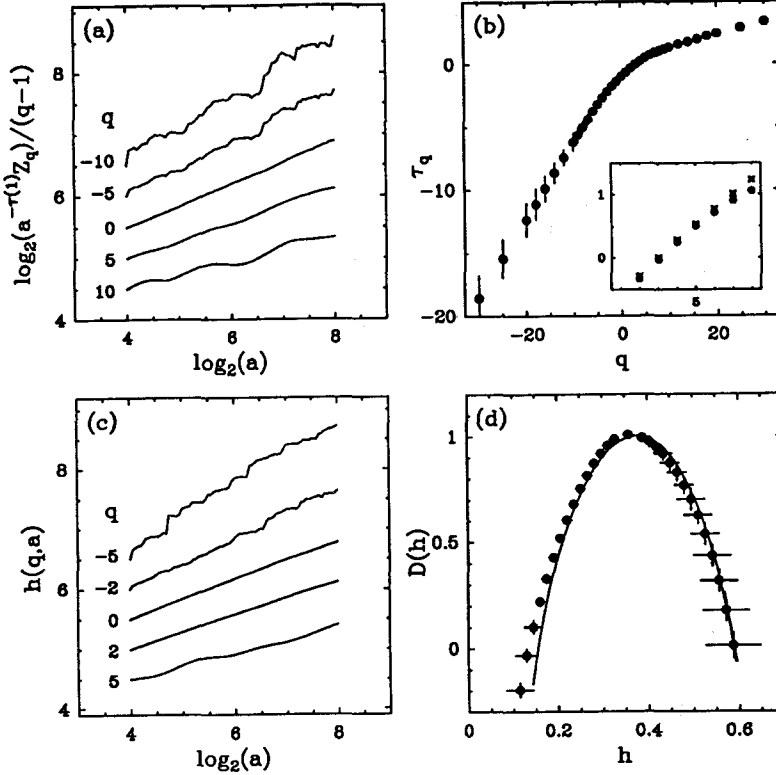


Fig. 35. WTMM measurement of the $\tau(q)$ and $D(h)$ spectra of the Modane turbulent velocity signal. (a) $\log_2(a^{-\tau^{(1)} Z(q,a)})/(q-1)$ versus $\log_2 a$. (b) $\tau(q)$ versus q . (c) Determination of the exponent $h(q)$ from Eq. (97). (d) $D(h)$ versus h . In (b) the symbols (\times) correspond to $\tau(q) = \zeta_q - 1$ obtained when computing the scaling exponent ζ_q with the SF method. In (d) the solid line corresponds to the average singularity spectrum obtained from dissipation field data via the Kolmogorov scaling relation (121). The results reported in this figure concern the analysis in the inertial range of about 100 integral length scales of the turbulent velocity signal.

using the local Kolmogorov scaling relation [Kolmogorov, 1962]:

$$\frac{1}{l} \int_{x-l}^{x+l} \varepsilon(x) dx \simeq \frac{\delta v_l^3}{l}, \quad (121)$$

where \simeq means that the two quantities have the same scaling laws. The fact that, for similar statistical samples, one cannot discriminate between these two singularity spectra within the experimental uncertainty, can be interpreted *a posteriori* as an experimental verification of the above Kolmogorov hypothesis. This observation can also be understood as an experimental confirmation of the universality of the multifractal singularity spectrum of fully developed turbulence with respect to Reynolds number. However, it is clear that considerable further work is needed to get definitive conclusions. In particular, long term statistical analysis must be carried out in order to capture more accurately the latent part ($D(h) < 0$) [Mandelbrot, 1989c] of the singularity spectrum, including possible violent

rare events that do not occur in every sample of inertial length scale. This analysis is likely to provide fundamental informations about the true role played by the vortex filaments in the intermittency phenomenon of the fine structures in fully developed turbulent flows.

6. Prospects: Solving the Inverse Fractal Problem from Wavelet Analysis

To summarize, we have presented in this tutorial, a first theoretical step towards a unified theory of singular distributions including multifractal measures and multifractal functions. Rigorous results have been mainly derived under specific hypothesis concerning the signal under study as well as the shape of the analyzing wavelet [Bacry *et al.*, 1993]. But the WTMM method is likely to remain valid under less stringent conditions [Jaffard, 1993]. The results of some numerical applications strongly

suggest that our theoretical results may extend to more general multifractal functions such as the realizations of some stochastic processes. Preliminary investigations in this context indicate that fractional Brownian motions [Flandrin, 1991a, 1991b] could well be amenable to such a rigorous treatment relying on the wavelet decomposition. Moreover, this wavelet based multifractal formalism provides algorithms for determining the $D(h)$ spectrum of Hölder exponents directly from the considered fractal distribution. From the comparative applications of the WTMM and SF methods on specific examples, we have pointed out the severe intrinsic limitations of the latter that fails to fully characterize the scaling properties of a multifractal signal. In contrast, we have demonstrated that the former does not introduce any bias in the estimate of the scaling exponents of some partition functions which are at the heart of this “generalized” multifractal formalism.

The efficiencies of the WTMM method originate from two main ingredients; on the one hand, the partition functions are based on discrete scale-dependent summations: the skeleton of the wavelet transform defined by the local maxima of its modulus provides a practical guide to achieve a scale adaptive partition; on the other hand, one uses sufficiently smooth and localized analyzing wavelets with an arbitrary large number of vanishing moments, which makes the entire range of singularities accessible to this method, even in the presence of regular behavior in the signal. The reported results of a preliminary analysis of a fully developed turbulent velocity signal show that this method is readily applicable to experimental situations. Indeed we believe that the WTMM method for determining the singularity spectrum of fractal signals is likely to become as useful as the well-known phase-portrait reconstruction, Poincaré section, and first return map techniques for the analysis of chaotic time series. Applications of this method to turbulent dynamics generated by fractal growth phenomena, critical fluctuations in colloidal systems, surface roughening in noise driven growth processes and DNA “walks” nucleotide sequences are currently in progress.

But beyond the statistical “thermodynamic” description of scale invariant objects that provides the multifractal formalism in either its (box counting) classical version or its wavelet based generalized version, there is a need to get deeper insight into the complexity of such objects and eventually to extract some “microscopic” information

about their underlying hierarchical structure. In many cases, the self-similarity properties of fractal objects can be expressed in terms of a dynamical system which leaves the object invariant. The inverse problem consists in recovering the dynamical system (or its main characteristics) from the data representing the fractal object. This problem has been previously approached within the theory of Iterated Function Systems [Barnsley & Demko, 1985; Barnsley, 1988; Handy & Mantica, 1990]. But the methods developed in this context are based on the search of a “best-fit” within a prescribed class of IFS attractors (mainly linear homogeneous attractors). In that sense, they approximate the self-similarity properties more than they reveal them. But as emphasized in Sec. 4.1 when analyzing the multiplicative structure of Bernoulli invariant measures of expanding Markov maps [Collet *et al.*, 1987; Rand, 1989], the space-scale unfolding that provides the wavelet transform generally enlightens the hierarchical structure of a fractal object and thus can possibly be used to reveal the renormalization operation which accounts for its construction process. To conclude this survey, we will describe a wavelet based tree matching algorithm that we have recently implemented and which provides some openings towards solving the so-called inverse fractal problem [Arneodo *et al.*, 1993a, 1993b].

The class of fractal objects we will use to carry out our demonstration are the invariant measures of “cookie-cutters.” A *cookie-cutter* [Rand, 1989] is a map on $A = [0, 1]$ which is hyperbolic ($|T'| > 1$) and so that $T^{-1}(A)$ is a finite union of s disjoint subintervals $(A_k)_{1 \leq k \leq s}$ of A . For each k , $T_k = T|_{A_k}$ is a one-to-one map on A . An invariant measure μ associated with T is a measure which satisfies $\mu \circ T^{-1} = \mu$. We will suppose that the weights are multiplicatively distributed on A , i.e.,

$$\mu \circ T_k^{-1} = p_k \mu, \quad \forall k \in \{1, \dots, s\}, \quad (122)$$

where $\sum p_k = 1$. As seen in Sec. 2, these self-similar (Bernoulli invariant) measures have been widely used for modeling a large variety of highly irregular physical distributions; notable examples include strange repellers which characterize transient behavior of nonlinear dynamical systems [Rand, 1989] and the spatial distribution of the dissipation field in fully developed turbulent flows [Paladin & Vulpiani, 1987; Meneveau & Sreenivasan, 1991]. Using a simple “smoothing wavelet” $\psi(x) = \exp(-x^2)$, one can reproduce the straightforward calculation carried out in Sec. 4.1 to derive Eqs. (70) and (78);

at the first order in a ($a \ll 1$) one gets

$$T_\psi[\mu](b, a) = \frac{1}{p_k} T_\psi[\mu](T_k^{-1}(b), T_k^{-1'}(b)a),$$

$$\forall k \in \{1, \dots, s\}, \quad (123)$$

where $T_k^{-1'}$ is the first derivative of T_k^{-1} . In the case where the T_k^{-1} 's are linear, i.e., $T_k^{-1}(x) = r_k x + t_k$ ($r_k < 1$), we thus obtain

$$T_\psi[\mu](b, a) = \frac{1}{p_k} T_\psi[\mu](r_k b + t_k, r_k a),$$

$$\forall k \in \{1, \dots, s\}. \quad (124)$$

These relations can be interpreted as self-similarity properties of the wavelet transform itself as previously illustrated in Figs. 13(a), 14(a) and 16. Indeed, in the linear case, the wavelet transform on the rectangle $[0, 1] \times]0, a_0]$ of the space-scale half-plane (b, a) is “similar” to the wavelet transform on each of the rectangles $[s_k, r_k + t_k] \times]0, r_k a_0]$ (a_0 is an appropriate coarsest scale which actually depends on the analyzing wavelet). Our goal is to study the self-similarity properties of μ through those of its wavelet transform $T_\psi[\mu]$. For that purpose, we are not going to deal with the whole wavelet transform but only with its skeleton. One can easily prove that the self-similarity relation (123) still holds when restricted to the set of modulus maxima of the wavelet transform [Figs. 13(b) and 14(b)]. For more details, we refer the reader to our previous work [Arneodo *et al.*, 1993a, 1993b; Bacry *et al.*, 1993] and to a recent preprint by Hwang & Mallat [1993] where an alternative approach to recover the affine self-similarity parameters through a voting procedure based on Eq. (123) is reported.

Let us illustrate our purpose on a particular example. For the sake of simplicity, we choose $s = 2$, $p_1 = 0.7$, $p_2 = 0.3$ and the T_k 's to be linear: $T_1(x) = 5x/3$ and $T_2(x) = 5x - 4$. The corresponding invariant measure is shown in Fig. 36(a) and the position of its wavelet transform modulus maxima in Fig. 36(b). As previously noticed, one can see that the part of the space-scale half-plane displayed in Fig. 36(b) (the entire rectangle $[0, 1] \times]0, a_0]$) is “similar” to the two rectangles delimited by the dashed lines ($[0, 3/5] \times]0, 3a_0/5]$ and $[4/5, 1] \times]0, a_0/5]$) (up to a global rescaling of the modulus of the wavelet transform). Let us describe on this particular example our technique for recovering from the wavelet transform modulus maxima, the discrete (cookie-cutter) dynamical system T .

We call *bifurcation point* any point in the space-scale half-plane located at a scale where a maxima line appears and which is equidistant to this line and to the closest longer line. The bifurcation points at coarse scales are displayed in Fig. 36(b) using the symbol (\bullet). They lie on a binary tree whose root is the bifurcation point at the coarsest scale. Each bifurcation point defines naturally a subtree which can be associated with a rectangle in the space-scale half-plane. This root corresponds to the original rectangle $[0, 1] \times]0, a_0]$ whereas its two sons correspond to reduced copies delimited by the dashed lines. As illustrated in Fig. 36(b), the self-similarity relation [Eq. (124)] amounts to matching the “root rectangle” with one of the “son rectangles,” i.e., the whole tree with one of the subtrees. More generally, this relation associates any bifurcation point (x_n, a_n) of an order n subtree with its hierarchical homologous (x_{n-1}, a_{n-1}) of an order $n-1$ subtree. It follows from Eq. (124) that $x_n = r_k x_{n-1} + t_k$ and $a_n = r_k a_{n-1}$. Thus by plotting x_{n-1} versus x_n , one can expect to recover the initial cookie-cutter T . This reconstructed 1D map is displayed in Fig. 36(c). As one can see, the two branches T_1 and T_2 of the cookie-cutter T provide a remarkable fit of the numerical data. Let us point out that the nonuniform repartition of the data points on the theoretical curve results from the lacunarity of the measure induced by the “hole” between the two branches T_1 and T_2 . In Fig. 36(d), we show the histogram of the (contracting) scale ratio values between the scales of two bifurcation points of successive generations $r = a_n/a_{n-1}$ as computed when investigating systematically the WTMM skeleton. As expected, it displays two peaks corresponding to the two slopes $r_1 = 3/5$ and $r_2 = 1/5$ of T_1^{-1} and T_2^{-1} respectively. Note that the peak corresponding to the smallest value of r is lower than the other one; this is a direct consequence of the finite cut-off we use in our wavelet transform calculation at small scales. On a finite range of scales, the construction process involves less steps with the smallest scale ratio r_2 than steps with the largest one r_1 . [The so-computed histogram can be artificially corrected in order to account for these finite size effects; actually it suffices to plot $N(r) \ln(1/r)$ instead of $N(r)$.] Figure 36(e) displays the histogram of amplitude ratio values $p = |T_\psi[\mu](x_n, a_n)|/|T_\psi[\mu](x_{n-1}, a_{n-1})|$; one clearly distinguishes two peaks in good agreement with the weights $p_1 = 0.7$ and $p_2 = 0.3$. Let us mention at this point, that the distribution $N(r)$ of scale ratios is in a way redundant with the 1D map

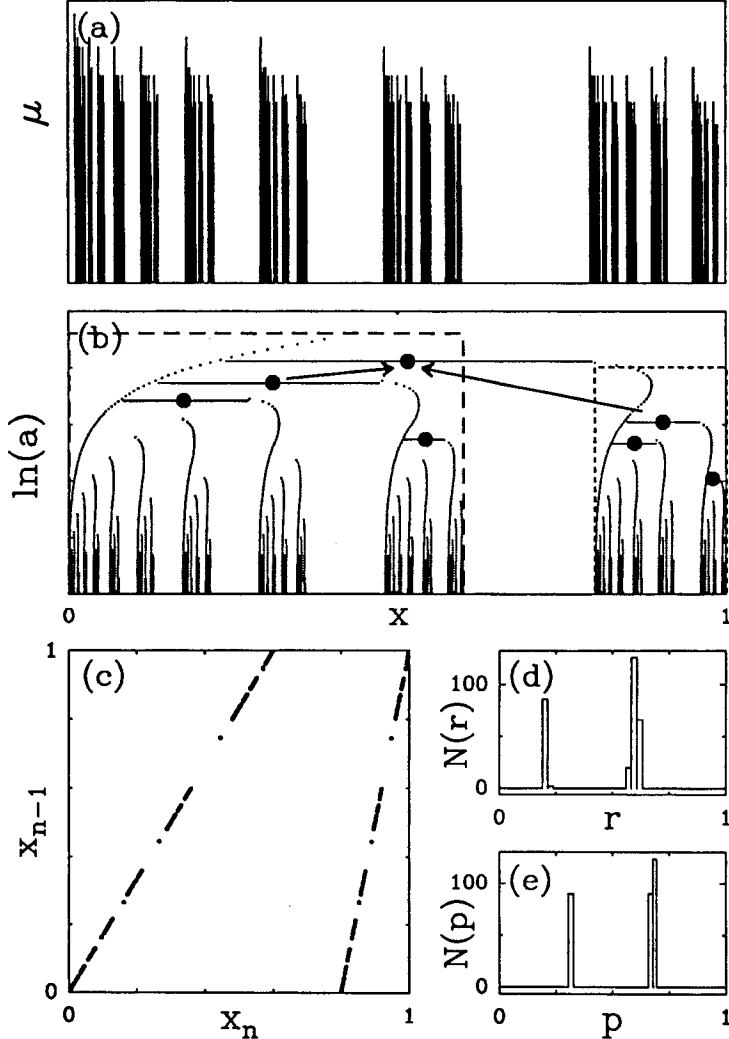


Fig. 36. (a) Invariant measure of the two branch cookie-cutter $T_1(x) = 5x/3$, $T_2(x) = 5x - 4$, distributed with the weights $p_1 = 0.7$, $p_2 = 0.3$ on the interval $[0, 1]$. (b) Position in the (x, a) half-plane of the local maxima of the modulus of the wavelet transform of the measure shown in (a), using a Gaussian analyzing wavelet; the large scales are at the top. According to the self-similarity relation [Eq. (124)], the maxima line arrangement in the two dashed rectangles is the same as in the original rectangle. The bifurcation points associated with each rectangle are represented by the symbols (\bullet). Arrows indicate the matching of these bifurcation points according to the self-similarity relation [Eq. (124)]. (c) 1D map that represents the position x_{n-1} of an order $n - 1$ bifurcation point versus the position x_n of the associated order n bifurcation point following the tree matching defined in (b). The graph of this map corresponds exactly to the original cookie-cutter. (d) Histogram of scale ratios $r = a_n/a_{n-1}$ between the scales of two associated bifurcation points. (e) Histogram of amplitude ratios $p = |T_\psi[\mu](x_n, a_n)|/|T_\psi[\mu](x_{n-1}, a_{n-1})|$ computed from two associated bifurcation points.

since it is basically made of two Diracs located at the inverse of the slopes of the two branches of this piecewise-linear map. On the contrary, the distribution $N(p)$ of amplitude ratios brings a very important piece of information which is not present in the 1D map: the repartition of the weights at each construction step. When this repartition is uniform, we get an histogram $N(p)$ which reduces to a single point $p = 1/2$. When the repartition is not uniform, as in Fig. 36, one can furthermore study the

joint law of p with r in order to find out the specific “rules” for associating a p with a r .

In the former example, we have described our technique to solve the inverse fractal problem for cookie-cutters made of two linear branches ($s = 2$ and T_1 , T_2 linear). Since Eq. (123) locally (in the space-scale half-plane) looks like Eq. (124), we can apply exactly the same technique for nonlinear expanding maps. [Let us point out that the hyperbolicity condition is *a priori* required for the first

derivative of T_k^{-1} involved in the right-hand side of Eq. (123), to be finite]. Figure 37(a) displays the 1D map extracted from the wavelet transform modulus maxima skeleton of the uniform Bernoulli measure associated to a nonlinear cookie-cutter made of two inverse hyperbolic tangent branches. Once again, the numerical results match perfectly the theoretical curve. In this case, the histogram of amplitude ratios is concentrated at a single point $p = 1/2$. The histogram of scale ratios, however, involves more than simply two scale ratios, as before, since the nonlinearity of the map implies that new scale ratios are actually operating at each construction step.

As a first application of our wavelet based tree matching algorithm to a physical problem, we show in Fig. 37(b) the results obtained when analyzing the natural measure associated with the iteration of quadratic unimodal maps at the accumulation of period doublings (Sec. 4.1.2). A well defined 1D map with two distinct hyperbolic branches is numerically reconstructed. A computation at finer resolution would reveal that the left-hand branch is linear with a slope $1/r = 1/\Phi_*(1) \simeq -2.5$, whereas the right-hand one is nonlinear. The computation of the scale-ratio histogram confirms this observation. One can also compute the amplitude ratio histogram and find that the weights associated with these two branches are equal $p_1 = p_2 = 1/2$. The period-doubling natural measure can thus be seen as the invariant measure of the (hyperbolic) cookie-cutter displayed in Fig. 37(b). The solid lines shown

in this figure correspond to the dynamical system defined in Eq. (76) and which was proved by Ledrappier & Misiurewicz [1985] to have the same invariant measure as the fixed point mapping $\Phi_*(x)$ [Eq. (75)] of the renormalization operation [Eq. (74)]. Our numerical data are in remarkable agreement with the theoretical prediction.

In the case where s is no longer equal to 2, one can easily adapt our technique by trying to match not only the root bifurcation point on its sons but also on its grandsons and so on. For instance, in the case $s = 3$, we will match the root with one of its sons and with each of the two sons of its other son. The general algorithm, that we have developed, uses a “best matching” procedure that automatically chooses the matching which is the most consistent (e.g., such that the different derivatives of $T_\psi[\mu]$ follow the same self-similarity rules as $T_\psi[\mu]$). Thus the algorithm is not looking for a given number s of branches that the user would have guessed *a priori*, it automatically comes up with the “best” value of s . In Fig. 38 are shown the 1D map, the histogram of scale ratios and the histogram of amplitude ratios obtained in the linear case where $s = 3$, $p_1 = p_2 = p_3 = 1/3$ and $r_1 = 0.2$, $r_2 = 0.3$, $r_3 = 0.5$. All these values are very accurately recovered by our algorithm. Let us notice that, so far, we have only considered measures which do not involve any “memory” effect in their hierarchical structure, i.e., the successive (backward) iterations always consist in applying the same dynamical system T , independently of the previous iterations. However, in a certain way, a construction rule involving a finite memory can be accounted for by increasing the number of branches of a “no memory” map T . As illustrated in Fig. 38, this class of dynamical systems is directly amenable to our WT algorithm procedure. Nevertheless, it is meaningless to look for some dynamical systems with rather high number of branches; generally, there would not be enough scales in the data in order to ensure the theoretical validity of the outcome discrete map.

This tree matching algorithm based on the wavelet transform modulus maxima representation is without any doubt a very promising step towards solving the inverse fractal problem. Its recent application to characterize the fractal properties of DLA azimuthal Cantor sets defined by intersecting the inner frozen region of large mass off-lattice diffusion limited aggregates with a circle, has revealed the existence of a Fibonacci multiplicative process in the apparently disordered arborescent

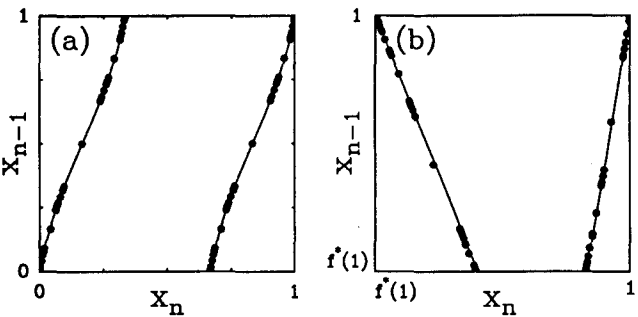


Fig. 37. (a) Inverse problem for a nonlinear cookie-cutter made of two inverse hyperbolic tangent branches. The data are obtained from the same wavelet transform tree matching analysis as in Fig. 36. The original dynamical system (solid lines) is recovered accurately. (b) Inverse problem for the invariant measure associated to the critical period-doubling dynamical system Φ_* (see text). The solid lines represent the theoretical prediction. Finer resolution computations would reveal that the right-hand branch is nonlinear. The left-hand branch is linear with a slope $1/\Phi_*(1) \simeq -2.5$.

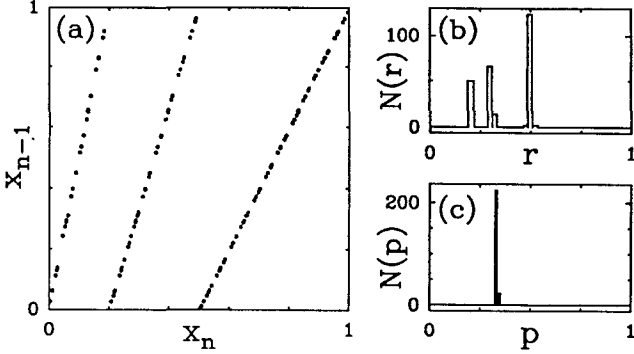


Fig. 38. (a) Inverse problem for the invariant measure of the three branch cookie-cutter $T_1(x) = 5x$, $T_2(x) = 10x/3 - 2/3$, $T_3(x) = 2x - 1$, distributed with equal weights $p_1 = p_2 = p_3 = 1/3$ on the interval $[0, 1]$. (b) Histogram of scale ratios $r = a_n/a_{n-1}$. (c) Histogram of amplitude ratios $p = |T_\psi[\mu](x_n, a_n)|/|T_\psi[\mu](x_{n-1}, a_{n-1})|$.

DLA morphology [Arneodo *et al.*, 1992c, 1992d, 1992e, 1993b]. This discovery is a very spectacular manifestation of the statistical relevance of the golden mean arithmetic to fractal growth phenomena. We are convinced that further applications of this wavelet based technique will lead to similar major breakthroughs in various fields where multi-scale phenomena are ubiquitous. The implementation of a tree matching algorithm that generalizes our wavelet based method from 1D to 2D is currently in progress.

Acknowledgments

We are very grateful to F. Argoul for very helpful discussions and a careful reading of the manuscript. This work was supported by the Direction des Etudes et Techniques under contract No. 92/097.

References

- Arneodo, A., Argoul, F., Bacry, E., Muzy, J. F. & Tabard, M. [1992c] "Golden mean arithmetic in the fractal branching of diffusion-limited aggregates," *Phys. Rev. Lett.* **68**, 3456–3459.
- Arneodo, A., Argoul, F., Muzy, J. F. & Tabard, M. [1992d] "Structural five-fold symmetry in the fractal morphology of diffusion-limited aggregates," *Physica A* **188**, 217–242.
- Arneodo, A., Argoul, F., Muzy, J. F. & Tabard, M. [1992e] "Uncovering Fibonacci sequences in the fractal morphology of diffusion-limited aggregates," *Phys. Lett. A* **171**, 31–36.
- Arneodo, A., Bacry, E. & Muzy, J. F. [1993a] "Solving the inverse fractal problem from wavelet analysis," *Europhysics Letters*, to appear.
- Arneodo, A., Argoul, F., Muzy, J. F., Tabard, M. & Bacry, E. [1993b] "Beyond classical multifractal analysis using wavelets: Uncovering a multiplicative process hidden in the geometrical complexity of diffusion limited aggregates," *Fractals* **1**, 629–649.
- Azencott, R. & Dacunha-Castelle, D. [1984] *Série d'Observations Irrégulières* (Masson, Paris).
- Bacry, E., Arneodo, A., Frisch, U., Gagne, Y. & Hopfinger, E. J. [1991] "Wavelet analysis of fully developed turbulence data and measurement of scaling exponents," in *Turbulence and Coherent Structures*, eds. Lesieur, M. & Metais, O. (Kluwer Academic Publishers), pp. 203–215.
- Bacry, E. [1992] *Thesis*, University of Paris VII.
- Bacry, E., Muzy, J. F. & Arnéodo, A. [1993] "Singularity spectrum of fractal signals from wavelet analysis: Exact results," *J. Stat. Phys.* **70**, 635–674.
- Badii, R. [1987] "Conservation laws and thermodynamic formalism for dissipative dynamical systems," *Thesis*, University of Zurich.
- Baddi, R. & Broggi, G. [1988] "Measurement of the dimension spectrum $f(\alpha)$: Fixed-mass approach," *Phys. Lett. A* **131**, 339–343.
- Barabási, A. L. & Vicsek, T. [1991] "Multifractality of self-affine fractals," *Phys. Rev. A* **44**, 2730–2733.
- Barnsley, M. F. & Demko, S. G. [1985] "Iterated function systems and the global construction of fractals," *Proc. Roy. Soc. London A* **339**, 243.
- Barnsley, M. F. [1988] *Fractals Everywhere* (Academic Press, INC. New York).
- Benzi, R., Paladin, G., Parisi, G. & Vulpiani, A. [1984] "On the multifractal nature of fully developed turbulence and chaotic systems," *J. Phys. A* **17**, 3521–3531.
- Besicovitch, A. S. [1935] "On the sum of digits of real numbers represented in the dyadic system," *Mathematische Annalen* **110**, 321–330.
- Bohr, T. & Tél, T. [1988] "The Thermodynamics of Fractals," in *Directions in Chaos*, Vol. 2, ed. Hao, B. L. (World Scientific, Singapore), pp. 194–237.
- Bowen, R. [1975] *Lect. Notes in Maths* **470**, 1 (Springer-Verlag, New York).
- Brachet, M. E., Meiron, D. I., Orszag, S. A., Nickel, B. G., Morf, R. H. & Frisch, U. [1983] "Small-scale structure of the Taylor-Green vortex," *J. Fluid Mech.* **130**, 411–452.
- Brachet, M. E. [1990] "Géométrie des structures à petite échelle dans le vortex de Taylor-Green," *C. R. Acad. Sci. Paris* **311**, 775–780.
- Brachet, M. E. [1991] "Direct simulations of three-dimensional turbulence in the Taylor-Green vortex," *Fluid Dyn. Research* **8**, 1–8.
- Bunde, A. & Havlin, S. (eds.) [1991] *Fractals and Disordered Systems* (Springer-Verlag, Berlin).

- Campanino, M. & Epstein, H. [1981] "On the existence of Feigenbaum's fixed point," *Comm. Math. Phys.* **79**, 261–302.
- Campanino, M., Epstein, H. & Ruelle, D. [1982] *Topology* **21**, 125.
- Castaing, B., Gagne, Y. & Hopfinger, E. J. [1990] "Velocity probability density functions of high Reynolds number turbulence," *Physica* **D46**, 177–200.
- Chhabra, A. & Jensen, R. V. [1989] "Direct determination of the $f(\alpha)$ singularity spectrum," *Phys. Rev. Lett.* **62**, 1327–1330.
- Chhabra, A. B., Meneveau, C., Jensen, R. V. & Sreenivasan, K. R. [1989] "Direct determination of the $f(\alpha)$ singularity spectrum and its application to fully developed turbulence," *Phys. Rev. A* **40**, 5284–5294.
- Collet, P. & Eckmann, J. P. [1980] *Iterated Maps on the Interval as Dynamical Systems* (Birkhäuser, Boston).
- Collet, P., Lebowitz, J. & Porzio, A. [1987] "The dimension spectrum of some dynamical systems," *J. Stat. Phys.* **47**, 609–644.
- Combes, J. M., Grossmann, A. & Tchamitchian, P. (eds.) [1989] *Wavelets* (Springer-Verlag, Berlin).
- Coullet, P. & Tresser, C. [1978] "Itérations d'endomorphismes et groupe de renormalisation," *J. Physique* **39**, Coll. C5–25.
- Coullet, P. & Tresser, C. [1981] "Some universal aspects of the transition to stochasticity for non-conservative dynamical systems," in *Field Theory, Quantization and Statistical Physics*, ed. Tirapegui, E. (D. Reidel Publishing Company, Dordrecht), pp. 249–261.
- Coullet, P. [1984] "Stability of the scenarios towards chaos," in *Chaos and Statistical Methods*, ed. Kuramoto, Y. (Springer-Verlag, Berlin), pp. 62–71.
- Crutchfield, J. P., Farmer, J. D. & Huberman, B. A. [1982] "Fluctuations and simple chaotic dynamics," *Phys. Rep.* **92**, 46–82.
- Cvitanovic, P. (ed.) [1984] *Universality in Chaos* (Hilger, Bristol).
- Cvitanovic, P. [1987] in *Proc. Group Theoretical Methods in Physics*, ed. Gilmore, R. (World Scientific, Singapore).
- Daubechies, I., Grossmann, A. & Meyer, Y. [1986] "Painless nonorthogonal expressions," *J. Math. Phys.* **27**, 1271–1283.
- Daubechies, I. [1988] "Orthonormal bases of compactly supported wavelets," *Comm. Pure Appl. Math.* **41**, 909–996.
- Daubechies, I. [1992] *Ten Lectures on Wavelets* (S.I.A.M., Philadelphie).
- Derrida, B., Gervois, A. & Pomeau, Y. [1979] "Universal metric properties of bifurcations of endomorphisms," *J. Phys.* **A12**, 269–296.
- Douady, S., Couder, Y. & Brachet, M. E. [1991] "Direct observation of the intermittency of intense vorticity filaments in turbulence," *Phys. Rev. Lett.* **67**, 983–986.
- Dubuc, B., Quiniou, J. F., Roques-Carmes, C., Tricot, C. & Zucker, S. W. [1989] "Evaluating the fractal dimension of profiles," *Phys. Rev. A* **39**, 1500–1512.
- Eckmann, J. P. [1981] "Roads to turbulence in dissipative dynamical systems," *Rev. Mod. Phys.* **53**, 643–654.
- Edgar, G. A. [1990] *Measure, Topology and Fractal Geometry* (Springer-Verlag, Berlin).
- Epstein, H. & Lascoux, J. [1981] "Analyticity properties of the Feigenbaum function," *Comm. Math. Phys.* **81**, 437–453.
- Epstein, H. [1986] "New proofs of the existence of the Feigenbaum functions," *Comm. Math. Phys.* **106**, 395–426.
- Everson, R., Sirovich, L. & Sreenivasan, K. R. [1990] "Wavelet analysis of the turbulent jet," *Phys. Lett.* **A145**, 314–322.
- Evertsz, C. J. & Mandelbrot, B. B. [1992] in *Chaos and Fractals*, eds. Peitgen, H. O., Jürgens, H. & Saupe, D. (Springer-Verlag, Berlin).
- Falconer, K. J. [1985] *The Geometry of Fractal Sets* (Cambridge Univ. Press, Cambridge).
- Family, F. & Vicsek, T. [1991] *Dynamics of Fractal Surfaces* (World Scientific, Singapore).
- Farge, M. [1992] "Wavelet transforms and their applications to turbulence," *Annu. Rev. Fluid Mech.* **24**, 395–457.
- Farmer, J. D., Ott, E. & Yorke, J. A. [1983] "The dimension of the chaotic attractors," *Physica* **D7**, 153–180.
- Farmer, J. D. [1984] in *Fluctuations and Sensitivity in Nonequilibrium Systems*, eds. Horstemke, W. & Kondepudi, D. (Springer-Verlag, Berlin), pp. 172.
- Feder, J. [1988] *Fractals* (Plenum Press, New York).
- Feigenbaum, M. J. [1978] "Quantitative universality for a class of nonlinear transformations," *J. Stat. Phys.* **19**, 25–52.
- Feigenbaum, M. J. [1979] "The universal metric properties of nonlinear transformations," *J. Stat. Phys.* **21**, 669–706.
- Feigenbaum, M. J., Kadanoff, L. P. & Shenker, S. J. [1982] "Quasiperiodicity in dissipative systems: A renormalization group analysis," *Physica* **D5**, 370–386.
- Feigenbaum, M. J. [1987a] "Some characterizations of strange sets," *J. Stat. Phys.* **46**, 919–924.
- Feigenbaum, M. J. [1987b] "Scaling spectrum and return times of dynamical systems," *J. Stat. Phys.* **46**, 925–932.
- Flandrin, P. [1991a] "Wavelet analysis and synthesis of fractional Brownian motion," preprint (ENS, Lyon).
- Flandrin, P. [1991b] "On the time-scale analysis of self-similar processes," (Springer-Verlag, Berlin) to appear.
- Frisch, U., Sulem, P. L. & Nelkin, M. [1978] "A simple dynamical model of intermittent fully developed turbulence," *J. Fluid. Mech.* **87**, 719–736.
- Frisch, U. [1985] "Où en est la turbulence pleinement développée?" *Physica Scripta* **T9**, 137–146.

- Frisch, U. & Parisi, G. [1985] "Fully developed turbulence and intermittency," and "Appendix: On the singularity structure of fully developed structure," in *Turbulence and Predictability in Geophysical Fluid Dynamics and Climate Dynamics*, eds. Ghil, M., Benzi, R. and Parisi, G. (North-Holland, Amsterdam), pp. 71–88.
- Frisch, U. & Orszag, S. A. [1990] "Turbulence: Challenges for theory and experiment," *Physics Today*, pp. 24–32.
- Frisch, U. [1991] "From global (Kolmogorov 1941) scaling to local (multifractal) scaling in fully developed turbulence," *Proc. Roy. Soc. A*, Special Issue on A. N. Kolmogorov, to appear.
- Gagne, Y. [1987] "Etude expérimentale de l'intermittence et des singularités dans le plan complexe en turbulence développée," *Thesis*, University of Grenoble.
- Gagne, Y., Hopfinger, E. J. & Frisch, U. [1988] "A new universal scaling for fully developed turbulence: The distribution of velocity increments," in *New Trends in Nonlinear Dynamics and Pattern-Forming Phenomena: The Geometry of Nonequilibrium*, eds. Coullet, P. & Huerre, P. (Plenum Press, New York), pp. 315–319.
- Ghez, J. M. & Vaidenti, S. [1992] "Integrated Wavelets on Fractal Sets: I. The Correlation Dimensions," *Nonlinearity* **5**, 777–790.
- Ghez, J. M. & Vaidenti, S. [1992] "Integrated wavelets on fractal sets: II. The generalized dimensions," *Nonlinearity* **5**, 791–804.
- Goodchild, M. [1980] *Math. Geo.* **12**, 85.
- Gouillaud, P., Grossmann, A. & Morlet, J. [1984] "Cycle-octave and related transforms in seismic signal analysis," *Geoexploration* **23**, 85–102.
- Grassberger, P. [1983] "Generalized dimensions of strange attractors," *Phys. Lett.* **A97**, 227–230.
- Grassberger, P. & Procaccia, I. [1983] "Measuring the strangeness of strange attractors," *Physica* **D9**, 189–208.
- Grassberger, P. & Procaccia, I. [1984] "Dimensions and entropies of strange attractors from a fluctuating dynamics approach," *Physica* **D13**, 34–54.
- Grassberger, P., Badii, R. & Politi, A. [1988] "Scaling laws for invariant measures on hyperbolic and nonhyperbolic attractors," *J. Stat. Phys.* **51**, 135–178.
- Grasseau, G. [1989] "Des techniques mathématiques aux outils numériques pour l'étude d'objets fractals," *Thesis*, University of Bordeaux I.
- Grossmann, A. & Morlet, J. [1984] "Decomposition of hardy functions into square integrable wavelets of constant shape," *S.I.A.M. J. Math. Anal.* **15**, 723–736.
- Grossmann, A. & Morlet, J. [1985] in *Mathematics and Physics, Lectures on Recent Results*, ed. Streit, L. (World Scientific, Singapore).
- Grossmann, A., Morlet, J. & Paul, T. [1985] "Transforms associated to square integrable group representations. I. General results. *J. Math. Phys.* **26**, 2473–2479.
- Grossmann, A., Morlet, J. & Paul, T. [1986] "Transform associated to square integrable group representation. II. Examples," *Ann. Inst. Henri Poincaré* **45**, 293–309.
- Guckenheimer, J. & Holmes, P. [1984] *Nonlinear Oscillations, Dynamical Systems and Bifurcations of Vector Fields* (Springer-Verlag, Berlin).
- Guttinger, W. & Dangelmayr, D. (eds.) [1987] *The Physics of Structure Formation* (Springer-Verlag, Berlin).
- Halsey, T. C., Jensen, M. H., Kadanoff, L. P., Procaccia, I. & Shraiman, B. I. [1986] "Fractal measures and their singularities: The characterization of strange sets," *Phys. Rev.* **A33**, 1141–1151.
- Handy, C. R. & Mantica, G. [1990] "Inverse problems in fractal construction: Moment method solution," *Physica* **D43**, 17–36.
- Hausdorff, F. [1919] "Dimension und äusseres Mass," *Mathematische Annalen* **79**, 157–179.
- Hentschel, H. G. E. & Procaccia, I. [1983] "The infinite number of generalized dimensions of fractals and strange attractors," *Physica* **D8**, 435–444.
- Holschneider, M. [1988a] "On the wavelet transformation of fractal objects," *J. Stat. Phys.* **50**, 963–993.
- Holschneider, M. [1988b] "L'analyse d'objets fractals et leur transformation en ondelettes," *Thesis*, University of Aix-Marseille II.
- Holschneider, M. [1990] "Inverse radon transform through inverse wavelet transform," preprint (CPT, Marseille), submitted to *Inverse Problems*.
- Holschneider, M. & Tchamitchian, P. [1990] in Lemarié, 1990, pp. 102.
- Hu, B. [1982] "Introduction to real-space renormalization-group methods in critical and chaotic phenomena," *Phys. Rep.* **91**, 233–295.
- Hwang, W. L. & Mallat, S. [1993] "Characterization of self-similar multifractals with wavelet maxima," New York University Technical Report N° 641 (Computer Science Department).
- Jaffard, S. [1989] "Exposants de Hölder en des points donnés et coefficients d'ondelettes," *C. R. Acad. Sci. Paris* **308**, série I, 79–81.
- Jaffard, S. & Meyer, Y. [1989a] "Bases d'ondelettes dans les ouverts de \mathbb{R}^n ," *J. de Math. Pures, et Appl.* **68**, 95–108.
- Jaffard, S. & Meyer, Y. [1989b] "Construction of wavelets on open sets," in *Combes et al., 1989*, 247–252.
- Jaffard, S. [1992] *C. R. Acad. Sci. Paris* **315**, série I, 19.
- Jaffard, S. [1993a] "Multifractal formalism for functions. Part I: Results valid for all functions," CERMA preprint.
- Jaffard, S. [1993b] "Multifractal formalism for functions. Part II: Self-similar functions," CERMA preprint.
- Jensen, M. H., Kadanoff, L. P. & Procaccia, I. [1987] "Scaling structure and thermodynamics of strange sets," *Phys. Rev.* **A36**, 1409–1420.

- Kahane, J. P. [1985] in *Recent Progress in Fourier Analysis*, eds. Peral, I. & Rubio di Francia, J. L. (North-Holland, Amsterdam), pp. 65–121.
- Kolmogorov, A. N. [1941] *C. R. Acad. Sci. USSR* **30**, 301.
- Kolmogorov, A. N. [1958] *Dokl. Akad. Nauka. USSR* **119**, 861.
- Kolmogorov, A. N. [1962] “A refinement of previous hypotheses concerning the local structure of turbulence in a viscous incompressible fluid at high Reynolds number,” *J. Fluid Mech.* **13**, 82–85.
- Lanford, O. E. [1982] “A computer-assisted proof of the Feigenbaum conjectures,” *Bull. Amer. Math. Soc.* **6**, 427–434.
- Lanford, O. E. [1984] “A shorter proof of the Feigenbaum fixed point,” *Comm. Math. Phys.* **96**, 521–538.
- Ledrappier, F. & Misiurewicz, M. [1985] *Ergodic. Th. Dyn. Syst.* **5**, 595.
- Lemarié, P. G. & Meyer, Y. [1986] “Ondelettes et bases hilbertiennes,” *Rev. Math. Iberoamericana* **2**, 1–18.
- Lemarié, P. G. (ed.) [1990] *Les Ondelettes en 1989* (Springer-Verlag, Berlin).
- Lévy, P. [1965] *Processus Stochastiques et Mouvement Brownien* (Gauthiers-Villars).
- Li, W. [1991] “Absence of $1/f$ spectra in Dow Jones daily average,” *Int. J. of Bifurcation and Chaos* **1**, 583–597.
- Mallat, S. G. [1989a] “A Theory for multiresolution signal decomposition: The wavelet representation,” *IEEE Trans. on Pattern Analysis and Machine Intelligence* **11**, 674–693.
- Mallat, S. [1989b] “Multiresolution approximations and wavelet orthonormal bases of $L^2(R)$,” *Trans. of the Am. Math. Soc.* **315**, 69–87.
- Mallat, S. & Hwang, W. L. [1992] “Singularity detection and processing with wavelets,” *IEEE Trans. on Information Theory* **38**, 617–643.
- Mallat, S. & Zhong, S. [1992] “Characterization of signals from multiscale edges,” *IEEE Trans. on Pattern Analysis and Machine Intelligence* **14**, 710–732.
- Mandelbrot, B. B. [1967] “The variation of some other speculative price,” *J. Bus. Univ. Chicago* **40**, 393–413.
- Mandelbrot, B. B. & Taylor, H. M. [1967] *Oper. Res.* **15**, 1057.
- Mandelbrot, B. B. & Van Ness, J. W. [1968] “Fractional Brownian motions, fractional noises and applications,” *S.I.A.M. Rev.* **10**, 422–437.
- Mandelbrot, B. B. [1974] “Intermittent turbulence in self-similar cascades: Divergence of high moments and dimension of the carrier,” *J. Fluid Mech.* **62**, 331–358.
- Mandelbrot, B. B. [1977] *Fractals: Form, Chance and Dimension* (W. H. FREEMAN and COMPANY, San Francisco).
- Mandelbrot, B. B. [1982] *The Fractal Geometry of Nature* (W. H. FREEMAN and COMPANY, San Francisco).
- Mandelbrot, B. B. [1984] “Fractals in physics: Squig clusters, diffusions, fractal measures, and the unicity of fractal dimensionality,” *J. Stat. Phys.* **34**, 895–930.
- Mandelbrot, B. B. [1988] “An introduction to multifractal distribution functions,” in *Random Fluctuations and Pattern Growth* ed. Stanley & Ostrowski (Kluwer Academic, Dordrecht), pp. 279–291.
- Mandelbrot, B. B. [1989a] *Fractals and Multifractals: Noise, Turbulence and Galaxies, Selecta Vol. 1* (Springer-Verlag, New York).
- Mandelbrot, B. B. [1989b] in *The Fractal Approach to Heterogeneous Chemistry*, ed. Avnir, D. (John Wiley & Sons, New York).
- Mandelbrot, B. B. [1989c] *Pure Appl. Geophys.* **131**, 5.
- Meakin, P. [1988] in *Phase Transitions and Critical Phenomena*, Vol. 12, ed. Domb, C. & Lebowitz, J. (Academic Press, New York), p. 355.
- Meneveau, C. & Sreenivasan, K. R. [1991] “The multifractal nature of turbulent energy dissipation,” *J. Fluid Mech.* **224**, 429–484.
- Meyer, Y. [1987] “Ondelettes, fonctions splines et analyses graduées,” *Cahier du CEREMADE* **8703** (Paris).
- Meyer, Y. [1990] *Ondelettes* (Herman, Paris).
- Meyer, Y. (ed.) [1992] *Wavelets and Applications* (Springer-Verlag, Berlin).
- Meyer, Y. & Roques, S. (eds.) [1993] *Progress in Wavelets Analysis and Applications* (Frontieres, Gif sur Yvette, France).
- Miller, P. L. & Dimotakis, P. E. [1991] “Stochastic geometric properties of scalar interfaces in turbulent jets,” *Phys. Fluids* **A3**, 168–177.
- Monin, A. S. & Yaglom, A. M. [1971] *Statistical Fluid Mechanics: Mechanics of Turbulence*, Vol. II (THE MIT PRESS).
- Morlet, J. [1983] “Sampling theory and wave propagations,” *NATO ASI series FI* (Springer, Berlin) 233–261.
- Muzy, J. F., Bacry, E. & Arneodo, A. [1991] “Wavelets and multifractal formalism for singular signals: Application to turbulence data,” *Phys. Rev. Lett.* **67**, 3515–3518.
- Muzy, J. F., Pouliquen, B., Freysz, E., Argoul, F. & Arneodo, A. [1992] “Optical-diffraction measurement of fractal dimensions and $f(\alpha)$ spectrum,” *Phys. Rev. A* **45**, 8961–8964.
- Muzy, J. F., Bacry, E. & Arneodo, A. [1993a] “Multifractal formalism for fractal signals: The structure-function approach versus the wavelet-transform modulus-maxima method,” *Phys. Rev. E* **47**, 875–884.
- Muzy, J. F., Bacry, E. & Arneodo, A. [1993b] “Multifractal formalism for singular signals based on wavelet analysis,” in *Progress in Wavelets Analysis and Applications*, eds. Meyer & Roques [1993], (Frontieres, Gif sur Yvette, France), pp. 323–336.
- Muzy, J. F. [1993] *Thesis*, University of Nice.
- Nelkin, M. [1989] “What do we know about self-similarity in fluid turbulence?” *J. Stat. Phys.* **54**, 1–15.
- Novikov, E. A. & Stewart, R. W. [1964] *Izv. Akad. Nauk. SSSR, Geofiz.* **3**, 408.

- Rand, D., Ostlund, S., Sethna, J. & Siggia, E. D. [1982] "Universal transition from quasiperiodicity to chaos in dissipative systems," *Phys. Rev. Lett.* **49**, 132–135.
- Ostlund, S., Rand, D., Sethna, J. & Siggia, E. [1983] "Universal properties of the transition from quasiperiodicity to chaos in dissipative systems," *Physica* **D8**, 303–342.
- Ott, E. [1981] "Strange attractors and chaotic motions of dynamical systems," *Rev. Mod. Phys.* **53**, 655–671.
- Paladin, G. & Vulpiani, A. [1987] "Anomalous scaling laws in multifractal objects," *Phys. Rep.* **156**, 147–225.
- Peano, G. [1973] *Selected Works*, ed. Kennedy, H. C. (Toronto Univ. Press, Toronto).
- Peitgen, H. O. & Saupe, D. (eds.) [1987] *The Science of Fractals Images* (Springer-Verlag, New York).
- Peng, C. K., Buldyrev, S. V., Goldberger, A. L., Havlin, S., Sciortino, F., Simons, M. & Stanley, H. E. [1992] "Long-range correlations in nucleotide sequences," *Nature* **356**, 168–170.
- Pietronero, L. & Tosatti, E. (eds.) [1986] *Fractals in Physics* (North-Holland, Amsterdam).
- Prasad, R. R., Meneveau, C. & Sreenivasan, K. R. [1988] "Multifractal nature of the dissipation field of passive scalars in fully turbulent flows," *Phys. Rev. Lett.* **61**, 74–77.
- Rand, D. [1989] *Ergodic Th. Dyn. Sys.* **9**, 527.
- Renyi, A. [1970] *Probability Theory* (North-Holland, Amsterdam).
- Ruelle, D. [1978] *Thermodynamic Formalism* (Addison-Wesley, Reading).
- Ruskai, M. B., Beyklin, G., Coifman, R., Daubechies, I., Mallat, S., Meyer, Y. & Raphael, L. (eds.) [1992] *Wavelets and Their Applications* (Jones and Bartlett Publishers, Boston).
- Schertzer, D. & Lejevov, S. [1987] *J. Geophys. Res.* **92**, 9693.
- She, Z. S., Jackson, E. & Orszag, S. A. [1990] "Intermittent vortex structures in homogeneous isotropic turbulence," *Nature* **344**, 226–228.
- Shenker, S. J. [1982] "Scaling behavior in a map of a circle onto itself: Empirical results," *Physica* **D5**, 405–411.
- Siggia, E. D. [1981] "Numerical study of small-scale intermittency in three-dimensional turbulence," *J. Fluid Mech.* **107**, 375–406.
- Sinai, Y. G. [1972] "Gibbs measures in ergodic theory," *Usp. Mat. Nauk.* **27**(4), 21–64 [*J. Russ. Math. Surveys* **27**(4), 21–69].
- Stanley, H. E. & Ostrowsky, N. (eds.) [1986] *On Growth and Form: Fractal and Nonfractal Patterns in Physics* (Martinus Nijhoff Publishers, Dordrecht).
- Stanley, H. E. & Ostrowsky, N. (eds.) [1988] *Random Fluctuations and Pattern Growth* (Kluwer Academic, Dordrecht).
- Tél, T. [1988] "Fractals, multifractals and thermodynamics: An introductory review," *Z. Naturforsch* **48a**, 1154–1174.
- Tresser, C. & Coullet, P. [1978] "Itérations d'endomorphismes et groupe de renormalisation," *C. R. Acad. Sci.* **287**, 577–580.
- Turchetti, G. (ed.) [1989] *Nonlinear Dynamics* (World Scientific, Singapore).
- Vergassola, M. & Frisch, U. [1991] "Wavelet transforms of self-similar processes," *Physica* **D54**, 58–64.
- Vergassola, M., Benzi, R., Biferale, L. & Pisarenko, P. [1991] "Wavelet analysis of a Gaussian Kolmogorov signal," (Springer-Verlag, Berlin) to appear.
- Vicsek, T. [1989] *Fractal Growth Phenomena* (World Scientific, Singapore).
- Vincent, A. & Meneguzzi, M. [1991] "The spatial structure and statistical properties of homogeneous turbulence," *J. Fluid Mech.* **225**, 1–20.
- Voss, R. F. [1987] "Fractals in nature: From characterization to simulation," in *The Science of Fractals Images*, eds. Peitgen, H. O. & Saupe, D. (Springer-Verlag, New York), pp. 21–69.
- Voss, R. F. [1989] "Random fractals: Self-affinity in noise, music, mountains, and clouds," *Physica* **D38**, 362–371.
- Vul, E. B., Sinai, Ya. G. & Khanin, K. M. [1984] "Feigenbaum universality and the thermodynamic formalism," *Usp. Mat. Nauk.* **39**(3), 3–37 [*J. Russ. Math. Surv.* **39**(3), 1–40].